MEASURING CONTINUOUS NITROUS OXIDE EMISSIONS WITH AN AUTOMATED FLUX CHAMBER SYSTEM IN AN AGRICULTURAL FIELD FROM A COVER CROP AND WINTER WHEAT SYSTEM

By

ALICIA IWANICKI

A thesis submitted in partial fulfillment of
the requirements for the degree of

MASTER OF SCIENCE IN CIVIL ENGINEERING

WASHINGTON STATE UNIVERSITY
Department of Civil and Environmental Engineering

AUGUST 2020

To the Faculty of Washington State University:

The members of the Committee appointed to examine the thesis of ALICIA IWANICKI find it satisfactory and recommend that it be accepted.

_____

Shelley N. Pressley, Ph.D., Chair

_____

Eric S. Russell, Ph.D.

_____

David R. Huggins, Ph.D.

ACKNOWLEDGMENTS

I am incredibly grateful to everyone who has helped and supported me through the process of completing my thesis is support of my M.Sc in Engineering at WSU. To my academic advisor, Dr. Shelley Pressley, the other members of my thesis supervisory committee, Dr. Eric Russell and Dr. David Huggins, and my mentor, Dr. Brian Lamb. Thank you for providing me with the opportunity to pursue graduate school, and for providing me with constant support, feedback, and encouragement. I would also like to thank the incredible students and faculty at the LAR – I'm not sure that a more supportive academic research lab exists. You have all helped me gain so much confidence in my abilities and overcome my imposter syndrome.

I'd like to thank Jeff Ritter, Jenny Carlson, and Milica Radanovich for helping with the setup of the research site, helping with the extensive amount of fieldwork and site maintenance, and overall just providing constant support with the project. Thanks to Ian Leslie for your involvement in the project, particularly with seeding and fertilization, and for answering all of my crops and soils related questions. To Patrick O'Keeffe for helping with instrument troubleshooting and tech-savvy expertise in making our setup remote-accessible. I would also like to acknowledge and thank the USDA-ARS research scientists and field technicians who work at the PCFS for all their help with fieldwork.

Huge thanks to my family and friends for their constant encouragement and support from both near and far, and to my partner for being more supportive than I ever could've imagined and for using all your vacation days to fly out to see me.

Finally, I would like to thank the "Landscapes in Transition" project and everyone involved, which was funded through award #2017-68002-26819 from the National Institute of Food and Agriculture.

MEASURING CONTINUOUS NITROUS OXIDE EMISSIONS WITH AN AUTOMATED FLUX CHAMBER SYSTEM IN AN AGRICULTURAL FIELD FROM A COVER CROP AND WINTER WHEAT SYSTEM

Abstract

by Alicia Iwanicki, M.S.
Washington State University
August 2020

Chair: Shelley N. Pressley

Globally, agroecosystems contribute approximately 60% of total anthropogenic N_2O emissions, a potent greenhouse gas (GHG), mainly due to excessive application of nitrogen (N) fertilizer to croplands. High spatiotemporal resolution flux measurements are necessary for improving our understanding of the episodic and microscale behavior of soil N_2O emissions and the complex biogeochemical processes that trigger them. This study used two Li-Cor 8100A Automated Soil CO_2 Flux Systems coupled with laser spectroscopic Los Gatos Research (LGR) N_2O analyzers to measure continuous soil GHG fluxes from an automated closed static chamber system. A small-scale study plot in an agricultural field was divided into 16 microplots and a chamber was installed on each one, ensuring high-spatial coverage. The system monitored CO_2 and N_2O fluxes from a cover crop (CC) study from 15 May - 23 August 2019, where four treatments with four replications were established on the microplots as a randomized block design. The treatments were: lynx winter pea (WP), verdant winter barley (WB), a WP+WB 50-50 mix, and fertilized WB (WB_{fert}; 112 kg N ha^{-1} fertilization rate). Combined mean cumulative emissions

from the CC study were 78 ± 21 g N_2O-N ha^{-1} d^{-1}. Daily emissions were generally low, however, a few N_2O pulses were observed following drying/rewetting cycles, which were likely nitrification driven. Mean cumulative emissions from the WB_{fert} microplots were higher than mean cumulative emissions from all unfertilized microplots by 34%. Following CC termination, a fertilized winter wheat (WW; 168 kg N ha^{-1} fertilization rate) treatment was implemented on each microplot and monitored from 16 October 2019 – 29 February 2020. Mean combined cumulative N_2O emissions were 1217 ± 99 g N_2O-N ha^{-1} d^{-1}, which were predominantly attributed to high denitrification rates driven by high moisture soil conditions following rainfall and snowmelt. During both studies, soil moisture and N availability were the main drivers of N_2O emissions. Overall, the automated flux chamber system provided high-quality long-term flux data that effectively captured the high spatial and temporal variability of N_2O fluxes from various cropping treatments, which is important for determining regional N_2O budgets and mitigating emissions through improved N use efficiency in agroecosystems.

TABLE OF CONTENTS

Page

LIST OF TABLES

LIST OF FIGURES

Page

Dedication

To my family and partner. Thank you for believing in me

that I could do this thing.

CHAPTER ONE:

INTRODUCTION

1.1 Overview and thesis organization

Nitrous oxide (N_2O) is a harmful greenhouse gas (GHG) with approximately 298 times the global warming potential of carbon dioxide (CO_2) over a 100-year time horizon and is the main contributor to stratospheric ozone depletion (EPA, 2020). Agroecosystems contribute approximately 60% (~ 5 Tg N_2O-N) of total global anthropogenic N_2O emissions, mainly due to excessive applications of nitrogen (N) fertilizers to croplands (IPCC, 2013). A better understanding of what influences the soil N_2O emissions and the complex biogeochemical processes that trigger them is important for determining regional N_2O budgets and mitigating emissions through improved N management. Manual closed static chambers (CSCs) have been widely used for decades to measure soil N_2O emissions, however, they do not effectively capture their sporadic and microscale nature (Lebegue et al., 2016). With recent technological advancements, robust optical spectrometers for N_2O measurements have become more accessible to researchers and can be used with automated CSCs to provide continuous soil N_2O flux measurements with a higher temporal resolution than manual CSCs.

This chapter will provide an overview of the terrestrial N cycle, the microbial processes involved in soil N transformations that produce N_2O, and how they are affected by environmental and anthropogenic influences. It will also compare the advantages and disadvantages of quantifying in-situ soil GHG emissions using manual versus automated CSCs. The overview aims to provide valuable background information for the research study presented in this thesis.

Following this general introduction and review, Chapters 2 and 3 are prepared in a stand-alone, manuscript format. Chapter 2 presents the performance of a Los Gatos Research (LGR) N_2O analyzer plumbed in-line with the Li-Cor Automated Soil CO_2 Flux System, which can measure continuous CO_2 and N_2O fluxes from eight automated flux chambers in an agricultural field. It also proposes a quality criteria (QC) protocol for obtaining high-quality soil N_2O flux datasets from automated CSCs. Chapter 3 presents the N_2O flux data results collected from two independent instrument setups measuring fluxes from 16 microplots located in an agricultural field. The data focuses on analyzing the environmental and anthropogenic influences on the spatiotemporal variability of N_2O fluxes from two different cropping systems: a cover crop (CC) system and a winter wheat (WW) system. The thesis concludes with a synthesis chapter (Chapter 4), which integrates and highlights important findings and limitations from Chapter 2 and 3 and outlines future research initiatives.

Initial work conducted by previous Washington State University (WSU) researchers to measure N_2O soil fluxes from agriculture was part of a USDA-funded project called **RE**gional **A**pproaches to **C**limate **CH**ange (REACCH). A compilation of articles have been published called *Building Resilience to Climate Change in Cereal Production Systems: Agroecosystem components and integrative approaches.* Specifically, publications from Kostyanovsky et al., (2017) and Waldo (2016) provided the initial framework for this work. Based on the foundation of REACCH, the research presented here is part of a collaborative and interdisciplinary USDA-funded project called Landscapes in Transition (LIT). One of the main objectives of the project is to study the impact of crop diversification by alternating between business-as-usual and alternative cropping systems to help farmers improve their nutrient use efficiencies and reduce GHG emissions.

1.2. The impact of nitrogen inputs to agricultural soils on the global nitrogen cycle

Anthropogenic activities have more than doubled global nitrogen N fixation of reactive nitrogen (N_r) in the last 50 years, mainly through application of synthetic N fertilizers to crops due to ever-increasing global food production demands (Vitousek and Matson, 1993; Galloway, 1998; Smil, 1999; Mosier et al., 2002; Cameron et al., 2013; Fowler et al., 2013). Applying N fertilizer to crops in one large dose at the beginning of a growing season is typical practice due to the difficulties and high cost associated with supplying nutrients according to crop demands through their stages of development (Glass et al., 2003; Ju et al., 2009).

Accumulation of N_r in soils has greatly affected the Earth's natural N cycle, resulting in numerous environmental consequences, such as alterations to major biogeochemical cycles, loss of biodiversity, eutrophication, and health problems, all driving a positive feedback loop that intensifies global climate change (Galloway et al., 1995; Vitousek, et al., 1997; Butterbach-Bahl and Dannenmann, 2011; Ollivier et al., 2011). Human impact on the terrestrial N cycle has caused a steady increase in global atmospheric concentration of N_2O. Current global atmospheric N_2O concentration is currently about 331 ppb, exceeding pre-industrial levels of 270 ppb by about 20%, and is continuing to increase at a rate of about 0.8 ppb (0.25%) per year (Hénault et al., 2012; IPCC, 2013). The dominant N transformation mechanisms in the terrestrial N cycle that impact soil N_2O production include: N fixation, mineralization, nitrification, and denitrification.

1.3 The main mechanisms of nitrous oxide production in soil

1.3.1 Nitrogen fixation

Earth's largest pool of biologically available N is the atmosphere, which is made up of 78% dinitrogen gas (N_2). Nitrogen is continuously exchanged between the atmosphere and biosphere while undergoing several chemical transformations that are predominantly controlled by soil microbial processes. Atmospheric N_2 is inaccessible to plants as the N_2 molecule is relatively unreactive due to its strong triple bond. Nitrogen in its gaseous form needs to be "fixed" into N_r before it can react with other elements to form nitrogenous compounds that can be taken up by plants, often making N a limiting nutrient in natural systems (Galloway et al., 2004). Nitrate (NO_3^-) and ammonium (NH_4^+) are the two forms of N that can be assimilated by plants, however, NO_3^- is the preferred form for most plants as it is more mobile (Millar et al., 2014).

There are multiple natural and anthropogenic sources of N_r to terrestrial systems (Figure 1.1). The two natural N fixing pathways in terrestrial systems are biological N fixation by soil bacteria (accounting for ~ 40 - 130 Tg N y^{-1}) and lightning (accounting for up to 10 Tg N y^{-1}) (Stedman and Shetter, 1983; Galloway et al., 1995; Vitousek et al., 1997; Mosier, 2002). In biological fixation, N_2 deposited from the atmosphere into soil is converted into ammonia (NH_3) by free-living bacteria in the soil or by plant-bacteria symbiosis (Galloway et al., 1995; Vitousek et al., 1997). In atmospheric fixation through lightning, the energy of lightning enables the reaction of N_2 with oxygen (O) to form nitrogen oxides (NO_x) or with hydrogen (H) to form NH_3. NO_x dissolves in water and forms NO_3^-, which is transported, along with NH_3, to the soil via rainfall. NH_3 in soil either remains in this form or is transformed into NH_4^+ in the presence of water and slightly acidic soils (Sawyer, 2014).

Anthropogenic activities have nearly doubled the amount of N_r entering the terrestrial pool, primarily through N fertilization with ammonium and nitrate fertilizers (Figure 1.1). N fertilizer is mainly created via the Haber-Bosch process, which involves fixing atmospheric N_2 and converting it into NH_3 (Galloway et al., 1995; Fowler et al., 2013). Currently, agricultural N fertilization adds about 109 Tg N y^{-1} to the global N-cycle, and world demand continues to increase at a yearly rate of about 1.5% (FAO, 2019). Cultivated legumes, mainly soybeans, alfalfa, and pulses, have contributed an additional 50 – 70 Tg N y^{-1} through symbiotic bacteria called rhizobia that live in the root nodules of legumes (Galloway et al., 1995; Vitousek et al., 1997; Herridge et al, 2008). Another major N_r source to soil is fossil fuel combustion, which adds more than 20 Tg N y^{-1} through atmospheric nitrogen oxide reactions and/or wet or dry deposition (Delmas et al., 1997; Vitousek et al., 1997).

Gaseous N loss via denitrification is a major N_r loss pathway from terrestrial systems. Davidson and Kanter (2014) have synthesized several studies on N_2O emission inventories determined from direct field measurements ("bottom-up") and indirect modeled estimates ("top-down") and determined that current (2005 – 2010) global N_2O emissions are likely around 10 – 12 Tg N_2O-N y^{-1}. Natural terrestrial sources account for about 6.6 Tg N_2O-N y^{-1} of this range, and anthropogenic sources about 5.3 Tg N_2O-N y^{-1}, with agriculture contributing to about 56 – 81% of total anthropogenic emissions. Bouwman et al. (2013) estimated that between 1900 and 2000, N_2O emissions from soil increased from about 10 to 12 Tg N y^{-1}. Despite researchers' continuing efforts to close the global N_2O budget, major uncertainties still remain in present-day and preindustrial estimates of terrestrial N_2O emissions from both natural and anthropogenic sources (Stein and Yung, 2003; Bouwman et al., 2013; Davidson and Kanter, 2014; Tian et al., 2019).

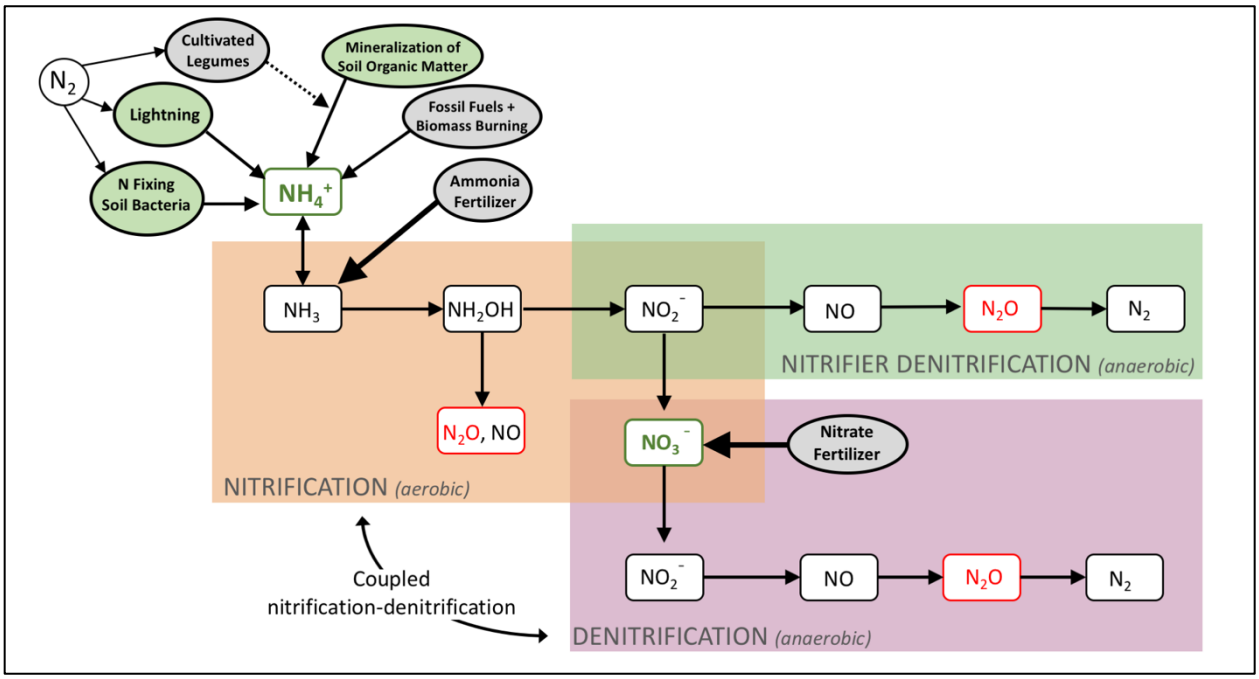

Figure 1.1. The main N_r inputs and loss pathways via N_2O emissions in terrestrial systems. The green bubbles signify natural N_r inputs to the terrestrial pool and the grey bubbles signify anthropogenic N_r inputs.

1.3.2 Mineralization

Mineralization is a two-step biological decomposition process where microbes and enzymes convert organic N in crop residues, dead animals, and nitrogenous animal waste into inorganic N (Robertson and Groffman, 2007; Figure 1.1). First, during aminization, bacteria break down the proteins of the organic N compounds into simple organic N compounds such as amides, amino sugars, and amino acids (Muruganandam et al., 2009). These organic N compounds are then further decomposed by ammonifying bacteria that release NH_3 from ammonification (Schimel and Bennett, 2004; Muruganandam et al., 2009). As NH_3 substrate availability for coupled nitrification-denitrification increases, N_2O production also increases (Figure 1.1).

1.3.3 Nitrification

Nitrification is an aerobic process carried out by autotrophic bacteria in the soil that convert porewater NH_4^+ or NH_3 into nitrite (NO_2^-) and then into NO_3^- (Perlman et al., 2013; Figure 1.1). The oxidation of NH_3 into NO_2^- is carried out by nitrosobacteria, and the oxidation of NO_2^- to NO_3^- is carried out by nitrobacteria (Pilegaard, 2013). N_2O and nitric oxide (NO) gases are released via the nitrification process from the decomposition of hydroxylamine (NH_2OH), a reactive intermediate following the oxidation of NH_3 (Cleemput and Samater, 1996). The intermediate NO_2^- can also decompose to produce NO and N_2O as by-products. Autotrophic nitrifiers also undergo nitrifier denitrification under anoxic conditions where NH_3 is oxidized to NO_2 then reduced to NO, N_2O, and finally N_2 (Poth and Focht, 1985; Wrage et al., 2001; Figure 1.1).

1.3.4 Denitrification

The reverse process, denitrification, is an anaerobic reduction of NO_3^- to N_2 carried out by heterotrophic bacteria (Perlman et al., 2013; Figure 1.1). In natural settings, denitrification is coupled to nitrification as denitrifying bacteria depend on it for the production of NO_3^- substrate. The reduction sequence does not always completely reduce to N_2, as some denitrifying bacteria can only partially denitrify NO_3^- (incomplete denitrifiers), forming other gaseous intermediates such as NO and N_2O (Stein and Klotz, 2016). Saturated soils with high organic carbon and NO_3^- and NO_2^- concentrations stimulate the reduction of NO to N_2O and almost completely inhibit the final reduction step to N_2, resulting in a higher N_2O to N_2 ratio (Blackmer and Bremner, 1978; Firestone et al., 1979; Gaskell et al., 1981; Baumgärtner and Conrad, 1992).

1.4 Influences of environmental and anthropogenic factors on nitrous oxide emissions

1.4.1 Environmental impacts

Soil-based N_2O emissions are correlated to changing environmental conditions and their effect on soil such as soil temperature and moisture, soil pH, and N substrate availability for nitrifying and denitrifying microbes (Clayton et al., 1994; Mosier et al., 2001; Galloway et al., 2003; Vitousek et al., 2008; Schlesinger et al., 2009; Jarvis et al., 2011; Henault et al., 2012).

Optimal soil temperature and moisture conditions are different for both nitrification and denitrification. Nitrification is at its optimum at a pH level between 6.6 – 8.5, a water-filled pore space (WFPS) below 60%, and soil temperature between ~ 25 – 35°C (Barnard et al., 2005; Pilegaard, 2013; Jalota et al., 2018). The oxidation process effectively stops at soil temperatures lower than 5°C and greater than 40°C (Jalota et al., 2018). Denitrification has an optimal pH between 7.0 – 7.5, a WFPS above 60%, and a similar optimal soil temperature to that of nitrification but is able to withstand higher temperatures (Barnard et al., 2005; Saleh-Lakha et al., 2009; Pilegaard, 2013). Low soil temperatures around 0°C have been observed to decrease denitrification rates but increase the denitrification gaseous $N_2O/(N_2O + N_2)$ end-product ratio (Holtan-Hartwig et al., 2002; Saleh-Lakha et al., 2009).

Slow-draining textured soils are more prone to saturation, resulting in high WFPS and thus higher denitrification rates (Cameron et al., 2013; Burger et al., 2016). Coarse-textured, fast-draining soils are not as prone to denitrification since rapidly draining soil pores allow for oxygen to re-enter the soil, creating a more favorable environment for nitrification. However, infiltration rates are generally higher in coarser soils, resulting in faster NO_3^- leaching through the soil profile, and thus a decrease in substrate availability for denitrification.

The dominant pathway of N_r loss from soil as gaseous N compounds is denitrification, which has been estimated to remove about 124 Tg N y^{-1} (35 – 40 %) of total N from terrestrial N_r (Seitzinger et al., 2006). Saturated soil conditions create anoxic environments driving denitrification in the presence of N substrate, catalyzing peak N_2O fluxes (Changsheng et al., 1992; Borken and Matzner, 2009). Event-based environmental drivers such as soil freeze-thaw and drying-rewetting events have shown to stimulate large increase in microbial reaction rates, causing hot moments and pulses (Birch, 1964; Kavdir et al., 2008; Wagner Riddle et al., 2017). Uncertainties still exist concerning the mechanisms that trigger N_2O emissions during these events.

Seasonal freeze-thaw events in cold winter regions can trigger enhanced soil N_2O emission rates over the non-growing season and can account for 30 – 90% of net annual N_2O emissions (Wagner-Riddle et al., 1997; 2007; Ludwig et al., 2004; Chen et al., 2018). Freeze-thaw induced N_2O pulses have often been attributed to the release of trapped N_2O produced under frozen surface soil layers (Bremner et al., 1980; Teepe et al., 2001) or from frozen soil layers or snowpack meltwater saturating the soil and driving denitrification (Wagner-Riddle et al., 1997; Risk et al., 2013).

Rewetting of dry soil can rapidly increase substrate availability for nitrifying bacteria as N and carbon (C) organic substrates in soil organic matter (SOM) are rapidly mineralized, resulting in increased soil respiration that returns to background levels after a few days and diminishes overall with each successive drying-rewetting cycle as the available SOM pool decreases (Birch, 1964; Borken and Matzner, 2009). This phenomenon is commonly referred to as the “Birch effect”. Several physicochemical and biological processes are at play during this process (Jarvis et al, 2007), including the release of organic N and C substrates through the

break-up of soil aggregates (Denef et al. 2001; Borken and Matzner, 2009) and from microorganisms killed during soil drying (Bottner, 1985), and the reactivation of soil microbes and increases in microbial populations in response to substrate and water availability (Griffiths and Birch 1961, Ludwig et al., 2001). Drying-rewetting cycles are responsible for a large portion of N_2O emissions during dry summer periods, however, they typically account for a much lower portion of annual N_2O emissions, sometimes less than 2% (Garcia-Montiel et al., 2003; Groffman et al., 2009; Congreves et al., 2018).

1.4.2 Anthropogenic impacts

Agricultural management practices such as N fertilization (timing, type, and placement), tillage, crop varieties, and irrigation influence the production, consumption, and transport of N_2O emissions (Halvorson et al., 2008; Perlman et al., 2013; Savage et al., 2014). Fertilization adds a surplus of N_r to the soil, increasing substrate availability for nitrification and denitrification processes and thereby N_2O production (Stein and Yung, 2003; Butterbach-Bahl and Dannenman, 2011). N_2O emissions typically increase in the first several days to weeks following fertilizer application with emissions scaling with the amount of fertilizer used (Clayton et al., 1994; Skiba et al., 2002; Drury et al., 2006; Liu et al., 2006; Halvorson et al., 2008; Kavdir et al., 2008; Millar et al., 2018). Timing, type, and placement of N fertilizers have significant effects on N_2O emissions, among other N losses, making fertilizer management a long-term and prominent area of research in agriculture. Examples of research topics include fertilizer placement location and depth (Schnier et al., 1990; Van Noordwijk and Scholten, 1994; Drury et al., 2006), improved application timing (Cole et al., 1997; Cassman et al., 1998; Kavdir et al., 2008), controlled-release fertilizers (Cole et al., 1997; Butterbach-Bahl and Dannenmann, 2011), and nitrification

inhibitors to improve fertilizer use efficiency and decrease N trace gas soil emissions (Cole et al., 1997; Akiyama et al., 2010).

Tillage effects on N_2O emissions are inconclusive (West and Post, 2002; Halvorson et al., 2008). Many studies found that N_2O emissions were greater from no-tillage (NT) systems compared to conventional tillage (CT) systems, explained by higher SOM in the top surface soil layers, resulting in increased substrate levels, soil density, and water content, creating optimal conditions for microbial activity and increasing microbial populations and diversity (Doran, 1980; Palma et al., 1997; Ball et al., 1999; Skiba et al., 2002; West and Post, 2002; Baggs et al. 2003; Gregorich et al., 2007; Rochette et al., 2008; Lognoul et al., 2017; Schmidt et al., 2018; Waldo et al, 2019). Alternatively, CT has been found to create less favorable surface soil temperatures for microbes due to breakup of surface soil layers, decreased microbial populations and diversity due to soil disturbance, increased soil aeration (decreased soil saturation favorable for denitrifiers), and increased nutrient export via runoff and erosion (Chatskikh and Olsen, 2007; Schmidt et al., 2018). Some studies found that emissions from CT soils were higher, explained by the incorporation of surface SOM deeper into the soil profile through turnover, increasing substrate availability for soil microbes at varying depths (Drury et al., 2006; Chatskikh and Olsen, 2007; Kavdir et al., 2008; Lehman et al., 2017). Kostyanovsky et al. (2019) studied N_2O emissions in four winter wheat cropping systems located in the inland Pacific Northwest that have both CT and NT treatments and found that CT treatments exhibited higher N_2O fluxes compared to NT following both soil rewetting and N fertilization events from three of the four sites. The site that exhibited higher N_2O emissions from NT versus CT was likely due to high levels of SOM in the NT plots.

Some studies also found no significant differences in N_2O emissions between NT and CT systems (Robertson et al. 2000; Jantalia et al., 2008; Hao et al., 2016; Behnke et al., 2018). Several researchers concluded that the impact of CT versus NT on N_2O emissions are site- and crop-specific and are often affected by the texture and physical properties of soil and their indirect influence on aeration and gas diffusion (Gregorich et al., 2005; Stöckle et al., 2012; Rochette, 2018; Petitjean et al., 2019).

Although there are still few studies examining the effect of crop rotations on GHG soil emissions, diversified crop rotations have been found to generally increase N_2O production (Halvorson et al., 2008; Lehman et al., 2017). The incorporation of grass species mixtures or cover crops into rotations improves soil health through increased residue, nutrient, and water retention (Huggins et al. 1998; Wilhelm et al., 2004; Hofstra and Bouwman, 2005). Legume-based cover crop mixtures also increase total soil N by fixing N symbiotically, enhancing soil nutrient availability for succeeding crops (Vitousek et al., 1997; Gage, 2006). Enhanced microbial abundance and diversity have also been correlated to cover cropping (Schmidt et al., 2018). High SOM levels typically result in increased mineralization rates and thus N_2O-producing microbial processes, however, sites with high SOM can also potentially offset global warming potential through the increased ability to sequester C in soil (Cole et al., 1997; West and Post, 2002).

1.5. Spatial and temporal variability of nitrous oxide soil emissions

Compared to GHGs that are usually emitted from soils in high concentrations, such as CO_2, N_2O soil emissions are difficult quantify due to their small magnitude and high spatiotemporal variability (Duxbury and Bouldin, 1982; Parkin, 1987, van Kessel et al., 1993).

The coefficient of variation for N_2O measurements is highly site-specific, however, authors have found the values to range between 80 to 425 % (Parkin et all., 1987; van Kessel et al., 1993; Palma et al., 1997; Gasche and Papen, 1999, Jones et al., 2011; Waldo et al., 2019). This variability is mainly due to denitrification processes, which exhibit highly irregular reaction rates as they are strongly influenced by environmental drivers and agricultural management practices (Jarvis et al., 1991; McClain et al., 2003; Groffman et al., 2009; Butterbach-Bahl and Dannenmann, 2011; Henault et al., 2012). High rates of soil N_2O emissions occur from discrete areas of enhanced N_2O emissions (hot spots) and over short periods of time (hot moments) that disproportionately increase cumulative field-scale N_2O emissions (McClain et al., 2003; Groffman et al., 2009; Bernhardt et al., 2017).

1.6. Measuring soil greenhouse gas emissions with flux chambers

For several decades, manual closed static chambers (CSCs) have been the most widely used method to measure soil GHG fluxes, including trace gas emissions such as N_2O and methane (CH_4) (Lundegårdh, 1927; Reiners, 1968; Pumpanen et al., 2004; Levy et al., 2011; de Klein and Harvey, 2015). About 95% of studies analyzing N_2O flux data have been obtained using manual CSCs, making them the main method used to define the global and national N_2O emission inventories from agricultural soils (de Klein and Harvey, 2015). Manual CSCs are labor-intensive as they need to be moved between soil sample locations and require repeated collection of syringe samples from the chamber headspace to be analyzed via gas chromatography (Smith and Dobbie, 2001; Levy et al., 2011). Although this method has the potential of capturing the spatial variability of soil N_2O emissions, it does not effectively capture the temporal variability.

Recently, automated CSCs have gained increased popularity for measuring GHG fluxes, which involves multiplexing an array of chambers to in-situ GHG analyzers that automatically and continuously sample soil GHG emissions. Automated CSCs are less laborious, can be left in the field relatively unattended for long-term periods of time, and they allow for accurate and repeatable GHG measurements from the same soil locations, capturing the dynamic nature of N_2O fluxes as well as diurnal and seasonal changes (Barton et al., 2008). The disadvantages of this method are that it is expensive, initial upfront set-up is time-intensive, spatial coverage is usually compromised, and access to line-power or generator power is typically required in rural settings.

With more automated CSCs appearing on the market, the need for a standardized chamber system and soil GHG sampling method is recognized by scientists (Rochette and Eriksen-Hamel, 2008; Pumpanen et al., 2004; Hall et al., 2014; Pavelka et al., 2018; Zhao et al., 2018). Due to the general lack of data interpretation, quality control, and reporting guidelines, biases are likely to occur, which inhibit inter-study comparisons (Rochette and Eriksen-Hamel, 2008; de Klein et al., 2015). By standardizing and optimizing the chamber system and sampling procedures, measurements would be more representative and repeatable (Hall et al., 2014).

1.7 References

Akiyama, H., Yan, X., & Yagi, K. (2010). Evaluation of effectiveness of enhanced-efficiency fertilizers as mitigation options for N2O and NO emissions from agricultural soils: Meta-analysis. *Global Change Biology*, *16*(6), 1837–1846. https://doi.org/10.1111/j.1365-2486.2009.02031.x

Baggs, E. M., Stevenson, M., Pihlatie, M., Regar, A., Cook, H., & Cadisch, G. (2003). Nitrous oxide emissions following application of residues and fertiliser under zero and conventional tillage. *Plant and Soil*, *254*(2), 361–370. https://doi.org/10.1023/A:1025593121839

Ball, B. C., Scott, A., & Parker, J. P. (1999). Adsorption Kinetics of CO2, O2, N2, and CH4 in Cation-Exchanged Clinoptilolite. *Soil and Tillage Research*, *53*, 1313–1319.

Barton, L., Kiese, R., Gatter, D., Butterbach-bahl, K., Buck, R., Hinz, C., & Murphy, D. V. (2008). Nitrous oxide emissions from a cropped soil in a semi-arid climate. *Global Change Biology*, *14*(1), 177–192. https://doi.org/10.1111/j.1365-2486.2007.01474.x

Baumgärtner, M., & Conrad, R. (1992). Role of nitrate and nitrite for production and consumption of nitric oxide during denitrification in soil. *FEMS Microbiology Letters*, *101*(1), 59–65. https://doi.org/10.1111/j.1574-6968.1992.tb05762.x

Behera, S. N., Sharma, M., Aneja, V. P., & Balasubramanian, R. (2013). Ammonia in the atmosphere: A review on emission sources, atmospheric chemistry and deposition on terrestrial bodies. *Environmental Science and Pollution Research*, *20*(11), 8092–8131. https://doi.org/10.1007/s11356-013-2051-9

Behnke, G. D., Zuber, S. M., Pittelkow, C. M., Nafziger, E. D., & Villamil, M. B. (2018). Long-term crop rotation and tillage effects on soil greenhouse gas emissions and crop production in Illinois, USA. *Agriculture, Ecosystems and Environment*, *261*, 62–70. https://doi.org/10.1016/j.agee.2018.03.007

Bernhardt, E. S., Blaszczak, J. R., Ficken, C. D., Fork, M. L., Kaiser, K. E., & Seybold, E. C. (2017). Control Points in Ecosystems: Moving Beyond the Hot Spot Hot Moment Concept. *Ecosystems*, *20*(4), 665–682. https://doi.org/10.1007/s10021-016-0103-y

Birch, H.F. (1964). Mineralisation of plant nitrogen following alternate wet and dry conditions. *Plant Soil*, *20*: 43-49. https://doi.org/10.1007/BF01378096

Blackmer, A.M. & Bremner, J.M. (1978). Inhibitory effect of nitrate on reduction of N2O to N2 by soil microorganisms. *Soil Biology and Biochemistry, 10*(3): 187-191. https://doi.org/10.1016/0038-0717(78)90095-0

Borken, W., & Matzner, E. (2009). Reappraisal of drying and wetting effects on C and N mineralization and fluxes in soils. *Global Change Biology*, *15*(4), 808–824. https://doi.org/10.1111/j.1365-2486.2008.01681.x

Bottner, P. (1985). Response of microbial biomass to alternate moist and dry conditions in a soil incubated with 14C and 15N labeled plant material. *Soil Biology and Biochemistry*, *17*: 329-337. https://doi.org/10.1016/0038-0717(93)90249-B

Bouwman, A. F., Beusen, A. H. W., Griffioen, J., Van Groenigen, J. W., Hefting, M. M., Oenema, O., … Stehfest, E. (2013). Global trends and uncertainties in terrestrial denitrification and N2O emissions. *Philosophical Transactions of the Royal Society B: Biological Sciences*, *368*(1621). https://doi.org/10.1098/rstb.2013.0112

Bremner, J. M., Robbins, S. G., & Blackmer, A. M. (1980). Seasonal variability in emission of nitrous oxide from soil. *Geophysical Research Letters*, *7*(9), 641–644. https://doi.org/https://doi.org/10.1029/GL007i009p00641

Butterbach-Bahl, K., & Dannenmann, M. (2011). Denitrification and associated soil N2O emissions due to agricultural activities in a changing climate. *Current Opinion in Environmental Sustainability*, *3*(5), 389–395. https://doi.org/10.1016/j.cosust.2011.08.004

Cassman, K. G., Peng, S., Olk, D. C., Ladha, J. K., Reichardt, W., Dobermann, A., & Singh, U. (1998). Opportunities for increased nitrogen-use efficiency from improved resource management in irrigated rice systems. *Field Crops Research*, *56*(1–2), 7–39. https://doi.org/10.1016/S0378-4290(97)00140-8

Changsheng, L., Frolking, S., & Frolking, T. A (1992). A model of nitrous oxide evolution from soil driven by rainfall events: Model structure and sensitivity. *Journal of Geophysical Research*, *97*(D9): 9759-9776. https://doi.org/10.1029/92JD00509

Chatskikh, D., & Olesen, J. E. (2007). Soil tillage enhanced CO2 and N2O emissions from loamy sand soil under spring barley. *Soil and Tillage Research*, *97*(1), 5–18. https://doi.org/10.1016/j.still.2007.08.004

Chen, Z., Yang, S. qi, Zhang, A. ping, Jing, X., Song, W. min, Mi, Z. rong, … Yang, Z. li. (2018). Nitrous oxide emissions following seasonal freeze-thaw events from arable soils in

Northeast China. *Journal of Integrative Agriculture*, *17*(1), 231–246. https://doi.org/10.1016/S2095-3119(17)61738-6

Cleveland, C. C., Townsend, A. R., Schimel, D. S., Fisher, H., Howarth, R. W., Hedin, L. O., … Wasson, M. F. (1999). Global patterns of terrestrial biological nitrogen (N2) fixation in natural ecosystems. *Global Biogeochemical Cycles*, *13*(2), 623–645. https://doi.org/10.1002/(ISSN)1944-9224

Cole, C. V., Duxbury, J., Freney, J., Heinemeyer, O., Minami, K., Mosier, A., … Zhao, Q. (1997). Global estimates of potential mitigation of greenhouse gas emissions by agriculture. *Nutrient Cycling in Agroecosystems*, *49*(1–3), 221–228. https://doi.org/10.1023/a:1009731711346

Coskun, D., Britto, D. T., Shi, W., & Kronzucker, H. J. (2017). Nitrogen transformations in modern agriculture and the role of biological nitrification inhibition. *Nature Plants*, *3*(June). https://doi.org/10.1038/nplants.2017.74

Crutzen, P. J. (1970). The influence of nitrogen oxides on the atmospheric ozone content. *Quarterly Journal of the Royal Meteorological Society*, *96*: 320–325. https://doi.org/10.1002/qj.49709640815

Davidson, E. A., & Kanter, D. (2014). Inventories and scenarios of nitrous oxide emissions. *Environmental Research Letters*, *9*(10). https://doi.org/10.1088/1748-9326/9/10/105012

De Klein, C. & Harvey, M. (2015). Nitrous Oxide Chamber Methodology Guidelines (version 1.1). Global Research Alliance of Agricultural Greenhouse Gases. Available at https://www.researchgate.net/profile/Mike_Harvey2/publication/236844607_Nitrous_Oxide_Chamber_Methodology_Guidelines/links/59b1c25fa6fdcc3f888e113c/Nitrous-Oxide-Chamber-Methodology-Guidelines.pdf

Delmas, R., Serça, D., & Jambert, C. (1997). Global inventory of NOx sources. *Nutrient Cycling in Agroecosystems*, *48*(1–2), 51–60. https://doi.org/10.1023/a:1009793806086

Denef, K., Six, J., Bossuyt, H., Frey, S. D., Elliott, E. T., Merckx, R., & Paustian, K. (2001). Influence of dry–wet cycles on the interrelationship between aggregate, particulate organic matter, and microbial community dynamics. *Soil Biology and Biochemistry*, *33*(2001), 1599–1611.

Doran, J.W. (1980). Soil microbial and biochemical changes associated with reduced tillage. *Soil Science Society of America*, *44*: 765–771. https://doi.org/10.2136/sssaj1980.03615995004400040022x

Drury, C. F., Reynolds, W. D., Tan, C. S., Welacky, T. W., Calder, W., & McLaughlin, N. B. (2006). Emissions of Nitrous Oxide and Carbon Dioxide. *Soil Science Society of America Journal*, *70*(2), 570–581. https://doi.org/10.2136/sssaj2005.0042

Duxbury, J. M., Bouldin, D. R., Terry, R. E., & Tate, R. L. (1982). Emissions of nitrous oxide from soils. *Nature*, *298*(5873), 462–464. https://doi.org/10.1038/298462a0

EPA (2020). *Inventory of U.S. Greenhouse Gas Emissions and Sinks: 1990–2018*.

FAO (2019). *World fertilizer trends and outlook to 2022*. Rome. Retrieved from: https://www.fao.org/3/ca6746en/CA6746EN.pdf?eloutlink=imf2fao

Firestone, M. K., Smith, M. S., Firestone, R. B., & Tiedje, J. M. (1979). The Influence of Nitrate, Nitrite, and Oxygen on the Composition of the Gaseous Products of Denitrification in Soil. *Soil Science Society of America Journal*, *43*(6), 1140–1144. https://doi.org/10.2136/sssaj1979.03615995004300060016x

Fowler, D., Coyle, M., Skiba, U., Sutton, M. A., Cape, J. N., Reis, S., … Voss, M. (2013). The global nitrogen cycle in the Twenty first century. *Philosophical Transactions of the Royal Society B: Biological Sciences*, *368*(1621). https://doi.org/10.1098/rstb.2013.0164

Gage, D. J. (2004). Infection and Invasion of Roots by Symbiotic, Nitrogen-Fixing Rhizobia during Nodulation of Temperate Legumes. *Microbiology and Molecular Biology Reviews: MMBR*, *68*(2), 280–300. https://doi.org/10.1128/MMBR.68.2.280

Galloway, J. N., Dentener, F. J., Capone, D. G., Boyer, E. W., Howarth, R. W., Seitzinger, S. P., … Vöosmarty, V. (2004). Nitrogen cycles: past, present, and future. *Biogeochemistry*, *70*, 153–226. Retrieved from https://doi.org/10.1007/s10533-004-0370-0

Galloway, J. N. (1998). The global nitrogen cycle: changes and consequences. *Environmental Pollution*, *102*(1), 15–24.

Galloway, J. N., Aber, J. D., Erisman, J. W., Seitzinger, S. P., Howrath, R., Cowling, E. B., & Cosby, B. J. (2003). The Nitrogen Cascade. *BioScience*, *53*(4), 341. https://doi.org/10.1641/0006-3568(2003)053[0341:tnc]2.0.co;2

Galloway, N., Schlesinger, W. H., Ii, H. L., Schnoor, L., & Tg, N. (1995). Nitrogen Fixation: Anthropogenic Enhancement - Environmental Response. *Global Biogeochemical Cycles*, *9*(2), 235–252.

Garcia-Montiel, D., Steudler, P.A., Piccolo, M., Neill, C., Melillo, J., and Cerri, G.C. (2003). Nitrogen oxide emissions following wetting of dry soils in forest and pastures in Rondônia, Brazil. *Biogeochemistry, 64*(3): 319-336. https://doi.org/10.1023/A:1024968802018

Gaskell, J. F., Blackmer, A. M., & Bremner, J. M. (1981). Comparison of Effects of Nitrate, Nitrite, and Nitric Oxide on Reduction of Nitrous Oxide to Dinitrogen by Soil Microorganisms. *Soil Science Society of America Journal*, *45*(6), 1124–1127. https://doi.org/10.2136/sssaj1981.03615995004500060022x

Gillam, K. M., Zebarth, B. J., & Burton, D. L. (2008). Nitrous oxide emissions from denitrification and the partitioning of gaseous losses as affected by nitrate and carbon addition and soil aeration. *Canadian Journal of Soil Science*, *88*(2), 133–143. https://doi.org/10.4141/CJSS06005

Gregorich, E. G., Rochette, P., St-Georges, P., McKim, U. F., & Chan, C. (2008). Tillage effects on N2O emission from soils under corn and soybeans in Eastern Canada. *Canadian Journal of Soil Science*, *88*(2), 153–161. https://doi.org/10.4141/CJSS06041

Groffman, P. M., Butterbach-Bahl, K., Fulweiler, R. W., Gold, A. J., Morse, J. L., Stander, E. K., … Vidon, P. (2009). Challenges to incorporating spatially and temporally explicit phenomena (hotspots and hot moments) in denitrification models. *Biogeochemistry*, *93*(1–2), 49–77. https://doi.org/10.1007/s10533-008-9277-5

Hall, M. K. D., Winter, A. J., & Rogers, G. S. (2014). Variations in the Diurnal Flux of Greenhouse Gases from Soil and Optimizing the Sampling Protocol for Closed Static Chambers. *Communications in Soil Science and Plant Analysis*, *45*(22). https://doi.org/10.1080/00103624.2014.956937

Halvorson, A. D., Grosso, S. J. Del, & Reule, C. A. (2008). Nitrogen, Tillage, and Crop Rotation Effects on Nitrous Oxide Emissions from Irrigated Cropping Systems. *Journal of Environmental Quality*, *37*, 1337–1344. https://doi.org/10.2134/jeq2007.0268

Halvorson, A. D., Del Grosso, S. J., & Reule, C. A. (2008). Nitrogen, Tillage, and Crop Rotation Effects on Nitrous Oxide Emissions from Irrigated Cropping Systems. *Journal of Environmental Quality*, *37*(4), 1337–1344. https://doi.org/10.2134/jeq2007.0268

Hao, Q., Jiang, C., Chai, X., Huang, Z., Fan, Z., Xie, D., & He, X. (2016). Drainage, no-tillage and crop rotation decreases annual cumulative emissions of methane and nitrous oxide from a rice field in Southwest China. *Agriculture, Ecosystems and Environment*, *233*, 270–281. https://doi.org/10.1016/j.agee.2016.09.026

Herridge, D. F., Peoples, M. B., & Boddey, R. M. (2008). Global inputs of biological nitrogen fixation in agricultural systems. *Plant and Soil*, *311*(1–2), 1–18. https://doi.org/10.1007/s11104-008-9668-3

Hofstra, N., & Bouwman, A. F. (2005). Denitrification in agricultural soils: Summarizing published data and estimating global annual rates. *Nutrient Cycling in Agroecosystems*, *72*(3), 267–278. https://doi.org/10.1007/s10705-005-3109-y

Huggins, D. R., Buyanovsky, G. A., Wagner, G. H., Brown, J. R., Darmody, R. G., Peck, T. R., … Bundy, L. G. (1998). Soil organic C in the tallgrass prairie-derived region of the corn belt: Effects of long-term crop management. *Soil and Tillage Research*, *47*(3–4), 219–234. https://doi.org/10.1016/S0167-1987(98)00108-1

IPCC (2007). In: Solomon, S., Qin, D., Manning, M., Chen, Z., Marquis, M., Averyt, K.B., Tignor, M., Miller, H.L. (Eds.), *Climate Change 2007: The Physical Science Basis. Contribution of Working Group I to the Fourth Assessment Report of the Intergovernmental Panel on Climate Change*. Cambridge, UK; New York, NY: Cambridge University Press..

IPCC (2013). *Climate Change 2013: The Physical Science Basis. Contribution of Working Group I to the Fifth Assessment Report of the Intergovernmental Panel on Climate Change* [Stocker, T.F., D. Qin, G.-K. Plattner, M. Tignor, S.K. Allen, J. Boschung, A. Nauels, Y. Xia, V. Bex and P.M. Midgley (eds.)]. Cambridge, United Kingdom and New York, NY, USA: Cambridge University Press.

Jalota, S.K., Vashisht, B.B., Sharma, S., & Kaur, S. (2018). *Understanding Climate Change Impacts on Crop Productivity and Water Balance*. Kelleher, L.S. (Ed.). London, UK: Elsevier.

Jansson, S.L. & Persson, J. (1982). Mineralization and immobilization of soil nitrogen. In F.J. Stevenson (Ed.), *Nitrogen in Agricultural Soils* (pp. 229–252). Madison, WI: Agronomy 22, ASA, CSSA, SSSA.

Jantalia, C. P., Dos Santos, H. P., Urquiaga, S., Boddey, R. M., & Alves, B. J. R. (2008). Fluxes of nitrous oxide from soil under different crop rotations and tillage systems in the South of Brazil. *Nutrient Cycling in Agroecosystems*, *82*(2), 161–173. https://doi.org/10.1007/s10705-008-9178-y

Jarvis, S.C., Barraclough, D., Williams, J., & Rook, A.J. (1991). Patterns of Denitrification Loss from Grazed Grassland: Effect of N Fertilizer Inputs at Different Sites. *Plant and Soil, 131*: 77-88. https://doi.org/10.1007/BF00010422

Jarvis, P., Rey, A., Petsikos, C., Wingate, L., Rayment, M., Pereira, J., … Valentini, R. (2007). Drying and wetting of Mediterranean soils stimulates decomposition and carbon dioxide emission: The "Birch effect." *Tree Physiology*, *27*(7), 929–940. https://doi.org/10.1093/treephys/27.7.929

Jones, S. K., Famulari, D., Di Marco, C. F., Nemitz, E., Skiba, U. M., Rees, R. M., & Sutton, M. A. (2011). Atmospheric Measurement Techniques Nitrous oxide emissions from managed grassland: a comparison of eddy covariance and static chamber measurements. *Atmos. Meas. Tech*, *4*, 2179–2194. https://doi.org/10.5194/amt-4-2179-2011

Ju, X. T., Xing, G. X., Chen, X. P., Zhang, S. L., Zhang, L. J., Liu, X. J., … Zhang, F. S. (2009). Reducing environmental risk by improving N management in intensive Chinese agricultural systems. *Proceedings of the National Academy of Sciences of the United States of America*, *106*(9), 3041–3046. https://doi.org/10.1073/pnas.0813417106

Kavdir, Y., Hellebrand, H. J., & Kern, J. (2008). Seasonal variations of nitrous oxide emission in relation to nitrogen fertilization and energy crop types in sandy soil. *Soil and Tillage Research*, *98*(2), 175–186. https://doi.org/10.1016/J.STILL.2007.11.002

Kostyanovsky, K. I., Huggins, D. R., Stockle, C. O., Waldo, S., & Lamb, B. (2018). Developing a flow through chamber system for automated measurements of soil N2O and CO2 emissions. *Measurement: Journal of the International Measurement Confederation*, *113*, 172–180. https://doi.org/10.1016/j.measurement.2017.05.040

Kostyanovsky, K. I., Huggins, D. R., Stockle, C. O., Morrow, J. G., & Madsen, I. J. (2019). Emissions of N2O and CO2 following short-term water and n fertilization events in wheat-based cropping systems. *Frontiers in Ecology and Evolution*, *7*, 1–10. https://doi.org/10.3389/fevo.2019.00063

Kroeze, C., Mosier, A., & Bouwman, L. (1999). Closing the global N20 budget: A retrospective analysis 1500 - 1994 the total N20 emissions increased from 11 Tg N yr. *Global Biogeochemical Cycles*, *13*(1), 1–8. Retrieved from https://doi.org/10.1029/1998GB900020

Lehman, R. M., Osborne, S. L., & Duke, S. E. (2017). Diversified No-Till Crop Rotation Reduces Nitrous Oxide Emissions, Increases Soybean Yields, and Promotes Soil Carbon Accrual. *Soil Science Society of America Journal*, *81*(1), 76–83. https://doi.org/10.2136/sssaj2016.01.0021

Liang, L. L., Campbell, D. I., Wall, A. M., & Schipper, L. A. (2018). Nitrous oxide fluxes determined by continuous eddy covariance measurements from intensively grazed pastures:

Temporal patterns and environmental controls. *Agriculture, Ecosystems and Environment*, *268*(July), 171–180. https://doi.org/10.1016/j.agee.2018.09.010

Liu, J., You, L., Amini, M., Obersteiner, M., Herrero, M., Zehnder, A. J. B., & Yang, H. (2010). A high-resolution assessment on global nitrogen flows in cropland. *Proceedings of the National Academy of Sciences of the United States of America*, *107*(17), 8035–8040. https://doi.org/10.1073/pnas.0913658107

Liu, S., Wang, F., Xue, K., Sun, B., Zhang, Y., He, Z., … Yang, Y. (2015). The interactive effects of soil transplant into colder regions and cropping on soil microbiology and biogeochemistry. *Environmental Microbiology*, *17*(3), 566–576. https://doi.org/10.1111/1462-2920.12398

Liu, X. J., Mosier, A. R., Halvorson, A. D., & Zhang, F. S. (2006). The impact of nitrogen placement and tillage on NO, N2O, CH4 and CO2 fluxes from a clay loam soil. *Plant and Soil*, *280*(1–2), 177–188. https://doi.org/10.1007/s11104-005-2950-8

Lognoul, M., Theodorakopoulos, N., Hiel, M. P., Regaert, D., Broux, F., Heinesch, B., … Aubinet, M. (2017). Impact of tillage on greenhouse gas emissions by an agricultural crop and dynamics of N2O fluxes: Insights from automated closed chamber measurements. *Soil and Tillage Research*, *167*, 80–89. https://doi.org/10.1016/j.still.2016.11.008

Ludwig, B., Wolf, I., & Teepe, R. (2004). Contribution of nitrification and denitrification to the emission of N2O in a freeze-thaw event in an agricultural soil. *Journal of Plant Nutrition and Soil Science*, *167*(6), 678–684. https://doi.org/10.1002/jpln.200421462

Lundegårdh, H. (1927). Carbon Dioxide Evolution of Soil and Crop Growth, *23*(6): 417-453.

McClain, M. E., Boyer, E. W., Dent, C. L., Gergel, S. E., Grimm, N. B., Groffman, P. M., … Pinay, G. (2003). Biogeochemical Hot Spots and Hot Moments at the Interface of Terrestrial and Aquatic Ecosystems. *Ecosystems*, *6*(4), 301–312. https://doi.org/10.1007/s10021-003-0161-9

Millar, N., Urrea, A., Kahmark, K., Shcherbak, I., Robertson, G. P., & Ortiz-Monasterio, I. (2018). Nitrous oxide (N2O) flux responds exponentially to nitrogen fertilizer in irrigated wheat in the Yaqui Valley, Mexico. *Agriculture, Ecosystems and Environment*, *261*(February), 125–132. https://doi.org/10.1016/j.agee.2018.04.003

Mosier, A. R. (2001). Exchange of Gaseous Nitrogen Compounds Between Terrestrial Systems and the Atmosphere. *Plant and Soil*, *228*, 17–27. https://doi.org/10.1016/B978-0-12-374347-3.00013-5

Mosier, A. R. (2002). Environmental challenges associated with needed increases in global nitrogen fixation. *Nutrient Cycling in Agroecosystems*, *63*(2–3), 101–116. https://doi.org/10.1023/A:1021101423341

Muruganandam, S., Israel, D. W., & Robarge, W. P. (2009). Activities of Nitrogen-Mineralization Enzymes Associated with Soil Aggregate Size Fractions of Three Tillage Systems. *Soil Science Society of America Journal*, *73*(3), 751–759. https://doi.org/10.2136/sssaj2008.0231

Oertel, C., Matschullat, J., Zurba, K., Zimmermann, F., & Erasmi, S. (2016). Greenhouse gas emissions from soils—A review. *Chemie Der Erde*, *76*(3), 327–352. https://doi.org/10.1016/j.chemer.2016.04.002

Ollivier, J., Töwe, S., Bannert, A., Hai, B., Kastl, E. M., Meyer, A., … Schloter, M. (2011). Nitrogen turnover in soil and global change. *FEMS Microbiology Ecology*, *78*(1), 3–16. https://doi.org/10.1111/j.1574-6941.2011.01165.x

Palma, R. M., Rímolo, M., Saubidet, M. I., & Conti, M. E. (1997). Influence of tillage system on denitrification in maize-cropped soils. *Biology and Fertility of Soils*, *25*(2), 142–146. https://doi.org/10.1007/s003740050294

Papen, H., & Butterbach-Bahl, K. (1999). A 3-year continuous record of nitrogen trace gas fluxes from untreated and limed soil of a N-saturated spruce and beech forest ecosystem in Germany. 2. NO and NO2 fluxes. *Journal of Geophysical Research Atmospheres*, *104*(15), 487–503.

Parkin, T. B. (1987). Soil Microsites as a Source of Denitrification Variability. *Soil Science Society of America Journal*, *51*(5), 1194–1199. https://doi.org/10.2136/sssaj1987.03615995005100050019x

Pavelka, M., Acosta, M., Kiese, R., Altimir, N., Brümmer, C., Crill, P., … Kutsch, W. (2018). Standardisation of chamber technique for CO2, N2O and CH4 fluxes measurements from terrestrial ecosystems. *International Agrophysics*, *32*(4), 569–587. https://doi.org/10.1515/intag-2017-0045

Petitjean, C., Le Gall, C., Pontet, C., Fujisaki, K., Garric, B., Horth, J.-C., … Perrin, A.-S. (2009). Soil N2O, CH4, and CO2 Fluxes in Forest, Grassland, and Tillage/No-Tillage Croplands in French Guiana (Amazonia). *Soil Systems*, *33*(3), 617–623. https://doi.org/10.3773/j.issn.1005-264x.2009.03.021

Pilegaard, K. (2013). Processes regulating nitric oxide emissions from soils. *Philosophical Transactions of the Royal Society B: Biological Sciences*, *368*(1621). https://doi.org/10.1098/rstb.2013.0126

Poth, M., & Focht, D. D. (1985). 15N Kinetic Analysis of N2O Production by Nitrosomonas europaea: an Examination of Nitrifier Denitrification. *Applied and Environmental Microbiology*, *49*: 1134-1141. https://doi.org/10.1128/AEM.49.5.1134-1141

Pumpanen, J., Kolari, P., Ilvesniemi, H., Minkkinen, K., Vesala, T., Niinistö, S., … Hari, P. (2004). Comparison of different chamber techniques for measuring soil CO 2 efflux. *Agricultural and Forest Meteorology*, *123*(3–4), 159–176. https://doi.org/10.1016/j.agrformet.2003.12.001

Ravishankara, A. R., Daniel, J. S., & Portmann, R. W. (2009). Nitrous oxide (N2O): The dominant ozone-depleting substance emitted in the 21st century. *Science*, *326*(5949), 123–125. https://doi.org/10.1126/science.1176985

Reiners, W.A. (1968). Carbon Dioxide Evolution from the Floor of Three Minnesota Forests. *Ecology, 49*: 471–483. https://doi.org/10.2307/1934114

Risk, N., Snider, D., & Wagner-Riddle, C. (2013). Mechanisms leading to enhanced soil nitrous oxide fluxes induced by freeze-thaw cycles. *Canadian Journal of Soil Science*, *93*(4), 401–414. https://doi.org/10.4141/CJSS2012-071

Robertson, G. P., Paul, E. A., & Harwood, R. R. (2000). Greenhouse gases in intensive agriculture: Contributions of individual gases to the radiative forcing of the atmosphere. *Science*, *289*(5486), 1922–1925. https://doi.org/10.1126/science.289.5486.1922

Robertson, G. P., & Groffman, P. M. (2006). *Nitrogen transformations*. *Soil Microbiology, Ecology and Biochemistry: Third Edition* (4th ed.). Elsevier Inc. https://doi.org/10.1016/b978-0-12-415955-6.00014-1

Rochette, P., & Eriksen-Hamel, N. S. (2008). Chamber Measurements of Soil Nitrous Oxide Flux: Are Absolute Values Reliable? *Soil Science Society of America Journal*, *72*(2), 331–342. https://doi.org/10.2136/sssaj2007.0215

Rochette, P., Liang, C., Pelster, D., Bergeron, O., Lemke, R., Kroebel, R., … Flemming, C. (2018). Soil nitrous oxide emissions from agricultural soils in Canada: Exploring relationships with soil, crop and climatic variables. *Agriculture, Ecosystems and Environment*, *254*(August 2017), 69–81. https://doi.org/10.1016/j.agee.2017.10.021

Saleh-Lakha, S., Shannon, K. E., Henderson, S. L., Goyer, C., Trevors, J. T., Zebarth, B. J., & Burton, D. L. (2009). Effect of pH and temperature on denitrification gene expression and activity in Pseudomonas mandelii. *Applied and Environmental Microbiology*, *75*(12), 3903–3911. https://doi.org/10.1128/AEM.00080-09

Savage, K., Phillips, R., & Davidson, E. (2014). High temporal frequency measurements of greenhouse gas emissions from soils. *Biogeosciences*, *11*(10), 2709–2720. https://doi.org/10.5194/bg-11-2709-2014

Schimel, J. P., & Bennett, J. (2004). Nitrogen Mineralization: Challenges of a Changing Paradigm. *Ecology*, *85*(3), 591–602. Retrieved from https://doi.org/10.1890/03-8002

Schnier, H.F., Dingkuhn, M., De Datta, S.K., Marquesses, E.P., & Faronilo, J.E. (1990). Nitrogen-15 balance in transplanted and direct-seeded flooded rice as affected by different methods of urea application. *Biology and Fertility of Soils*, 10: 89-96. https://doi.org/10.1007/BF00336242

Schlesinger, W. H. (2009). On the fate of anthropogenic nitrogen. *Proceedings of the National Academy of Sciences of the United States of America*, *106*(1), 203–208. https://doi.org/10.1073/pnas.0810193105

Schmidt, R., Gravuer, K., Bossange, A. V., Mitchell, J., & Scow, K. (2018). Long-term use of cover crops and no-till shift soil microbial community life strategies in agricultural soil. *PLoS ONE*, *13*(2), 1–19. https://doi.org/10.1371/journal.pone.0192953

Seitzinger, S., Harrison, J. A., Böhlke, J. K., Bouwman, A. F., Lowrance, R., Peterson, B., … Drecht, G. Van. (2006). Denitrification across landscapes and waterscapes: a synthesis. *Ecological Applications*, *16*(6), 2064–2090.

Skiba, U., van Dijk, S., & Ball, B. C. (2002). The influence of tillage on NO and N2O fluxes under spring and winter barley. *Soil Use and Management*, *18*(4), 340–345. https://doi.org/10.1079/sum2002141

Smil, V. (1999). Nitrogen in crop production: An account of global flows adds. *Global Biogeochemical Cycles*, *13*(2), 647–662.

Smith, P., Martino, D., Cai, Z., Gwary, D., Janzen, H., Kumar, P., McCarl, B., Ogle, S., O'Mara, F., Rice, C., Scholes, B., & Sirotenko, O. (2007). *Agriculture. In Climate Change 2007: Mitigation. Contribution of Working Group III to the Fourth Assessment Report of the Intergovernmental Panel on Climate Change*. B. Metz, O.R. Davidson, P.R. Bosch, R.

Dave, L.A. Meyer (Eds.). Cambridge, United Kingdom and New York, NY, USA: Cambridge University Press.

Smith, P., House, J. I., Bustamante, M., Sobocká, J., Harper, R., Pan, G., … Pugh, T. A. M. (2016). Global change pressures on soils from land use and management. *Global Change Biology*, *22*(3), 1008–1028. https://doi.org/10.1111/gcb.13068

Stedman, D.H. & Shetter, R.E. (1983). *The global budget of atmospheric nitrogen species*. S.E. Schwartz (Ed.), Trace Atmospheric Constituents: Properties, Transformations and Fates. pp. 411-454. New York, NY: Wiley.

Stein, L. Y., & Klotz, M. G. (2016). The nitrogen cycle. *Current Biology*, *26*(3), R94–R98. https://doi.org/10.1016/j.cub.2015.12.021

Stein, L. Y., & Yung, Y. L. (2003). Production, Isotopic Composition, and Atmospheric Fate of Biologically Produced Nitrous Oxide. *Annual Review of Earth and Planetary Sciences*, *31*(1), 329–356. https://doi.org/10.1146/annurev.earth.31.110502.080901

Stöckle, C., Higgins, S., Kemanian, A., Nelson, R., Huggins, D., Marcos, J., & Collins, H. (2012). Carbon storage and nitrous oxide emissions of cropping systems in eastern Washington: A simulation study. *Journal of Soil and Water Conservation*, *67*(5), 365–377. https://doi.org/10.2489/jswc.67.5.365

Sun, R., Guo, X., Wang, D., & Chu, H. (2015). Effects of long-term application of chemical and organic fertilizers on the abundance of microbial communities involved in the nitrogen cycle. *Applied Soil Ecology*, *95*, 171–178. https://doi.org/10.1016/j.apsoil.2015.06.010

Teepe, R., Brumme, R., & Beese, F. (2001). Nitrous oxide emissions from soil during freezing and thawing periods. *Soil Biology and Biochemistry*, *33*(9), 1269–1275. https://doi.org/10.1016/S0038-0717(01)00084-0

Tian, H., Yang, J., Xu, R., Lu, C., Canadell, J. G., Davidson, E. A., … Zhang, B. (2019). Global soil nitrous oxide emissions since the preindustrial era estimated by an ensemble of terrestrial biosphere models: Magnitude, attribution, and uncertainty. *Global Change Biology*, *25*(2), 640–659. https://doi.org/10.1111/gcb.14514

United States Environmental Protection Agency (2020). *Inventory of U.S. Greenhouse Gas Emissions and Sinks: 1990–2018*. Available at https://www.epa.gov/ghgemissions/inventory-us-greenhouse-gas-emissions-and-sinks-1990-2016

Van Cleemput, O. & Samater, A. H. (1996). Nitrite in soils: accumulation and role in the formation of gaseous N compounds. *Fertilizer Research*, *45*: 81–89. https://doi.org/10.1007/BF00749884

van Kessel, C., Pennock, D. J., & Farrell, R. E. (1993). Seasonal Variations in Denitrification and Nitrous Oxide Evolution at the Landscape Scale. *Soil Science Society of America Journal*, *57*(4), 988–995. https://doi.org/10.2136/sssaj1993.03615995005700040018x

Van Noordwijk, M. & Scholten, J.H.M. (1994). Effects of fertilizer price on feasibility of efficiency improvement: case study for an urea injector for lowland rice. *Fertilizer Research*. *39*: 1-9. https://doi.org/10.1007/BF00750151

Veraart, A. J., de Klein, J. J. M., & Scheffer, M. (2011). Warming can boost denitrification disproportionately due to altered oxygen dynamics. *PLoS ONE*, *6*(3), 2–7. https://doi.org/10.1371/journal.pone.0018508

Vitousek, P. M., Mooney, H. A., Lubchenco, J., & Melillo, J. M. (1997). Human domination of Earth's ecosystems. *Urban Ecology: An International Perspective on the Interaction Between Humans and Nature*, *277*(July), 3–13. https://doi.org/10.1007/978-0-387-73412-5_1

Wagner-Riddle, C., Thurtell, G. W., Kidd, G. K., Beauchamp, E. G., & Sweetman, R. (1997). Estimates of nitrous oxide emissions from agricultural fields over 28 months. *Canadian Journal of Soil Science*, *77*(2), 135–144. https://doi.org/10.4141/S96-103

Wagner-Riddle, C., Congreves, K. A., Abalos, D., Berg, A. A., Brown, S. E., Ambadan, J. T., … Tenuta, M. (2017). Globally important nitrous oxide emissions from croplands induced by freeze-thaw cycles. *Nature Geoscience*, *10*(4), 279–283. https://doi.org/10.1038/ngeo2907

Wagner-Riddle, C., Furon, A., Mclaughlin, N. L., Lee, I., Barbeau, J., Jayasundara, S., … Warland, J. (2007). Intensive measurement of nitrous oxide emissions from a corn-soybean-wheat rotation under two contrasting management systems over 5 years. *Global Change Biology*, *13*(8), 1722–1736. https://doi.org/10.1111/j.1365-2486.2007.01388.x

Waldo, S. (2016). Using micrometerorological methods and modeling to determine greenhouse gas budgets over agricultural systems in the inland Pacific Northwest. Washington State University PhD Dissertation.

Waldo, S., Russell, E. S., Kostyanovsky, K., Pressley, S. N., O'Keeffe, P. T., Huggins, D. R., … Lamb, B. K. (2019). N2O Emissions From Two Agroecosystems: High Spatial Variability and Long Pulses Observed Using Static Chambers and the Flux-Gradient Technique.

Journal of Geophysical Research: Biogeosciences, *124*(7), 1887–1904. https://doi.org/10.1029/2019JG005032

Wang, C., Wang, N., Zhu, J., Liu, Y., Xu, X., Niu, S., … He, N. (2018). Soil gross N ammonification and nitrification from tropical to temperate forests in eastern China. *Functional Ecology*, *32*(1), 83–94. https://doi.org/10.1111/1365-2435.13024

West, T. O., & Post, W. M. (2002). Soil Organic Carbon Sequestration Rates by Tillage and Crop Rotation. *Soil Science Society of America Journal*, *66*(6), 1930–1946. https://doi.org/10.2136/sssaj2002.1930

Wilhelm, W. W., Johnson, J. M. F., Hatfield, J. L., Voorhees, W. B., & Linden, D. R. (2004). Crop and Soil Productivity Response to Corn Residue Removal: A Literature Review. *Agronomy Journal*, *96*(1), 1–17. https://doi.org/10.2134/agronj2004.0001

Wrage N., Velthof, G.L., van Beusichem, M.L., & Oenema, O. (2001). Role of nitrifier dentification in the production of nitrous oxide. *Soil Biology and Biochemistry*, *33*: 1723–732. http://doi.org/10.1016/S0038-0717(01)00096-7

Zhao, P., Hammerle, A., Zeeman, M., & Wohlfahrt, G. (2018). On the calculation of daytime CO2 fluxes measured by automated closed transparent chambers. *Agricultural and Forest Meteorology*, *263*(August), 267–275. https://doi.org/10.1016/j.agrformet.2018.08.022

Zhu, X., Burger, M., Doane, T. A., & Horwath, W. R. (2013). Ammonia oxidation pathways and nitrifier denitrification are significant sources of N2O and NO under low oxygen availability. *Proceedings of the National Academy of Sciences of the United States of America*, *110*(16), 6328–6333. https://doi.org/10.1073/pnas.1219993110

CHAPTER TWO:

MEASURING SOIL GREENHOUSE GAS FLUXES IN AN AGRICULTURAL FIELD USING A LONG-TERM AUTOMATED FLUX CHAMBER SYSTEM

2.1 Introduction

Manual closed static chambers (CSCs) are a widely used method to quantify greenhouse gas (GHG) emissions between the soil surface and the atmosphere, especially trace gases like nitrous oxide (N_2O) and methane (CH_4) (Lundegårdh, 1927; Livingston and Hutchinson, 1995; Kutzbach et al., 2007; Pumpanen et al., 2010). This method involves sealing a closed chamber over a known area of soil for a period of time and allowing the soil gases to accumulate in the chamber's headspace. Traditionally, the gas has been sampled at regular intervals with a syringe and subsequently analyzed in the lab via gas chromatography (Davidson et al., 2008; Peterson et al., 2012). The flux is calculated as the rate of change of gas concentration per unit time, per surface area of soil (Davidson et al., 2008; Levy et al., 2011).

Manual CSCs are inexpensive and easy to transport, making it possible to achieve a high spatial resolution, however, this method is labor-intensive and time-consuming, resulting in reduced sampling intervals and low temporal resolution (Smith and Dobbie, 2001; Forbrich et al., 2010, Görres et al., 2016). Automated CSCs are a well-suited option for achieving high temporal resolution for soil trace gas measurements because they provide continuous high-frequency measurements, making them more effective in capturing the variability and episodic dynamics associated with soil biogeochemical cycling (Savage and Davidson, 2003; Görres et al., 2016; Petrakis et al., 2017).

There are currently many solutions available for conducting long-term automated soil carbon dioxide (CO_2) flux measurements (Livingston and Hutchinson, 1995; Pumpanen et al.,

2004; Kutzbach et al., 2007; Görres et al., 2016), with the most popular being the standardized eddy covariance method (Pavelka et al., 2018). Technological advancements in spectroscopic analyzers have only recently enabled the development of high-frequency and high-precision N_2O analyzers that are portable and rugged enough for field deployment (Fassbinder et al., 2013; Savage et al., 2014; Görres et al., 2016; Lebegue et al., 2016). Although chambers are the most popular method for measuring N_2O soil fluxes, there are few studies using N_2O analyzers in the field as they are expensive and require housing in a controlled environment due to their limited operating ranges (Denmead, 2008; Görres et al., 2016; Kostyanovsky et al., 2017; Pavelka et al., 2018; Waldo et al., 2019).

Manual CSC sampling methods are standardized by the GRACENet protocol (Parkin and Venterea, 2010), however, there is currently no standardization of sampling protocols for soil-based trace gas flux measurements using automated CSC. Simple first-order polynomial linear regression has been widely used among researchers to calculate GHG emissions from soils using manual CSCs due to its simplicity (Livingston et al., 2006; Hendriks et al., 2007, 2010). Many studies have demonstrated that using linear models with inherently nonlinear data can lead to inaccuracy and underestimation of fluxes because it assumes that the rate of concentration change is constant (Hutchinson and Mosier, 1981; Healy et al., 1996; Livingston et al., 2006; Kutzbach et al., 2007; Kroon et al., 2008; Forbrich et al., 2010; Levy et al., 2011; Silva et al., 2015; Kandel et al., 2016). Following Fick's law, a decrease in the concentration gradient between the soil-to-chamber air over time will result in a nonlinear increase in chamber gas concentration, making a nonlinear (exponential) regression model analysis more appropriate (Davidson et al., 2002; Livingston et al., 2006; Kutzbach et al., 2007; Hüppi et al., 2018). Recently, the development of nonlinear models for calculating flux from change in chamber

concentration data are becoming more popular (Livingston et al., 2006; Kroon et al., 2008, Levy et al., 2011).

A lack of standardization for automated CSC sampling methods and data analysis has also resulted in inconsistencies in the literature regarding quality assurance (QA) and quality control (QC) considerations for system performance and flux data validation (Rochette and Ericksen-Hamel, 2008; Pavelka et al., 2018; Zhao et al., 2018). In particular, there are inconsistencies in determining goodness-of-fit of nonlinear, or exponential, models to soil GHG concentration curves measured by automated CSCs. Several authors use the coefficient of determination (R^2) as a QC indicator to determine how well their nonlinear model fits the measured concentration curves (Forbrich et al., 2010, Petrakis et al., 2017, 2018; Courtois et al, 2019), however, this is an invalid goodness-of-fit statistic for nonlinear curves since R^2 is based on the assumption of fitting data with a linear model. R^2 is calculated as the explained sum of squares of the regression model (SSE) divided by the total sum of squares (SST), where SST is the SSE plus the residual sum of squares (SSR). R^2 will always be between 0 – 100 % for linear models, but for nonlinear models, the SST is not equal to the SSE plus the SSR, invalidating R^2 as it will no longer be between 0 – 100 %. This can result in a high R^2 values for both well and poorly fitted models, and thereby leading to false conclusions on model fit evaluation (Spiess and Neumeyer, 2010). Spiess and Neumeyer (2010) believe that authors and reviewers continue to use this statistical evaluation method incorrectly because almost all statistical software calculates R^2 for nonlinear models.

For this study, a robust automated soil respiration system was constructed to continuously and simultaneously monitor high-frequency CO_2 and N_2O soil emissions from an agricultural field over multiple growing seasons. To achieve this, two independent Li-Cor Automated Soil

CO_2 Flux Systems (LI-8100A, Li-Cor Biosciences, Lincoln, NE, USA) were integrated in-line with laser spectroscopic Los Gatos Research (LGR) N_2O analyzers (Los Gatos Research Inc, Mountain View, CA) and housed in on-site trailers with line-power. The plumbing of the analytical instrumentation was done per Li-Cor guidelines (Li-Cor Biosciences, 2019) and the configuration of the instrument housing trailers was adapted from previous work of Kostyanovsky et al. (2018) and Waldo et al. (2019).

This chapter describes the effectiveness of the chamber system and analytical instruments to capture the spatial and temporal variability of soil respiration throughout various seasons and environmental conditions. The first part of this analysis consisted of evaluating the flux dataset derived from automated CSC system by developing and processing the data through an optimized QC protocol. And secondly, the importance of choosing the right regression type for modeling gas flux estimates from CSCs is presented.

2.2 Materials and Methods

2.2.1 Field site

This study was conducted in an agricultural field at the Palouse Conservation Field Station (PCFS, 46°44′ N, 117°8′ W, 762 m above mean sea level), in Pullman, Washington. Two on-site line-powered trailers (Trailer 1 and Trailer 2) house analytical instrumentation that operate an array of chambers measuring the soil-based GHG emissions from the microplots. Continuous chamber measurements occurred between 15 May 2019 and 23 August 2019 during a cover crop (CC) system, and between 16 October 2019 and 29 February 2020 during a winter wheat (WW) system. A schematic and photographs of the experimental setup are shown in

Figure 2.1. The technical specifications of the analytical instruments and chamber system are displayed in Table 2.1.

2.2.2 Experimental design

2.2.2.1 Continuous gas analyzers and housing trailers

Two independent instrument setups each include eight long-term automated flux chambers (LI8100-104, LI-COR Biosciences, Lincoln, NE) connected to a multiplexer (LI-8150, LI-COR Biosciences, Lincoln, NE). The multiplexer cycles through each chamber and sampled air from the chamber headspace is analyzed (1 Hz frequency) for CO_2 and H_2O (LI-8100A, LI-COR Biosciences, Lincoln, NE), and for N_2O using a laser spectroscopic Los Gatos Research (LGR) N_2O analyzer (Los Gatos Research Inc.) connected in parallel (Figure 2.1). Average flow rate through the LI-8100A was approximately 2 L min^{-1}, and 0.25 L min^{-1} through the LGR. The air sample was then directed back to the chamber for a continuous flow-through chamber system set-up. Chambers 1 – 8 are connected to Trailer 1 and were installed on 8 full microplots. Chambers 9 – 16 were connected to Trailer 2 during the CC study and were installed on four full microplots and four half-microplots (Figure 2.1b). Four additional chambers were added during the WW study to the remaining four half-microplots, chambers 17 – 20. The data from these four additional chambers are not included in this work. The LGR in Trailer 1 (LGR_1) used during the CC study failed on 23 August 2019 and was replaced with an enhanced precision LGR (LGR_{EP}) prior to commencing the WW study. Trailer 2 has an isotopic LGR (LGR_{ISO}), measuring N_2O as well as $\delta^{15}N$ and $\delta^{17}O$. The trailers are connected to AC power for near-continuous year-round operation. A heating and cooling system inside the trailers ensures that the ambient air remains within the instruments' required operating ranges. Since the LGRs are sensitive to abrupt power

shut-off, an uninterruptible power source (UPS) was installed in case of power surges or blackouts.

The set-up in Trailer 2 was different than Trailer 1 in that a multiport unit (MIU) was connected between the LI-8100A and LGR_{ISO} with Tygon® tubing. The MIU allows for the addition of reference gas to be sampled and analyzed by the LGR_{ISO} for calibration purposes, necessary for isotopic analysis. This level of calibration precision was necessary for isotopic analysis of N_2O emissions from microplots that had ^{15}N-labelled fertilizer applied to them.

2.2.2.2 Automated chamber flux system

Sixteen 1.14 x 0.61 m microplots were arranged on a 4.6 x 2.7 m study plot (Figure 2.1b). Four of the microplots were divided into half-microplots (0.57 x 0.61 m), for a total of 12 "full microplots" and 8 "half-microplots". Soil emissions were measured using automated CSCs at each of the 16 microplots. Four different crop and fertilizer treatments were applied to the microplots during the CC study, and all microplots had the same seeding and fertilizer treatment applied during the WW study. More details about the microplots treatments can be found in Chapter 3.

A PVC soil collar was inserted into the soil to provide a stable supporting foundation for the chamber baseplates and an interface between the soil surface and baseplates. Collars were inserted between the crop rows during the CC system several months prior to commencing flux measurements and remained in-place during seeding and fertilization of the WW system. During a flux measurement, the chamber lid closes down onto the baseplate surrounding the collar forming an airtight seal, leaving the collar undisturbed. The collars also minimize lateral

diffusion of GHGs in the soil column below the chamber (Healy et al., 1996; Hutchinson and Livingston, 2001).

Chambers were connected to the multiplexer with 15 m long Bev-a-line® tubing and powered via an electronic cable. The multiplexer is programmed to cycle through each chamber one-by-one for a pre-programmed measurement period, and a pre- and post- purge period where ambient air is sampled to flush the tubing and restore the system to ambient N_2O levels. It takes three hours to cycle through each of the eight chambers once, including reference gas sampling (Trailer 2 only). For Trailer 1 during both the CC and WW studies, and Trailer 2 during just the CC study, the chamber measurement period was 12 minutes and the pre- and post- purge periods were 5 minutes each.

In Trailer 2 during the CC study, two 10 L Restek polypropylene multi-layer bags containing a 1 ppm and a 2 ppm N_2O gas standard were sampled by the LGR_{ISO} for two minutes each during the five-minute post-purge period of the last chamber of the cycle (chamber 12). During the WW system, four extra chambers were added to Trailer 2, and 1 ppm, 500 ppb, and N_2O-free reference gases in Restek bags, and ambient air from inside the trailer, were analyzed for two minutes each after the post-purge period of the last chamber of the cycle (chamber 20). The purpose of introducing the ambient air sampling was to restore the system to ambient N_2O levels after sampling N_2O concentrations at elevated levels. In order for the chamber and reference gas sampling sequence to fit into the 3-hour cycle, the measurement period was adjusted to 11 minutes and the pre- and post-purge timing was adjusted to 1.6 minutes each.

With the complete chamber sampling sequence for each trailer during both systems repeating every 3 hours, approximately 128 chamber measurements were completed each day from both trailers during the CC system (16 total chambers) and 160 during the WW system (20

total chambers), of which only 128 chamber measurements per day were used study since data from chamber 17 – 20 were not used in this study.

2.2.2.3 Additional instrumentation

Soil temperature and volumetric water content were monitored at each microplot in the top 0 – 10 cm using 5-TM (METER Group, Inc., Pullman, WA) sensors that were installed vertically into the soil surface. All probes were connected to EM50 dataloggers (METER Group, Inc.) and data were averaged and recorded in 5-minute intervals. Precipitation measurements were recorded using a TRP-525I tipping bucket rain gauge with a 15 cm wide collector (Texas Electronics Inc., Dallas, TX) located approximately 1 km east of the study site and the data were recorded in 30-minute intervals. All data were converted to Pacific Standard Time (PST) prior to analysis. Data were collected from the analyzers and 5-TM sensors weekly.

A WiFi router was installed inside Trailer 1 to provide internet access to the LI-8100A and LGR computers and to help diminish time-drift with automatic synchronization of instrument clocks. Remote access allowed us to monitor the system health and data quality in real-time and address any potential issues expediently.

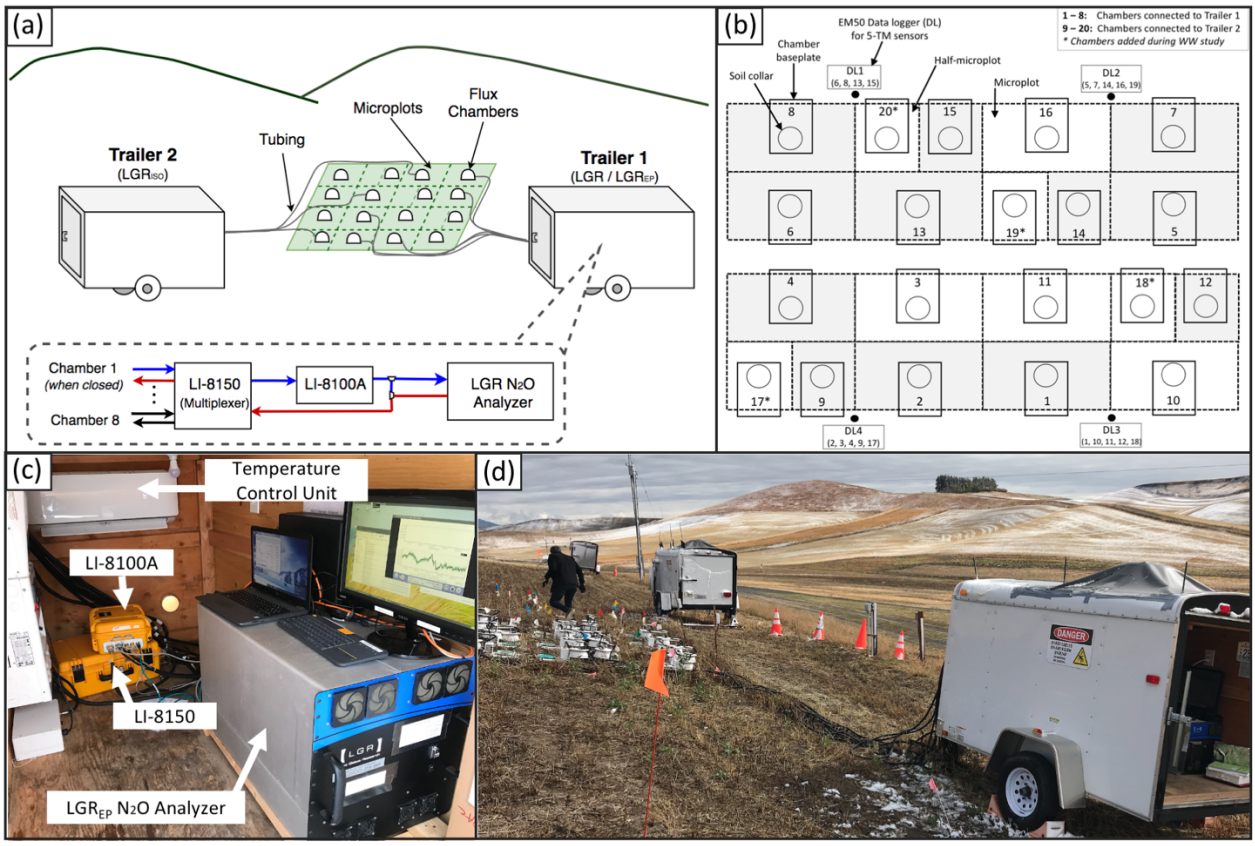

Figure 2.1. **(a)** Schematic of the microplots, flux chambers, trailers and analytical instrumentation setup at the study site (diagram is not to scale). **(b)** Layout of microplots, soil collars, chamber baseplates, and EM50 dataloggers on the study site. **(c)** Picture of instrumentation inside Trailer 1. **(d)** Picture of the chamber setup at the study site.

Table 2.1. Technical Specifications of the instrumentation at the study site.

Instrumentation	Specifications	
Long-Term Automated Flux Chambers	Model Name / Manufacturer	LI8100-104 / LI-COR Biosciences, Lincoln, NE
	Dimensions	48.3 cm L x 38.1 cm W x 33.0 cm H (20 cm collar opening)
	Headspace Volume	4076 cm^3
	Material	White coated stainless steel, black rubber soil collar gasket (seal)
	Operating Range (thermistor)	-20 – 45°C
	Accuracy (thermistor)	± 0.5°C over 0 – 70°C
	Power Requirement	Powered by LI-8150
PVC Soil Collars	Dimensions	21.34 cm (O.D.), 20 cm (I.D.), 12 cm H
	Enclosed Soil Area	317.8 cm^3
	Insertion Depth / Offset	~ 9 cm / ~ 3 cm
	Material	Thick-walled 8" SDR 35 PVC Sewer Pipe
Tubing	Model Name / Manufacturer	Bev-a-Line® Tubing / LI-COR Biosciences, Lincoln, NE
	Dimensions	3.2 mm (I.D.), 15 mL
	Material	Bev-a-Line®
Analyzer Control Unit & Infrared Gas Analyzer (IRGA)	Model Name / Manufacturer	LI-8100A / LI-COR Biosciences, Lincoln, NE
	Trace Gases Analyzed	CO_2, H_2O
	Dimensions	29 cm L x 38.1 cm W x 16.5 H cm
	Internal Cavity Volume	19 cm^3
	Operating Range	-20 – 45 °C, non-condensing (0 – 95% RH)
	Power Requirement	10.5 – 28 VDC (LI-8150 powers LI-8100A)
	Measurement Range (Pressure Sensor)	15 – 115 kPa
	Accuracy (Pressure Sensor)	1.5% over 0 – 85°C
	Measurement Range (CO_2 / H_2O reading)	0 – 20,000 ppm (CO_2) / 0 – 60 mmol/mol (H_2O)
	Accuracy (CO_2 & H_2O)	1.5% of reading
Multiplexer (16-port)	Model Name / Manufacturer	LI-8150 / LI-COR Biosciences, Lincoln, NE
	Dimensions	40.6 cm L x 57.2 cm W x 21.1 H cm
	Internal Cavity Volume	55 cm^3
	Operating Range	-20 – 45°C, 0 – 95% RH, non-condensing
	Power Requirement	10.5-14.5 VDC, 2.1 Amps (@ 12.5 VDC), 27 Watts (for 8 chambers & LI-8100A)
	Pump Type	Diaphragm
N_2O/CO Analyzer (LGR_1)*	Manufacturer	Los Gatos Research Inc, Mountain View, CA
	Model Name / Model Number	N_2O/CO-23d / 907-0014-0000 (S/N 12-0044)
	Trace Gases Analyzed	N_2O, CO, H_2O
	Dimensions	80 cm L x 48.3 cm W x 22.2 cm H
	Internal Cavity Volume	434 cm^3 (Effective volume: 50 cm^3)
	Operating Range	85 torr, 10 – 35°C, 0 – 98% RH, non-condensing
	Power Requirement	150 Watts
	Precision (1sec / 3min)	0.1 ppb / 0.050 pbb (N_2O, CO), 50ppm / 10ppm (H_2O)
Enhanced Precision N_2O/CO Analyzer (LGR_{EP})†	Manufacturer	Los Gatos Research Inc, Mountain View, CA
	Model Name / Model Number	N_2O/CO-23-EP / 913-0014-0001 (S/N 13-0199)
	Trace Gases Analyzed	N_2O, CO, H_2O
	Dimensions	80 cm L x 48.3 cm W x 48.9 cm H
	Internal Cavity Volume	401 cm^3 (Effective volume: 50 cm^3)
	Operating Range	85 torr, 0 – 45°C, 0 – 98% RH, non-condensing
	Power Requirement	300 Watts
	Precision (1σ, 0.1 sec / 1 sec)	0.3 ppb / 0.08 ppb (N_2O), 0.3 ppb / 0.1 ppb (CO), 150 ppm / 50 ppm (H_2O)
Isotopic N_2O Analyzer (LGR_{ISO})‡	Manufacturer	Los Gatos Research Inc, Mountain View, CA
	Model Name / Model Number	N_2OIA-23e-EP / 914-00027
	Dimensions	114 cm L x 43 cm W x 36 cm H
	Internal Cavity Volume	915 cm^3 (Effective volume: 50 cm^3)
	Operating Range	40 torr, 0 – 45°C, 0 – 100% RH, non-condensing
	Power Requirement	115/230 VAC, 50/60 Hz, 400 watts (steady state)
	Precision (1σ, 300 sec)	0.2 ppb (N_2O: 0.2), better than 1 ‰ ($\delta^{15}N$, $\delta^{15}N_a$, $\delta^{15}N_b$), better than 2 ‰ ($\delta^{18}O$)
Soil Temperature & Moisture Sensors	Model Name / Manufacturer	5-TM / METER Group, Inc., Pullman, WA
	Dimensions	10.1 cm L x 3.4 cm W x 1.0 cm H (5.0cm prong length)
	Operating temperature	-40 – 60°C
	Resolution, Accuracy (Temperature)	0.1°C ± 1°C
	Resolution, Accuracy (VWC)	0.0008 m^3/m^3 from 0% – 50% VWC, ± 0.03 m^3/m^3
Tipping Bucket Rain Gauge	Model Name / Manufacturer	TRP-5251 / Texas Electronics Inc., Dallas, TX
	Dimensions	26.0 cm H x 16.3 W (I.D.)
	Operating Range	0 – 70°C, 0 – 100% RH
	Resolution / Accuracy	0.2 mm / 50mm per hour (± 1%)

** LGR used during cover crop (CC) system only in Trailer 1.*

† LGR used during winter wheat (WW) system only in Trailer 1.

‡ LGR used during CC and WW system in Trailer 2.

2.2.3 Site Maintenance

Throughout the growing seasons, the areas in and around the chambers were weeded and the canopy growing inside the soil collars was trimmed to the top of the collar to prevent interference with chamber closure (Figure 2.2a; Kostanovsky et al., 2017). The weeds growing in the unplanted area surrounding the study site were regularly mowed throughout the duration of the experiment.

During the winter, the system was only shut down once prior to a snowstorm on 12 January 2020 to avoid damage to the chambers from snow interference. The system remained in operation during light snow events and snow removal was done the following day. Typically, most of the snow was removed from the study plot, but if there was a significant amount of snow, berms were formed along the borders of the microplots in order to create enough clearance for the chamber head swivel-path (Figure 2.2b). Snow was removed from inside the soil collar to the top lip of the collar. Ice that had formed on the soil collar gaskets was carefully cleared to ensure that the gasket seal was not compromised.

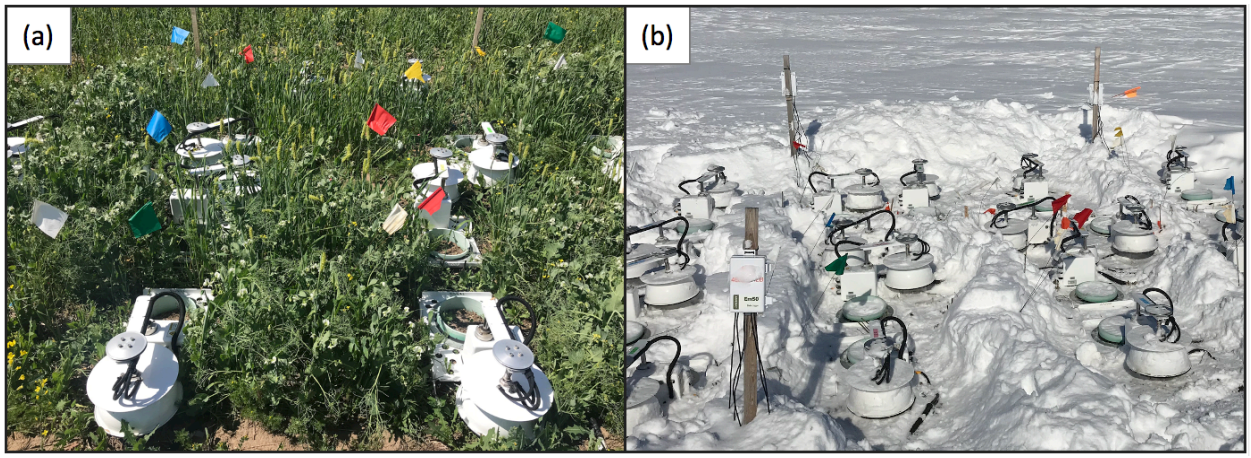

Figure 2.2. Pictures of the microplots showing **(a)** cover crop canopy maintenance and **(b)** snow removal.

2.2.4 Flux Calculations

N_2O and CO_2 fluxes were calculated using Li-Cor's SoilFluxPro Software (version 4.0.1; LI-COR Biosciences), which allows for the integration of data files from third party analyzers. Weekly LI-8100A data files and daily LGR data files were uploaded or imported into SoilFluxPro and the program matched the timestamps from the LGR datafiles to each record of the of the LI-8100A datafiles. Instrument clock synchronization between the two instruments is important for file integration, and if there was not an exact match between time stamp, SoilFluxPro interpolated between the two closest timestamps.

System volume (chamber, collar offset, tubing, and effective instrument volume) and the soil collar area are constants that were manually input within the software for flux calculation. SoilFluxPro automatically adjusts the ambient pressure and temperature variables via recorded LI-8100A readings from each chamber measurement. Figure 2.3 illustrates a typical N_2O chamber flux measurement from SoilFluxPro. The program allows for visual inspection of each measurement so that the "start" and "stop" times for computing the flux can be adjusted to omit any data irregularities in the curve. It takes approximately 15 s for the chamber dome to swing closed, which is accounted for in the LI-8100A and excluded from the flux measurement data. The first 30 s of each chamber measurement was omitted from the flux calculation to account for the time needed to establish well-mixed conditions within the chamber headspace. This is referred to as the dead band. SoilFluxPro applies both linear and non-linear (exponential) equations to maximize the fit between the change in gas concentration over time.

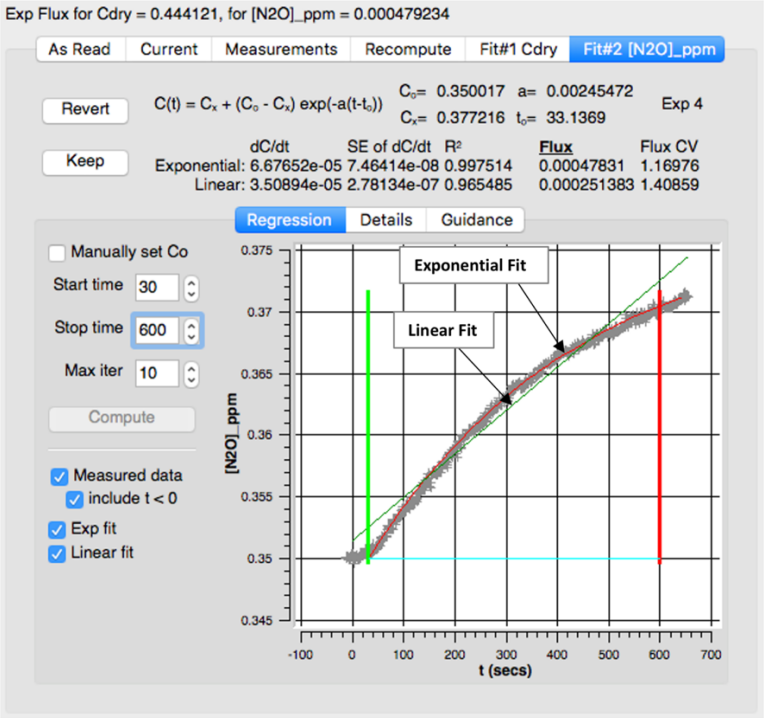

Figure 2.3. Detailed view of single N_2O flux observation concentration curve in SoilFluxPro showing a linear and exponential curve fit, shown by the thin green and red lines, respectively. The thick green and red vertical lines at 30 s and 600 s, respectively, indicate "start" and "stop" times for the flux emission duration used in determining the average flux for this measurement cycle.

Linear and exponential fluxes computed by SoilFluxPro used Equation 2.1, which accounts for water vapor dilution effects (LI-COR Biosciences, 2015):

$$F = \frac{10VP_0\left(1 - \frac{W_0}{1000}\right)}{RS(T_0 + 273.15)} \frac{\partial C'}{\partial t} \quad (2.1)$$

where F is the CO_2 or N_2O efflux rate (μmol m^{-2} s^{-1}), V is the combined volume of the chamber headspace, the Bev-a-Line® tubing, the internal cavity effective volumes of the analytical instruments, multiplexer (4076.1 cm^3), and the volume within the soil collar offset, P_0 is the initial pressure (kPa), W_0 is the initial water vapor mole fraction (mmol mol^{-1}), S is soil surface

area (317.8 cm^2), T_0 is initial air temperature (°C), and $\partial C'/\partial t$ is the initial rate of change in water-corrected CO_2 or N_2O mole fraction (μmol mol^{-1} s^{-1}). For linear flux computation, $\partial C'/\partial t$ is computed as the difference between the specified "start" and "stop" time gas concentrations.

SoilFluxPro calculates exponential flux by fitting the time-series concentration data to the empirical equation shown in Equation 2.2 (LI-COR Biosciences, 2015):

$$C'(t) = C_x' + (C_0' - C_x')e^{-a(t-t_0)} \quad (2.2)$$

where *C'(t)* is the water-corrected chamber CO_2 or N_2O concentration at any time along the concentration curve (μmol mol^{-1}), C_0' is the initial water-corrected value of *C'(t)* computed from the intercept of a linear regression of the first 10 points following the deadband after chamber closure (μmol mol^{-1}), C_x' is a fitted parameter that defines the asymptote (μmol mol^{-1}), and *a* (s^{-1}) is a parameter that defines the curvature of the fit. The regression of C_0' against time yields values for the parameters C_x', *a, and* t_0.

When $t = t_0$ in Equation 2.2, this yields Equation 2.3 (LI-COR Biosciences, 2015). Equation 2.3 is used to calculate the soil-to-chamber exponential flux that is most representative of a soil-to-atmosphere flux.

$$\left.\frac{dC'}{dt}\right|_{t=t_0} = a(C_x' - C_0') \quad (2.3)$$

This initial rate of CO_2 or N_2O concentration change ($\partial C'/\partial t$) calculated by Equation 2.3 following chamber closure once well-mixed conditions are achieved is then plugged into

Equation 2.1 to calculate the corrected exponential flux. If Equation 2.3 reaches the maximum number of 10 iterations without convergence, then SoilFluxPro reports the calculated linear flux value as the best fit.

2.2.5 Minimum detectable fluxes of N_2O

The minimum detectable flux (MDF) of N_2O for each LGR were calculated using methodology developed by Christiansen et al. (2015) and modified by Nickerson (2016) for high frequency gas concentration measurements:

$$MDF = \left(\frac{A_a}{t_c \sqrt{\frac{t_c}{p_s}}} \right) \left(\frac{VP}{SRT} \right) \quad (2.4)$$

where A_a is the analytical accuracy of the instrument, which was measured in the field by passing a 0.5 ppm N_2O calibration gas through each LGR and determining the effective noise, t_C is the closure time of the chamber (720 s), V is the chamber volume (0.0053905 m^3), p_s is the sampling periodicity of the instrument (Table 2.2), P is average ambient pressure for Pullman, WA (92 000 Pa), S is the chamber surface area (0.03178 m^2), R is the ideal gas constant (8.314 m^3 Pa K^{-1} mol^{-1}) and T is ambient air temperature (298.15°K). The computed MDFs for each LGR are listed in Table 2.2.

Table 2.2. Unit values for MDF equation for each LGR analyzer. LGR_1 was the LGR used in Trailer 1 during the CC system, LGR_{EP} was the LGR used in Trailer 1 during the WW system, and LGR_{ISO} was the LGR used in Trailer 2 during both the CC and WW systems.

Analyzer	Analytical Accuracy, A_a (ppb)	Sampling periodicity, p_s (s)	MDF ($\mu mol\ m^{-2}\ s^{-1}$)
LGR_1	1.620	1	5.28×10^{-7}
LGR_{ISO}	1.050	2	4.84×10^{-7}
LGR_{EP}	0.396	1	1.29×10^{-7}

2.2.6 Data quality control

A quality control (QC) protocol was established for the GHG flux datasets (CO_2 and N_2O) to ensure that only high-quality data were used in the data analyses. Each step of the QC protocol is summarized in Table 2.3. The first three steps of the QC process (QC1-3) were applied consistently to both CO_2 and N_2O fluxes within SoilFluxPro, at which point data were imported into Python and we used a script to complete the final QC steps. QC1-3 are performed as raw datafiles are imported into SoilFluxPro and fluxes are calculated. Overall, they filter out unreliable fluxes. QC4 uses CO_2 fluxes to help evaluate corresponding N_2O fluxes and QC5 compares calculated fluxes to the MDF, and QC6 identifies the final flux value for each chamber measurement based on the quality of fit (i.e., linear or exponential). Flux datasets were analyzed every 2-3 weeks to ensure high quality data was being collected throughout the experiment.

QC1 was focused on the input parameters used to calculate fluxes, such as temperatures (instrument and ambient), instrument voltage, pressure, flow rates, etc. Outliers were identified in each case using set bounds based on realistic or physically possible values. For CO_2 and N_2O concentrations, SoilFluxPro provides a column showing the mean gas concentration (water-corrected) observed during each individual chamber measurement as “Cdry_IV” and

"N2Odry_IV", respectively. An outlier was defined as a Cdry_IV and N2Odry_IV value that exceeded the mean Cdry_IV and N2Odry_IV of the entire dataset by two standard deviations. For instance, a Cdry_IV of 1273 ppm was removed from the dataset as an unreasonable value since the remaining dataset ranged from 366 – 617 ppm (mean of 492 ppm). QC2 evaluated the normalized residual sum of squares (SSN) of linear and exponential models to determine the goodness-of-fit to the concentration curve, depending on which SoilFluxPro selected to be the appropriate model (CrvFitStatus). As previously mentioned, although the linear and exponential R^2 values were provided for each flux measurement, R^2 is invalid for nonlinear regression so it was not used as a statistical measure of how well the nonlinear model fit the measured concentration curve data. High values of SSN could indicate laser failure of the analyzer, poor chamber closure, incorrect data file integration, or reference gas interference, for example. If SSN values were considerably higher than the remainder of the dataset, a visual inspection of the flux measurement was done, and if appropriate, start and stop times were manually adjusted otherwise the flux measurement was deleted. There is no fixed CO_2 and/or N_2O SSN value that can be used as a threshold to separate good flux measurements from bad ones, per se. Li-Cor recommends sorting the data on SSN and looking for clear outliers (Hall, C., personal communication, August 11, 2020), as each dataset is unique. While the LGR_1 was used to measure the CC system fluxes, visual inspection of each concentration curve was required for all of the flux observations due to gradual laser card driver failure which resulted in frequent data dropouts. As shown in Figure 2.4, data dropouts caused poor linear and/or exponential regression fits to the concentration curve data resulting in high SSN values. Grouped data dropouts lasting up to 200 s could be deleted from the raw 1 Hz concentration data within SoilFluxPro while still preserving the integrity of the concentration curve (Figure 2.4b), however, curves with longer

periods of faulty data (greater than 200 s) were deemed unreliable and deleted from the dataset. If the dropouts occurred immediately following chamber closure, the flux measurement would be deleted from the dataset, as the initial change in gas concentration over time at time "zero" is required for Equation 2.3. Faulty flux curves could only be used if the dropouts occurred within one 0 – 200 s grouping, as shown in Figure 2.4b, whereas flux curves with several dropouts occurring throughout the entirety of the curve or as several groups were unusable.

Once QC2 was completed to identify faulty fluxes as a result of instrumentation failures, a second pass to flag high or low fluxes (outliers) was conducted as part of QC3. If fluxes seemed unreasonably large compared to the rest of the dataset, a visual inspection of the concentration curve was conducted to verify whether SoilFluxPro used appropriate start and stop times. Outliers were removed if an error in the curve fit procedure was identified, otherwise the flux measurement remained in the dataset. Once QC1-3 were completed, the data were imported into Python for the remainder of the QC.

QC4 is based on Li-Cor guidelines (Li-Cor Biosciences, 2020) and previous studies (Savage et al., 2014; Petrakis et al., 2018; Courtois et al., 2019; Capooci et al., 2019; Barba et al., 2019) that show flux measurements are not reliable unless the chamber volume is well-mixed. The linear regression coefficient (R^2) for CO_2 fluxes has been shown to indicate a well-mixed chamber. Based on this, both CO_2 and N_2O fluxes for a corresponding chamber measurement were discarded from the dataset if the linear R^2 value for CO_2 was less than 0.9. QC5 compared calculated N_2O fluxes against the MDF of the LGR used to measure them (Table 2.2), removing N_2O fluxes below the possible detection limit. And finally, QC6 evaluated which final flux value to use for each chamber observation based on whichever regression model (linear or exponential) had a lower SSN, specifying the best fitting model. SoilFluxPro reports this in the "CrvFitStatus"

column as either “Linear” or “Exponential”. The “Exponential” fit status also had a number associated with it depending on the number of iterations that were required for the model to converge (i.e., Exp 1 through 10).

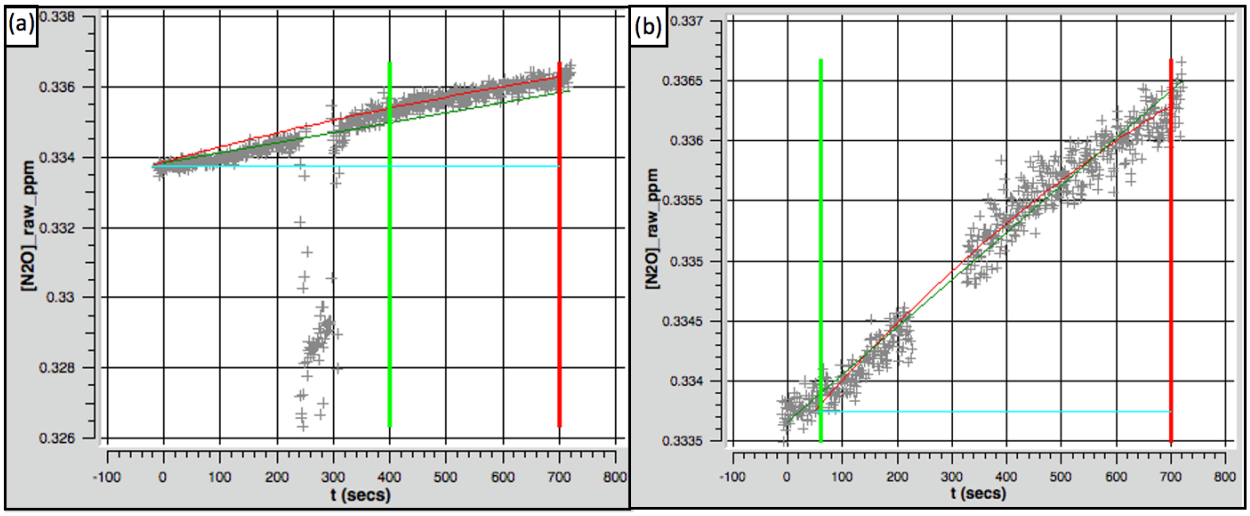

Figure 2.4. (a) Example of an N_2O flux curve with data dropouts. **(b)** The same N_2O flux curve corrected within SoilFluxPro. The green and red vertical lines indicate “start” and “stop” times for the flux emission duration used in determining the average flux for this measurement cycle.

Table 2.3. Quality control (QC) procedure for calculating chamber fluxes. SFP is SoilFluxPro; IRGA is Infrared Gas Analyzer; $Flux_{exp}$ and $Flux_{lin}$ are fluxes computed in SFP using exponential or linear equations, respectively; SSN is the normalized residual sum of squares for both the linear and exponential curve fit; CrvFitStatus is a curve fit solution variable calculated in SFP that determines whether the concentration curve was better fitted with the exponential or linear model.

	QC Criteria	Reasoning	Action	Data QC Flag*	References
QC1	Instrument Diagnostics & Flux Calculation Variables	Sort column headers containing instrument diagnostic data and flux calculation variables to identify unreasonable values, including: instrument temperatures (IRGA, multiplexer and LGR), system voltage, multiplexer flow, chamber closure time, atmospheric pressure, relative humidity, air temperature, and water dilution corrected CO_2 and N_2O concentration.	Discard corresponding CO_2 & N_2O flux observations	3	LI-COR Biosciences, 2011
QC2	High SSN	Sort CO_2 & N_2O linear and exponential SSN column headers from high to low to identify outliers and inspect concentration curves with for irregularities. Irregular curves may indicate issues with instrumentation (ie. LGR laser failure), chamber closure (ie. snow impact), clock sync (ie. improper LI-8100A and LGR datafile integration).	Adjust start/stop times used for flux calculation if possible, otherwise, discard corresponding CO_2 & N_2O flux observations	3	LI-COR Biosciences, 2011
QC3	GHG Flux Outliers	Sort CO_2 and N_2O linear and exponential flux column headers to identify high/low outliers. An outlier may be due to a faulty fit of the exponential or linear regression model, or the flux can be explained by a relevant environmental driver (ie. temperature/ moisture).	Determine if flux outliers are justified, otherwise, discard corresponding CO_2 & N_2O flux observations	3	LI-COR Biosciences, 2011
QC4	CO_2 Linear Flux $R^2 < 0.9$	CO_2 linear fluxes with $R^2 < 0.9$ likely indicate poor gas mixing inside the chamber and/or mechanical errors such as incorrect chamber closure, resulting in a concentration curve that abruptly tapers off horizontally. The exponential flux R^2 cannot be used because the model will fit itself to the faulty curve.	Discard corresponding CO_2 & N_2O flux observations	3	Savage et al., 2014; Petrakis et al., 2018; Coutrois et al., 2019; Capooci et al., 2019; Barba et al., 2019
QC5	N_2O Flux < MDF	N_2O fluxes < MDF are theoretically non-detectable by the LGR (based on measured effective noise). Not applicable for the LI-8100A because CO_2 fluxes are well above the MDF.	N_2O linear and/or exponential flux not used in analyses	2	Savage et al., 2014; Coutrois et al., 2019
QC6	$Flux_{lin}$ or $Flux_{exp}$ (CrvFitStatus in SFP)	Select the flux value calculated either by linear or exponential regression based on whichever has a lower SSN.	Use either $Flux_{lin}$ or $Flux_{exp}$ for the given chamber observation	1	Görres et al., 2016; LI-COR Biosciences, 2019

** Data QC Flag ranges from 1 to 3, where 3 means the data were unreliable and discarded, 2 means the data were suspect and was not included in data analyses, and 1 means the data were of the highest quality.*

2.3 Results and Discussion

2.3.1 Instrument performance and response

During the CC system (15 May 2019 to 23 August 2019), Trailer 1 (which contained LGR_1) was in operation for the entirety of the study period for a total of 101 days (~ 3 months), and Trailer 2 (LGR_{ISO}) was in operation for 95 days as it was out of service from 5 – 10 July 2019 for LGR maintenance. In total, 6385 and 5993 chamber measurements were recorded in Trailer 1 and Trailer 2, respectively. The LGR_1 experienced laser failure, which resulted in the trailer being out of operation until it was replaced with the LGR_{EP} for the WW system. The LGR_{ISO} in Trailer 2 continued to operate through to the WW study, however, the data were not used in order to keep the CC study flux results from both trailers within the same timeframe.

The WW system study period was 137 days (~ 4.5 months; 16 October 2019 to 29 February 2020), with Trailer 1 (LGR_{EP}) in operation for 127 days and Trailer 2 for 121 days (LGR_{ISO}). Trailer 2 was down from 14 – 25 November 2019 for maintenance and both trailers were shut down before and during a major snowstorm event from 11 – 20 January 2020. In total, 8052 and 7537 chamber measurements were recorded from Trailer 1 and Trailer 2 during the WW study, respectively.

Figure 2.5 illustrates a 3-day time series of raw unfiltered data from the WW system. For every chamber measurement during the WW system, the CO_2 and N_2O concentrations were observed to increase simultaneously during a chamber closure from the LI-8100A and LGR instruments, respectively. Both large and small amounts of rainfall consistently triggered a soil moisture response 9 hours later to varying degrees, as shown by the double-ended red arrows in Figure 2.5. This lag in response time was likely due to the sensors being installed vertically into the soil. A large enough increase in soil moisture across the depth of the soil sensor prongs

would be required to elevate VWC since it is averaged over the entire 10 cm length of the soil sensor. Therefore, VWC is likely underestimated at the study site and installing the sensors parallel to the soil surface might have been a better option. A 10 – 20% variability between the 5-TM VWC readings was observed during both studies, which is reasonable and likely attributed to the spatial heterogeneity of soil.

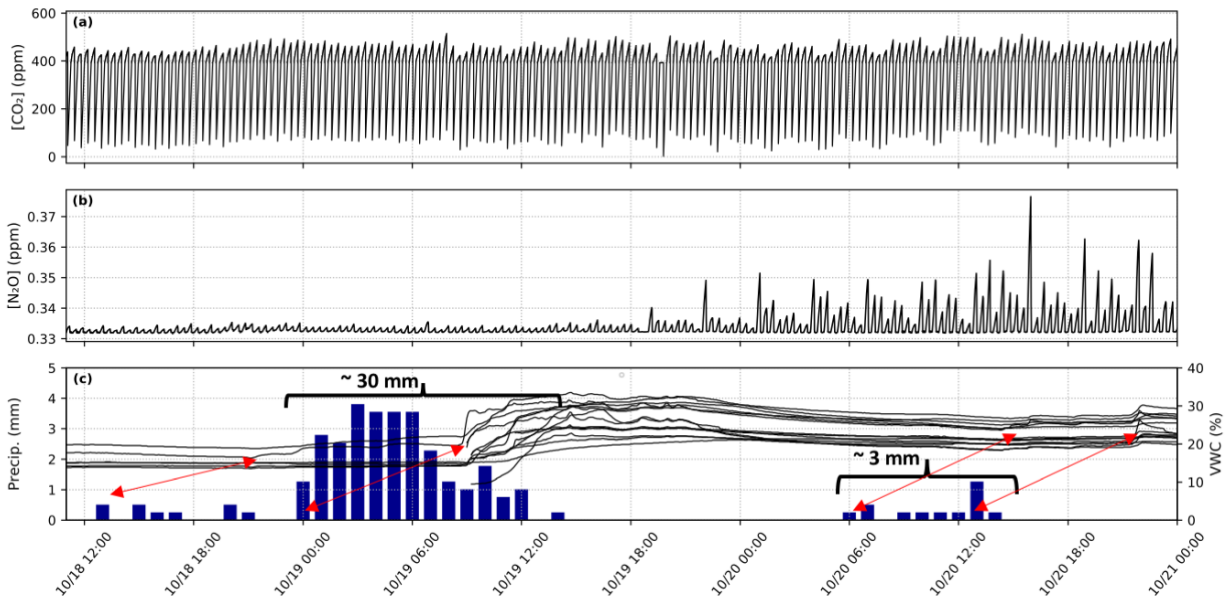

Figure 2.5. Example of the raw unfiltered soil gas concentration data, precipitation and volumetric water content (VWC) from 18 - 21 Oct 2019 during the WW study. **(a)** Unfiltered water-corrected CO_2 data (ppm) measured using LI-8100A. **(b)** Unfiltered water-corrected N_2O data (ppm) from the LGR_{EP}. **(c)** Half-hourly precipitation data (left axis, blue vertical bars, mm) and VWC (right axis, solid black lines, %) from 14 of the 16 soil sensors (5-TM) installed in the top 0 – 10 cm of surface soil. The red arrows indicate the 5-TM response to precipitation.

2.3.2 Flux results

The final flux datasets for the CC system calculated using the QC protocol consisted of 91% (5833 observations) and 92% (5487 observations) flux measurements from the original dataset for Trailer 1 (LGR_1) and Trailer 2 (LGR_{ISO}), respectively. The WW system retained 97% (7809 fluxes) and 95% (7126 fluxes) from the original data set for Trailer 1 (LGR_{EP}) and Trailer 2 (LGR_{ISO}), respectively. Table 2.4 summarizes the number of observations per chamber and numbers of fluxes filtered during each QC step. The majority (n= 68; 0.5% of entire dataset) of the fluxes that were filtered (or removed) during QC1 for both trailers were due to instrument audits, with a smaller number filtered due to relative humidity exceeding 100%, unreasonable water dilution corrected CO_2 concentrations and unreasonable chamber temperature readings. QC2 resulted in the highest number of filtered fluxes during the CC system from both Trailer 1 (n = 393; 6%) and Trailer 2 (n = 299; 5%). The majority of filtered fluxes were due to unsalvageable concentration curves with considerable data dropouts from LGR_1 in the Trailer 1 dataset, and issues with reference gas readings interfering with chamber 9 measurements caused by instrument clock drift and sync issues between the LI-8100A and LGR_{ISO} in the Trailer 2 dataset. Otherwise, the remaining fluxes filtered out during QC2 (from both trailers) were a result of extremely low N_2O fluxes during the CC system. Oftentimes, no discernible trend was detected in the measured N_2O concentration readings during a chamber closure due to low soil N_2O emissions. SoilFluxPro was unable to fit the regression models to this data, resulting in incorrectly reported fluxes and high SSN values. During the WW system, only 21 faulty fluxes were filtered out during QC2 from both trailers as soil N_2O emissions were generally high and produced well-behaved concentration curves. No flux data were filtered during QC3 as there

were no unjustifiably high or low CO_2 or N_2O fluxes identified following QC1 and QC2 filtering.

Overall, CO_2 soil emissions from the microplots were consistently high, producing concentration curves with well-behaved data and low residuals, resulting in consistently high linear regression R^2 values. After filtering the flux data from both trailers through QC3, 2% (n = 272) of the chamber measurements had CO_2 fluxes with linear $R^2 < 0.90$ for the CC system, and 4% (n = 559) for the WW system. CO_2 concentration curves with low linear R^2 values typically exhibited "jumpy" concentration data (example data shown in Figure 2.6), which was likely caused by incomplete chamber closure. During the CC measurements, flux measurements were removed from the dataset from chambers with persistent mechanical issues. On occasion, the canopy interfered with chamber closure, resulting in low linear R^2 values. The LI-8100A typically recognized if a chamber was unable to close properly due to an obstruction and would issue a warning flag in the datafile. Sometimes, however, the LI-8100A would still continue collecting data for a chamber measurement even if the chamber had closed improperly. The chamber closing mechanism does not stop at the first sign of resistance, but rather pushed through the obstruction. This was particularly problematic when heavy wet snow or frozen snow covered the study plot during the WW system (mid-January). The chambers are programmed to swing open a specific number of degrees from the closed position (typically 180°), however pushing through an obstruction resulted in the swing trajectory to become skewed. The swivel arm would overshoot the trajectory in subsequent measurements, resulting in the chamber lid closing on the side of the baseplate rather than directly over the soil collar. There were a few instances where the chamber lid forced itself closed onto a thick snow layer, resulting in the

pressure vent plate that connects the chamber lid to the swivel arm to bend out of alignment resulting in the chamber closing down onto the soil collar lid crookedly.

A particularly problematic period was the snowstorm on 12 January 2020. The chamber systems were shut down prior to snow and turned back on following snow removal on 15 January. Data collected during 15 – 21 January 2020 was not used from either trailer because it continued to snow throughout the week and nearly every chamber measurement had an error message associated with it within the datafile. This resulted in the removal of 350 chamber observations from Trailer 1 and 513 observations from Trailer 2 (257 of which were from chambers 9 – 12).

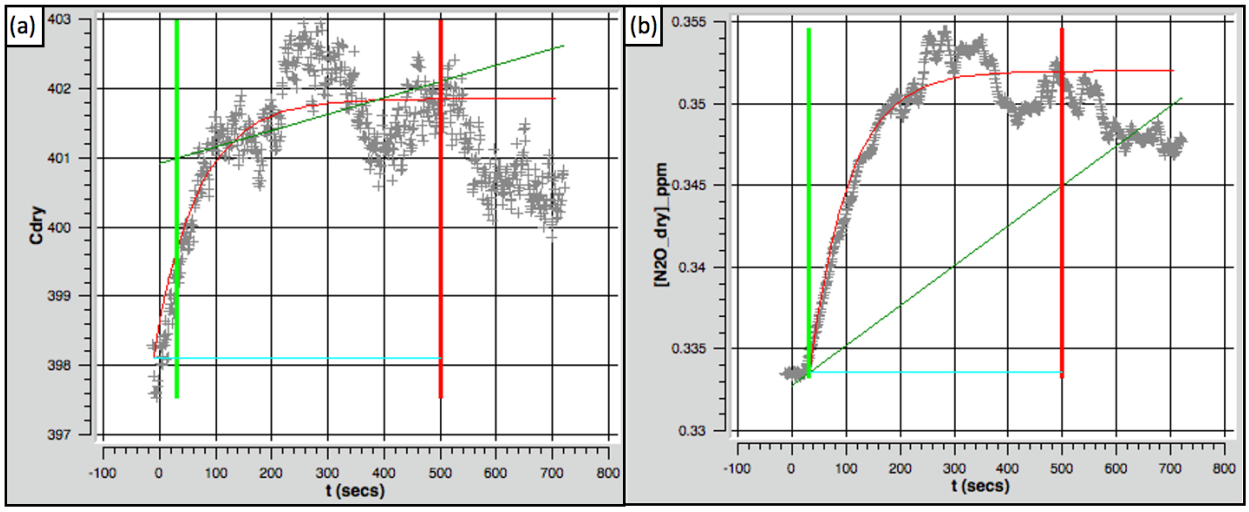

Figure 2.6. Chamber concentration curve data from chamber 7 (Trailer 1) on 20 January 2020 during a snowstorm for **(a)** CO_2, with an R^2 of 0.19 for the linear fit and 0.32 for the exponential fit, and **(b)** N_2O, with an R^2 of 0.49 for the linear fit and 0.91 for the exponential fit. The flux observations for both gases were filtered out during QC4 for this chamber measurement due to chamber lid not properly closing.

The final QC step for filtering unreliable fluxes, QC5, compared the N_2O fluxes to the MDF of the LGRs. Only 26 flux observations were below the MDF for the entire dataset from both studies. QC5 was not necessary for CO_2 fluxes as they were all well above the LI-8100A effective noise level. Following QC1 – 5 filtering, the total CO_2 and N_2O flux data retention from the CC study was 92% for both gases, and 96 % for both gases during the WW study. From the filtered dataset, QC6 was applied to determine whether the linear or exponential model quality of fit was better for a given flux observation. This step selects the model that gives the best description of the gas concentration change inside the chamber headspace (Kutzbach et al., 2007; Forbrich et al., 2010). During the CC study, 99% of CO_2 fluxes and 88% of N_2O fluxes were best-fitted with the exponential model, and during the WW study, 91% of CO_2 fluxes and 94% of N_2O fluxes were best-fitted with the exponential model. The remaining flux curves were fit with the linear model. This outcome aligns with several similar studies that have demonstrated that exponential curve-fit models better describe the behavior of soil gas efflux (Healy et al., 1996; Livingston et al., 2006; Kutzbach et al., 2007; Kroon et al., 2008; Forbrich et al., 2010; Levy et al., 2011; Silva et al., 2015; Kandel et al., 2016).

Table 2.4. Summary of raw unfiltered flux observations and numbers of observations removed during each QC step. Data are presented by chamber number as well as separated into observations from the CC and WW systems. From left to right, the table presents the number of unfiltered CO_2 and N_2O fluxes pre-QC, the number of discarded fluxes after each QC step (QC1 – 5), the number and percent of fluxes deleted after filtering through QC1 – 5, and how many of those remaining fluxes were best fit with linear or exponential regression for the flux datasets (QC6). Under the QC6 columns, the percentages show the percent of remaining fluxes post-QC for CC and WW, and the percent of fluxes that were best fit with the linear or exponential regression.

	Unfiltered		QC1: Diagnostics & Flux Variables		QC2: High SSN		QC3: Flux Outliers		QC4: CO_2 $R^2 < 0.9$		QC5: Flux < MDF (N_2O only)		N_2O Fluxes				CO_2 Fluxes			
													No. Remaining Fluxes		QC 6: $Flux_{lin}$ or $Flux_{exp}$ LIN | EXP		No. Remaining Fluxes		QC 6: $Flux_{lin}$ or $Flux_{exp}$ LIN | EXP	
Trailer 1 Chambers	*CC*	*WW*	*CC*	*WW*	*CC*	*WW*	*CC*	*WW*	*CC*	*WW*	*CC*	*WW*	*CC*	*WW*	*CC*	*WW*	*CC*	*WW*	*CC*	*WW*
Chamber 1	800	1015	11	1	36	1	0	0	13	20	3	0	737	993	67 | 670	104 | 889	740	993	4 | 736	75 | 918
Chamber 2	799	1012	6	0	55	0	0	0	49	24	1	0	688	988	49 | 639	21 | 967	689	988	13 | 676	54 | 934
Chamber 3	801	1012	4	0	65	0	0	0	15	60	1	0	716	952	47 | 669	17 | 935	717	952	2 | 715	49 | 903
Chamber 4	796	1009	5	0	43	0	0	0	4	19	5	0	739	990	63 | 676	29 | 961	744	990	4 | 740	82 | 908
Chamber 5	797	1005	8	0	43	0	0	0	2	17	2	0	742	988	43 | 699	15 | 973	744	988	2 | 742	86 | 902
Chamber 6	797	1004	4	3	51	0	0	0	6	39	4	0	732	962	59 | 673	37 | 925	736	962	2 | 734	82 | 880
Chamber 7	798	1001	6	2	47	0	0	0	0	45	2	0	743	954	61 | 682	40 | 914	745	954	10 | 735	84 | 870
Chamber 8	797	994	3	0	53	0	0	0	3	12	2	0	736	982	68 | 668	14 | 968	738	982	4 | 734	71 | 911
	6385	**8052**	**47**	**6**	**393**	**1**	**0**	**0**	**92**	**236**	**20**	**0**	**5833**	**7809**	**457 | 5376**	**277 | 7532**	**5853**	**7809**	**41 | 5812**	**583 | 7226**
			1%	*0%*	*6%*	*0%*	*0%*	*0%*	*1%*	*3%*	*0%*	*0%*	*91%*	*97%*	*8% | 92%*	*4% | 96%*	*92%*	*97%*	*1% | 99%*	*7% | 93%*
Trailer 2 Chambers																				
Chamber 9	750	941	1	8	221	15	0	0	1	92	1	0	526	826	182 | 344	165 | 661	527	826	8 | 519	157 | 669
Chamber 10	747	942	2	8	14	1	0	0	0	10	1	0	730	923	73 | 657	36 | 887	731	923	17 | 714	114 | 809
Chamber 11	750	943	1	8	10	0	0	0	0	38	0	0	739	897	94 | 645	25 | 872	739	897	0 | 739	90 | 807
Chamber 12	749	943	1	8	7	0	0	0	14	7	2	0	725	928	118 | 607	41 | 887	727	928	12 | 715	96 | 832
Chamber 13	749	942	0	8	10	2	0	0	2	11	1	0	736	921	83 | 653	77 | 844	737	921	2 | 735	88 | 833
Chamber 14	749	942	7	8	9	2	0	0	21	139	1	0	711	793	105 | 606	36 | 757	712	793	8 | 704	29 | 764
Chamber 15	750	942	3	9	20	0	0	0	142	10	0	0	585	923	87 | 498	39 | 884	585	923	7 | 578	169 | 754
Chamber 16	749	942	6	11	8	0	0	0	0	16	0	0	735	915	126 | 609	154 | 761	735	915	2 | 733	90 | 825
	5993	**7537**	**21**	**68**	**299**	**20**	**0**	**0**	**180**	**323**	**6**	**0**	**5487**	**7126**	**868 | 4619**	**573 | 6553**	**5493**	**7126**	**56 | 5437**	**833 | 6293**
			0%	*1%*	*5%*	*0%*	*0%*	*0%*	*3%*	*4%*	*0%*	*0%*	*92%*	*95%*	*16% | 84%*	*8% | 92%*	*92%*	*95%*	*1% | 99%*	*12% | 88%*

2.3.3 Behavior of CO_2 and N_2O flux data

2.3.3.1 CO_2 and N_2O flux distribution

The distribution of CO_2 fluxes were right skewed for both the CC and WW systems (Figure 2.7), indicating a larger number of low fluxes compared to high fluxes. CO_2 fluxes calculated using exponential regression were on average 28 ± 29 % higher for the CC system and 33 ± 41 % higher for the WW system compared to a linear regression. The CC system CO_2 flux distribution is bimodal, and the fluxes estimated using linear and exponential models had medians of 1.3 and 1.7 μmol CO_2 m^{-2} s^{-1}, respectively. The distribution of the WW system CO_2 flux data are unimodal with medians of 0.3 and 0.4 μmol CO_2 m^{-2} s^{-1} for the linear and exponential models, respectively. The spread of the CO_2 flux data from the CC system is broader than the WW system, indicating that a larger range of fluxes were measured during the CC system with larger fluxes overall.

The distribution of N_2O fluxes for both the CC and WW studies were reverse J-shaped towards a flux value of 0 nmol N_2O m^{-2} s^{-1} (Figure 2.7b), indicating that the large majority of chamber measurements exhibited low flux rates and few high flux rates. N_2O flux data have been reported for other field studies to follow highly skewed probability distributions, typically reverse J-shaped or right-skewed, with high coefficients of variability (Parkin, 1987, 2007; van Kessel et al., 1993; Corre et al., 1996; Yates et al., 2006; Wagner-Riddle et al., 2007; Savage et al., 2014; Courtois et al., 2019), which is attributed to the inherent highly variable and dynamic nature of N_2O-producing soil microbial processes and the environmental and anthropogenic drivers that influence them. Overall, fluxes were higher during the WW system than during the CC system (Figure 2.7b). N_2O fluxes calculated using exponential regression are on average 45 ± 120% higher for the CC system and 36 ± 61% higher for the WW system than when using linear

regression. The CC system N_2O median fluxes using the linear and exponential models are 1.8 x 10^{-2} and 2.4 x 10^{-2} nmol N_2O m^{-2} s^{-1}, respectively. The WW system N_2O median fluxes using the linear and exponential models are 0.1 and 0.2 nmol N_2O m^{-2} s^{-1}, respectively.

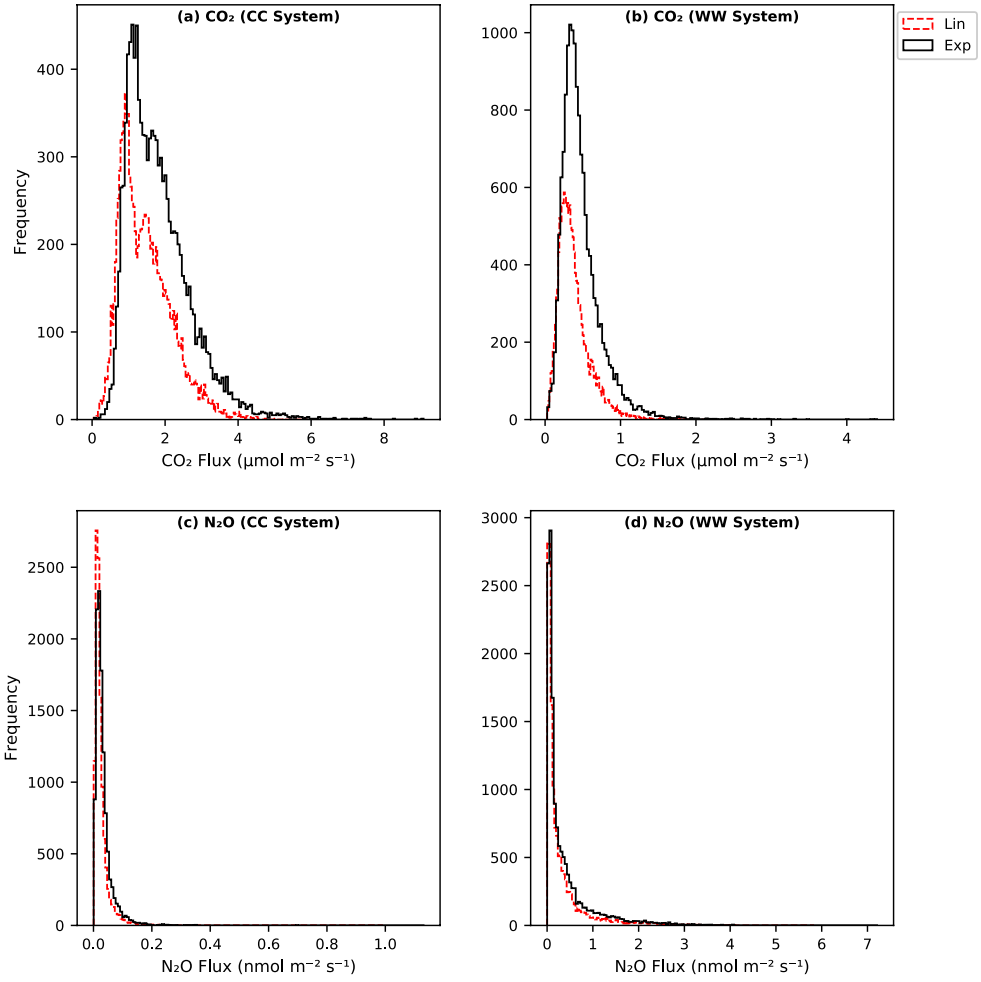

Figure 2.7. (a-b) Frequency distribution of CO_2 fluxes during the CC and WW system and **(c-d)** N_2O fluxes during the CC and WW system from all chambers. Fluxes estimated using linear regression are shown as a red dotted line and exponential regression are shown as a black solid line. The horizontal axes show the full range of flux values measured from each system for each gas.

2.3.3.2 CO_2 and N_2O flux variability

A key feature of the automated multi-chamber system is the ability to capture spatial and temporal variability in fluxes. In this section, we briefly present results which demonstrate this capability. Further analyses of the variability is presented in Chapter 3 in terms of the environmental and soil condition drivers for the observed spatial and temporal variability. An important aspect of assessing the variability is to show that the difference among chamber fluxes are real reflections of the dynamics of soil biogeochemical gas emissions and not due to methodological variability.

By analyzing continuous GHG data from 16 soil locations on our small study site, we were able to capture the spatial and temporal variability in soil gas respiration of CO_2 and N_2O (Figure 2.8 and 2.9). Our results demonstrated that even on a seemingly uniform site, small-scale spatial variability was high, which was expected and "forced" to a certain degree through the implementation of various microplot treatments. Spatial variability over short distance intervals has frequently been observed in comparable agricultural field studies for N_2O flux (Bellingrath-Kimura et al., 2014; McDaniel et al., 2017), and similarly for CO_2, although CO_2 soil emissions are generally more evenly distributed (Stoyan et al., 2000; Heilmann and Beese, 1992; Maestre and Cortina, 2003; Wright et al., 2013; Bellingrath-Kimura et al., 2014).

Frequent and repetitive measurements of the same soil locations allowed us to capture the changes in soil respiration responses to various environmental and anthropogenic drivers (Chapter 3). Pulse emissions of CO_2 and N_2O were observed throughout both studies, which were triggered by increase in soil moisture caused by manual soil-wetting, rain events, and snowmelt. This observation is consistent with the literature (Mulvaney et al., 1997; Chatskikh and Olesen, 2007; Halvorson et al., 2008; Alvarez et al., 2012; Carmo et al., 2015; Kostyanovsky

et al., 2019; Waldo et al., 2019). Pulses decreased with time as the surface soil moisture decreased by evaporation and drainage (Xu et al., 2004; Savage et al., 2014). The largest pulse responses of CO_2 and lowest pulse responses of N_2O were during the CC study, and the opposite trend was observed during the WW study (Figure 2.8 and 2.9). It was generally warm and dry during the CC study period. Vegetation began emerging mid-April, had developed a full canopy by the beginning of June, and was cut down and left on the microplots mid-July. The WW study period was generally cold and wet, and emergence of WW was minimal.

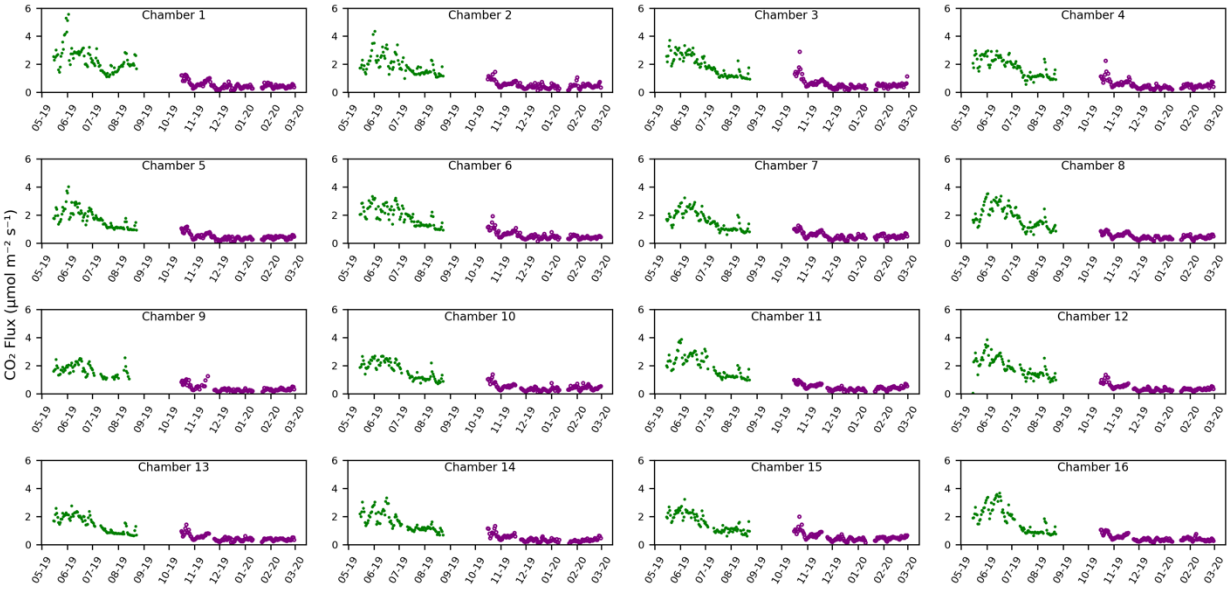

Figure 2.8. Individual CO_2 fluxes from each chamber split up by treatment type during the cover crop system (15 May to 23 August 2019) represented in green solid markers, and during the winter wheat system (16 October 2019 to 29 February 2020) represented in purple circular markers.

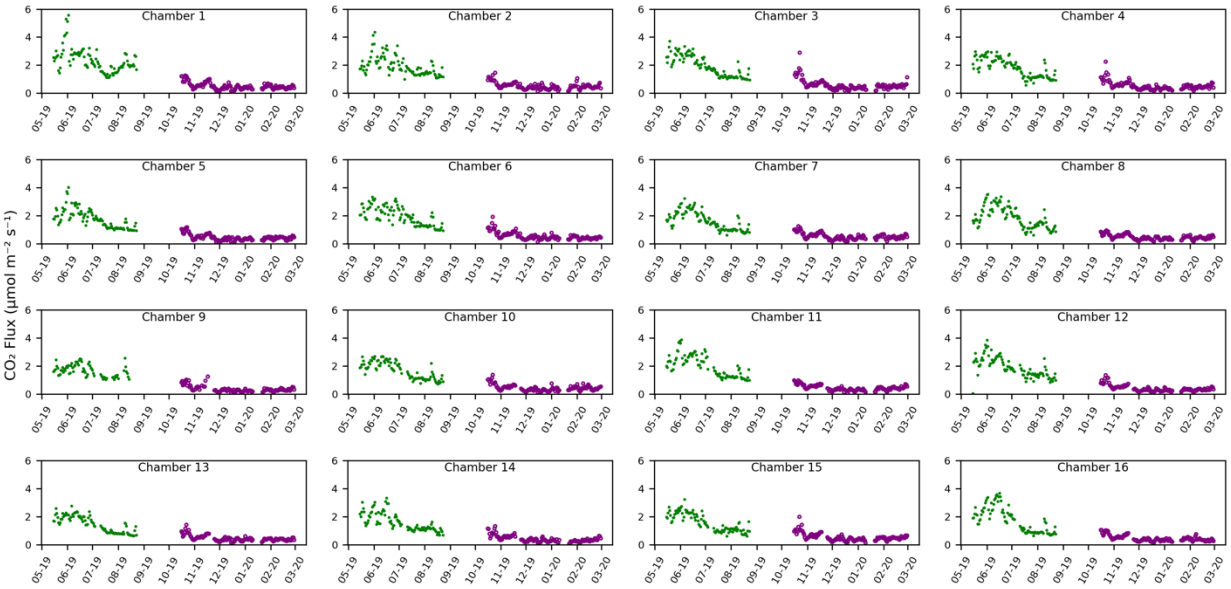

Figure 2.9. Individual N_2O fluxes from each chamber split up by treatment type during the cover crop system (15 May to 23 August 2019) represented in green solid markers, and during the winter wheat system (16 October 2019 to 29 February 2020) represented in purple circular markers.

2.4 Conclusions

Overall, a multiplexed LI-8100A system plumbed in parallel with an LGR analyzer showed high robustness while being continuously operated in the field over multiple seasons and various weather conditions. Connecting the LGR in parallel with the LI-8100A and multiplexer with short pieces of tubing worked well in controlling the different flow specifications between the LI-8100A, multiplexer, and LGR instruments. The parallel configuration also allowed for a fast and synchronized response between instruments during sampling.

It was important to maintain a temperature-controlled environment for the instruments to ensure that they were within their optimal operating ranges. This would not have been possible had line-power not been a possibility at the site. This is a major limitation of this system as more agricultural fields are remote, cover large areas, and do not have line-power connection. Line

power also ensured continuous operation of the chamber systems and analytical instrumentation. Overall, on-site line power was a key requirement for this study to be successful.

Installing remote access capabilities on the analytical instrument computers allowed for site operations to be remotely monitored. This was particularly important in the winter due to snowfall events that led to chamber closure issues. The chamber concentration data could be monitored in real-time and observed for irregularities, such as "jumpy" data, which usually indicates improper chamber closure. A program on the computers also notified the user if any of the monitored parameters were ever out of range or if/when the power shut down at the site. With these systems in place, issues on-site could be resolved expediently.

The QC protocol was developed and altered throughout the process of the study in order to automate it as much as possible and also to ensure that that low-quality data was filtered out of the flux dataset. Half of the QC process still had to be performed manually within SoilFluxPro, which requires a large amount of time input from the user. The CC study produced lower quality data than the WW study due to the failing LGR in Trailer 1 (LGR_1) which caused several data dropouts during chamber measurements. The majority of the data lost during the WW study was a result of snow interfering with chamber closure. Overall, CO_2 and N_2O flux data retention was high throughout both studies, at 92% during the CC study and 96% during the WW study for both gases.

Spatial and temporal variability of CO_2 and N_2O fluxes were well captured by the chamber system. There was greater variability in CO_2 fluxes from the CC study compared to CO_2 from WW. The opposite was true for N_2O fluxes, where greater variability was observed during the WW study compared to the CC study. Overall, the system was able to measure GHG fluxes with a time scale of hours to days after environmental drivers such as rain or snowmelt.

This type of detailed analysis and insight can only be accomplished with an automated chamber system, as a manual static chamber system is not able to capture fluxes at a high temporal frequency and would have missed important flux events.

2.5 References

Alvarez, C., Costantini, A., Alvarez, C. R., Alves, B. J. R., Jantalia, C. P., Martellotto, E. E., & Urquiaga, S. (2012). Soil nitrous oxide emissions under different management practices in the semiarid region of the Argentinian Pampas. *Nutrient Cycling in Agroecosystems*, *94*(2–3), 209–220. https://doi.org/10.1007/s10705-012-9534-9

Barba, J., Poyatos, R., & Vargas, R. (2019). Automated measurements of greenhouse gases fluxes from tree stems and soils: magnitudes, patterns and drivers. *Scientific Reports*, *9*(4005), 1–13. https://doi.org/10.1038/s41598-019-39663-8

Bellingrath-Kimura, S. D., Kishimoto-Mo, A. W., Oura, N., Sekikawa, S., Yonemura, S., Sudo, S., … Hara, H. (2014). Differences in the Spatial Variability Among CO2, CH4, and N2O Gas Fluxes from an Urban Forest Soil in Japan. *Ambio*, *44*(1), 55–66. https://doi.org/10.1007/s13280-014-0521-z

Capooci, M., Barba, J., Seyfferth, A. L., & Vargas, R. (2019). Experimental influence of storm-surge salinity on soil greenhouse gas emissions from a tidal salt marsh. *Science of the Total Environment*, *686*, 1164–1172. https://doi.org/10.1016/j.scitotenv.2019.06.032

Corre, M. D., van Kessel, C., & Pennock, D. J. (1996). Landscape and Seasonal Patterns of Nitrous Oxide Emissions in a Semiarid Region. *Soil Science Society of America Journal*, *60*(6), 1806–1815. https://doi.org/10.2136/sssaj1996.03615995006000060028x

Courtois, E. A., Stahl, C., Burban, B., Van Den Berge, J., Berveiller, D., Bréchet, L., … August Janssens, I. (2019). Automatic high-frequency measurements of full soil greenhouse gas fluxes in a tropical forest. *Biogeosciences*, *16*(3), 785–796. https://doi.org/10.5194/bg-16-785-2019

Davidson, E. A., Savage, K., Verchot, L. V., & Navarro, R. (2002). Minimizing artifacts and biases in chamber-based measurements of soil respiration. *Agricultural and Forest Meteorology*, *113*(1–4), 21–37. https://doi.org/10.1016/S0168-1923(02)00100-4

Davidson, E. A., Nepstad, D. C., Ishida, F. Y., & Brando, P. M. (2008). Effects of an experimental drought and recovery on soil emissions of carbon dioxide, methane, nitrous oxide, and nitric oxide in a moist tropical forest. *Global Change Biology*, *14*(11), 2582–2590. https://doi.org/10.1111/j.1365-2486.2008.01694.x

Denmead, O. T. (2008). Approaches to measuring fluxes of methane and nitrous oxide between landscapes and the atmosphere. *Plant and Soil*, *309*(1–2), 5–24. https://doi.org/10.1007/s11104-008-9599-z

Fassbinder, J. J., Schultz, N. M., Baker, J. M., & Griffis, T. J. (2013). Automated, Low-Power Chamber System for Measuring Nitrous Oxide Emissions. *Journal of Environmental Quality*, *42*(2), 606–614. https://doi.org/10.2134/jeq2012.0283

Forbrich, I., Kutzbach, L., Hormann, A., & Wilmking, M. (2010). A comparison of linear and exponential regression for estimating diffusive CH4 fluxes by closed-chambers in peatlands. *Soil Biology and Biochemistry*, *42*(3), 507–515. https://doi.org/10.1016/j.soilbio.2009.12.004

Görres, C. M., Kammann, C., & Ceulemans, R. (2016). Automation of soil flux chamber measurements: Potentials and pitfalls. *Biogeosciences*, *13*(6), 1949–1966. https://doi.org/10.5194/bg-13-1949-2016

Healy, R.W., Striegi, S.C., Russell, T.F., Hutchison, G.L. and Livingston, G.P (1996). Numerical evaluation of static-chamber measurements of soil–atmosphere gas exchange: identification of physical processes. *Soil Science Society of America Journal*, *60*: 740–7. https://doi.org/10.2136/sssaj1996.03615995006000030009x

Heilmann, B., & Beese, F. (1992). Miniaturized Method to Measure Carbon Dioxide Production and Biomass of Soil Microorganisms. *Soil Science Society of America Journal*, *56*(2), 596–598. https://doi.org/10.2136/sssaj1992.03615995005600020041x

Hüppi, R., Felber, R., Krauss, M., Six, J., Leifeld, J., & Fuß, R. (2018). Restricting the nonlinearity parameter in soil greenhouse gas flux calculation for more reliable flux estimates. *PLoS ONE*, *13*(7), 1–17. https://doi.org/10.1371/journal.pone.0200876

Hutchinson, G. L., & Livingston, G. P. (2001). Vents and seals in non-steady-state chambers used for measuring gas exchange between soil and the atmosphere. *European Journal of Soil Science*, *52*(4), 675–682. https://doi.org/10.1046/j.1365-2389.2001.00415.x

Hutchinson, G. L., & Mosier, A. R. (1981). Improved Soil Cover Method for Field Measurement of Nitrous Oxide Fluxes. *Soil Science Society of America Journal*, *45*(2), 311–316. https://doi.org/10.2136/sssaj1981.03615995004500020017x

Kandel, T. P., Lærke, P. E., & Elsgaard, L. (2016). Effect of chamber enclosure time on soil respiration flux: A comparison of linear and non-linear flux calculation methods. *Atmospheric Environment*, *141*, 245–254. https://doi.org/10.1016/j.atmosenv.2016.06.062

Kostyanovsky, K. I., Huggins, D. R., Stockle, C. O., Waldo, S., & Lamb, B. (2018). Developing a flow through chamber system for automated measurements of soil N2O and CO2 emissions. *Measurement: Journal of the International Measurement Confederation*, *113*, 172–180. https://doi.org/10.1016/j.measurement.2017.05.040

Kroon, P. S., Hensen, A., Van Den Bulk, W. C. M., Jongejan, P. A. C., & Vermeulen, A. T. (2008). The importance of reducing the systematic error due to non-linearity in N2O flux measurements by static chambers. *Nutrient Cycling in Agroecosystems*, *82*(2), 175–186. https://doi.org/10.1007/s10705-008-9179-x

Kutzbach, L., Schneider, J., Sachs, T., Giebels, M., Nykänen, H., Shurpali, N. J., … Wilmking, M. (2007). CO2 flux determination by closed-chamber methods can be seriously biased by inappropriate application of linear regression. *Biogeosciences*, *4*(6), 1005–1025. https://doi.org/10.5194/bg-4-1005-2007

Li-Cor Biosciences (2015). *Using the LI-8100A Soil Gas Flux System and the LI-8150 Multiplexer* (2e). Lincoln, Nebraska, USA. Available at: https://licor.app.boxenterprise.net/s/jtpq4vg358reu4c8r4id

Li-Cor Biosciences (2019). Capturing and processing soil GHG fluxes using the LI-8100A. Available at: https://www.licor.com/env/support/LI-8100A/topics/trace-gas-flux-measurements.html

Lebegue, B., Schmidt, M., Ramonet, M., Wastine, B., Yver Kwok, C., Laurent, O., … Conil, S. (2016). Comparison of nitrous oxide (N2O) analyzers for high-precision measurements of atmospheric mole fractions. *Atmospheric Measurement Techniques*, *9*(3), 1221–1238. https://doi.org/10.5194/amt-9-1221-2016

Levy, P. E., Gray, A., Leeson, S. R., Gaiawyn, J., Kelly, M. P. C., Cooper, M. D. A., … Sheppard, L. J. (2011). Quantification of uncertainty in trace gas fluxes measured by the static chamber method. *European Journal of Soil Science*, *62*(6), 811–821. https://doi.org/10.1111/j.1365-2389.2011.01403.x

Livingston, G.P. and Hutchinson, G.L. (1995). Enclosure-based measurement of trace gas exchange: applications and sources of error. In: Matson, P.A. and Harris, R.C., Eds., Biogenic trace gases: measuring emissions from soil and water. Blackwell Science Ltd., Oxford, UK. 14–51.

Livingston, G. P., Hutchinson, G. L., & Spartalian, K. (2006). Trace Gas Emission in Chambers. *Soil Science Society of America Journal*, *70*(5), 1459–1469. https://doi.org/10.2136/sssaj2005.0322

Lundegårdh, H. (1927). Carbon Dioxide Evolution of Soil and Crop Growth, *23*(6): 417 - 453. https://doi.org/10.1097/00010694-192706000-00001

Maestre, F. T., & Cortina, J. (2003). Small-scale spatial variation in soil CO2 efflux in a Mediterranean semiarid steppe. *Applied Soil Ecology*, *23*(3), 199–209. https://doi.org/10.1016/S0929-1393(03)00050-7

McDaniel, M. D., Simpson, R. G., Malone, B. P., McBratney, A. B., Minasny, B., & Adams, M. A. (2017). Quantifying and predicting spatio-temporal variability of soil CH4 and N2O fluxes from a seemingly homogeneous Australian agricultural field. *Agriculture, Ecosystems and Environment*, *240*, 182–193. https://doi.org/10.1016/j.agee.2017.02.017

Nickerson, N. (2016). *Evaluating gas emission measurements using Minimum Detectable Flux (MDF),* Eosense Inc., Dartmouth, Nova Scotia, Canada.

Parkin, T. B. (1987). Soil Microsites as a Source of Denitrification Variability. *Soil Science Society of America Journal*, *51*(5), 1194–1199. https://doi.org/10.2136/sssaj1987.03615995005100050019x

Parkin, T. B. (2008). Effect of Sampling Frequency on Estimates of Cumulative Nitrous Oxide Emissions. *Journal of Environmental Quality*, *37*(4), 1390–1395. https://doi.org/10.2134/jeq2007.0333

Parkin, T.B. & Venterea, R.T. (2010). *Chamber-based trace gas flux measurements*. R.F. Follet (Ed.), GRACEnet Sampling Protocols, 3-1 to 3-39. Available at: https://www.ars.usda.gov/anrds/gracenet/

Pavelka, M., Acosta, M., Kiese, R., Altimir, N., Brümmer, C., Crill, P., … Kutsch, W. (2018). Standardisation of chamber technique for CO2, N2O and CH4 fluxes measurements from terrestrial ecosystems. *International Agrophysics*, *32*(4), 569–587. https://doi.org/10.1515/intag-2017-0045

Petersen, S. O., Hoffmann, C. C., Schäfer, C. M., Blicher-Mathiesen, G., Elsgaard, L., Kristensen, K., … Greve, M. H. (2012). Annual emissions of CH 4 and N 2O, and ecosystem respiration, from eight organic soils in Western Denmark managed by agriculture. *Biogeosciences*, *9*(1), 403–422. https://doi.org/10.5194/bg-9-403-2012

Petrakis, S., Barba, J., Bond-lamberty, B., & Vargas, R. (2018). Using greenhouse gas fluxes to define soil functional types. *Plant Soil*, *423*, 285–294.

Petrakis, S., Seyfferth, A., Kan, J., Inamdar, S., & Vargas, R. (2017). Influence of experimental extreme water pulses on greenhouse gas emissions from soils. *Biogeochemistry*, *133*(2), 147–164. https://doi.org/10.1007/s10533-017-0320-2

Pumpanen, J., Kolari, P., Ilvesniemi, H., Minkkinen, K., Vesala, T., Niinistö, S., … Hari, P. (2004). Comparison of different chamber techniques for measuring soil CO 2 efflux. *Agricultural and Forest Meteorology*, *123*(3–4), 159–176. https://doi.org/10.1016/j.agrformet.2003.12.001

Pumpanen, J., Longdoz, B., & Kutsch, W. L. (2010). Field measurements of soil respiration: Principles and constraints, potentials and limitations of different methods. *Soil Carbon Dynamics: An Integrated Methodology*, 16–33. https://doi.org/10.1017/CBO9780511711794.003

Savage, K. E., & Davidson, E. A. (2003). A comparison of manual and automated systems for soil CO2 flux measurements: Trade-offs between spatial and temporal resolution. *Journal of Experimental Botany*, *54*(384), 891–899. https://doi.org/10.1093/jxb/erg121

Silva, J. P., Lasso, A., Lubberding, H. J., Peña, M. R., & Gijzen, H. J. (2015). Biases in greenhouse gases static chambers measurements in stabilization ponds: Comparison of flux estimation using linear and non-linear models. *Atmospheric Environment*, *109*, 130–138. https://doi.org/10.1016/j.atmosenv.2015.02.068

Smith, K. A., & Dobbie, K. (2001). The impact of sampling frequency and sampling times on chamber-based measurements of N2O emissions from fertilized soils. *Global Change Biology*, *7*(8), 933–945. https://doi.org/10.1046/j.1354-1013.2001.00450.x

Spiess, A. N., & Neumeyer, N. (2010). An evaluation of R2as an inadequate measure for nonlinear models in pharmacological and biochemical research: A Monte Carlo approach. *BMC Pharmacology*, *10*, 1–11. https://doi.org/10.1186/1471-2210-10-6

Stoyan, H., De-Polli, H., Böhm, S., Robertson, G. P., & Paul, E. A. (2000). Spatial heterogeneity of soil respiration and related properties at the plant scale. *Plant and Soil*, *222*(1–2), 203–214. https://doi.org/10.1023/a:1004757405147

Wagner-riddle, C., Furon, A., Mclaughlin, N. L., Lee, I., Barbeau, J., Jayasundara, S., … Warland, J. (2007). Intensive measurement of nitrous oxide emissions from a corn-soybean-wheat rotation under two contrasting management systems over 5 years. *Global Change Biology*, *13*(8), 1722–1736. https://doi.org/10.1111/j.1365-2486.2007.01388.x

Waldo, S., Russell, E. S., Kostyanovsky, K., Pressley, S. N., O'Keeffe, P. T., Huggins, D. R., … Lamb, B. K. (2019). N2O Emissions From Two Agroecosystems: High Spatial Variability and Long Pulses Observed Using Static Chambers and the Flux-Gradient Technique. *Journal of Geophysical Research: Biogeosciences*, *124*(7), 1887–1904. https://doi.org/10.1029/2019JG005032

Wright, E. L., Black, C. R., Turner, B. L., & Sjögersten, S. (2013). Environmental controls of temporal and spatial variability in CO2 and CH4 fluxes in a neotropical peatland. *Global Change Biology*, *19*(12), 3775–3789. https://doi.org/10.1111/gcb.12330

Yates, T. T., Si, B. C., Farrell, R. E., & Pennock, D. J. (2006). Probability Distribution and Spatial Dependence of Nitrous Oxide Emission. *Soil Science Society of America Journal*, *70*(3), 753–762. https://doi.org/10.2136/sssaj2005.0214

Zhao, P., Hammerle, A., Zeeman, M., & Wohlfahrt, G. (2018). On the calculation of daytime CO2 fluxes measured by automated closed transparent chambers. *Agricultural and Forest Meteorology*, *263*(January), 267–275. https://doi.org/10.1016/j.agrformet.2018.08.022

CHAPTER THREE:

SOIL NITROUS OXIDE FLUXES FROM A COVER CROP AND WINTER WHEAT SYSTEM

3.1 Introduction

Agricultural soils contribute about 60% (~ 5 Tg N_2O-N) of total global anthropogenic nitrous oxide (N_2O) emissions, a harmful ozone-depleting greenhouse gas, primarily due to the application of synthetic nitrogen (N) fertilizer to cropping systems (Vitousek et al., 1997; Mosier, 2001, 2002; IPCC, 2013; EPA, 2020). N_2O soil emissions remain poorly understood among researchers due to their extremely high spatiotemporal variability, resulting in high uncertainties in predicting fluxes at the ecosystem and landscape scales, particularly from agroecosystems (Pattey et al., 2007; Hénault et al., 2012). Improving our understanding of the physical and biological mechanisms that cause increased pulses of soil N_2O efflux is imperative in order to derive appropriate N_2O mitigation strategies through improved nitrogen-use efficiency, which is generally considered quite poor in most conventional agricultural cropping systems worldwide (Hénault et al., 2012).

Humans have more than doubled global N fixation of reactive N (N_r) in the last 50 years through frequent fertilizer applications due to high food production demands (Galloway et al. 2003; Fowler et al., 2013; Smith et al., 2016). Ammonium hydroxide (NH_4OH) solution or ammonium sulfate ($(NH_4)_2SO_4$) are commonly used fertilizers that supply the soil with ammonium (NH_4^+). Potassium nitrate (KNO_3) is a water-soluble fertilizer that supplies the soil-plant system with nitrate ions (NO_3^-). Plants are able to assimilate N in both forms, however, NO_3^- more available for uptake because it is more mobile (Boczulak et al., 2014).

Crop diversification and integrating alternative crops into crop rotations can help farmers improve their nutrient use efficiencies and reduce N_2O emissions (Camargo et al., 2013; Liu et al., 2016; Behnke et al., 2018). Symbiotic bacteria called rhizobia that live in the root nodules of legumes, such as peas or beans, are able to fix atmospheric N_2 directly for plant assimilation (Gage, 2006). Adoption of cover cropping with legumes can build and retain soil organic matter (SOM) and replenish nutrients back into the soil for subsequent crops through natural mineralization processes, allowing for reduced N fertilizer use (Jeuffroy et al., 2013; Li et al., 2017).

Microbial bacteria involved in nitrification and denitrification processes are the main source of N_2O production from soils (Firestone and Davidson, 1989; Nelson, 1992). Nitrification is an aerobic process carried out by autotrophic nitrifying prokaryotes in the soil that convert NH_4^+ or ammonia (NH_3) into nitrite (NO_2^-) then NO_3^- (Perlman et al., 2013; Pilegaard, 2013). Intermediates of the nitrification process release N_2O as a by-product (Cleemput and Samater, 1996). Autotrophic nitrifiers can also undergo a process termed nitrifier denitrification under anoxic conditions, where NO_2^- produced during nitrification is reduced to NO, N_2O, and N_2 (Poth and Focht, 1985; Wrage et al., 2001). This is the main N_2O production pathway from ammonia-based fertilizers under anoxic conditions (Zhu et al., 2013).

Denitrification is a sequential anaerobic heterotrophic reduction of NO_3^-- to N_2 that occurs in water-logged soil conditions (Perlman et al., 2013). Denitrification is typically an incomplete pathway as denitrifying bacteria are typically only able to partially denitrify NO_3^-, forming gaseous intermediates in the process such as nitric oxide (NO) and N_2O (Stein and Klotz, 2016). Denitrification is the dominant pathway of N_2O loss from soils, however, it is intrinsically linked to nitrification rates which provide the NO_3^- substrate for denitrifying

bacteria. Alternatively, NO_3^- can be applied to soil directly through fertilization, evoking a greater potential for N losses by denitrification under saturated soil conditions.

Nitrification and denitrification rates depend on and are driven by different variables such as climate, seasonality, soil temperature and moisture, soil pH, and fertilizer types and application rate (Clayton et al., 1994; Mulvaney et al., 1997; Jarvis et al., 2011; Henault et al., 2012; Perlman et al., 2013). Soil moisture has been found to be a dominant driver as it controls the level of soil aeration and availability of oxygen (Zhu et al., 2013; Linn and Doran, 1984). Optimum soil moisture conditions for denitrification have been found to exist at water-filled pore space (WFPS) above 60%, whereas nitrification has been attributed to lower WFPS (Grundmann and Rolston, 1987; Davidson et al., 1991; Clayton et al., 1994; Scmidt et al., 2000; Bateman and Braggs, 2005; Rafique et al., 2011; Laville et al., 2010; Petitjean et al., 2019).

Prolonged periods of precipitation, soil rewetting, and freeze-thaw cycles have been shown to trigger high rates of soil N_2O emissions to occur from discrete areas of enhanced N_2O emissions (hot spots) and over short periods of time (hot moments) that disproportionately increase cumulative field-scale N_2O emissions (McClain et al., 2003; Wagner-Riddle et al., 2008; Borken and Matzner, 2009; Groffman et al., 2009; Bernhardt et al., 2017). Hot moments can be prolonged when microbial degradation rate of substrates are mobilized and intensified, creating pulses of N_2O (Borken and Matzner, 2009; Leitner et al., 2017).

Soil rewetting is an extended dry period followed by rapid wetting, accelerating mineralization of SOM in the soil creating substrate for nitrifying and denitrifying bacteria (Grierson et al., 1998; Fierer and Schimel, 2002; Miller et al., 2005; McIntyre et al., 2009; Kuzyakov and Blagodatskaya, 2015; Petitjean et al., 2019). It can create temporarily saturated anoxic areas within the soil. Freeze-thaw events occur during the non-growing season when

either trapped N_2O produced under frozen surface soil layers is released, or when frozen soil layers or snow thaw and saturates the soil, driving denitrification (Risk et al., 2013; Wagner-Riddle et al., 1997). N_2O loss from agricultural soils during the winter and spring has been observed to account for about 60 – 80 % of the annual N_2O emissions (Wagner-Riddle et al. 1997; Papen and Butterbach-Bahl, 1999; Ludwig et al., 2004; Chen et al., 2018).

In this study, sixteen automated static soil flux chambers measured continuous N_2O fluxes from sixteen microplots (one chamber per microplot) at a high temporal frequency from a cover crop (CC) study (15 May to 23 August 2019) followed by a winter wheat (WW) study (16 October 2019 to 29 February 2020). The microplots were situated in a grid on a small study plot, ensuring high spatial coverage over a small and seemingly homogeneous area of soil.

The purpose of this experiment is to gain insight into the episodic nature and spatiotemporal variability of agricultural soil N_2O emissions associated with drying/wetting cycles, freeze-thaw events, prolonged water-logged soil, seasonality, weather patterns, N fertilizer type and timing of application. The impact of crop diversification through four legume cover crop treatments on N_2O emissions was investigated during both the CC study and the succeeding WW study. Cumulative N_2O nitrogen (N_2O-N) loss from the soil relative to fertilizer N inputs are also presented for the study periods from both systems.

3.2 Materials and methods

3.2.1. Description of the Palouse Conservation Field Station (PCFS)

This study was conducted at the Palouse Conservation Field Station (PCFS, 46.76°N, 117.19°W, 762 m above mean sea level), a United States Department of Agriculture (USDA) Agricultural Research Service (ARS) study farm located near Pullman, Washington (Figure 3.1).

The climate in this region is classified as Dsb (warm, dry summer Mediterranean). In 2019, PCFS recorded an annual total precipitation of 447 mm and an average annual temperature of 9°C, typical of this region. The majority of precipitation occurs in the fall, winter and spring as rain or snowfall, while the summers are predominantly dry and temperate. The soil is classified as a Palouse silt loam (a fine-silty, mixed, superactive, mesic Pachic Ultic Haploxeroll) (Prabhakar et al., 2009). The PCFS comprises about 200 acres of rolling cropland and has been used to conduct various soil, water, and crop experiments since 1931. The land is divided into ten individual study fields that are used for individual studies.

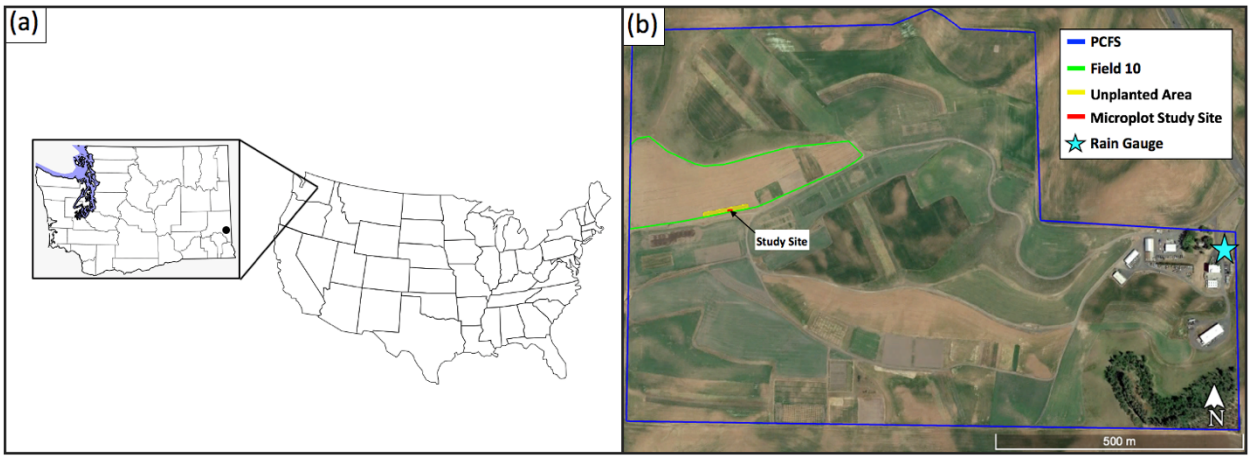

Figure 3.1 (a) Map showing the location of the study site in Washington State (black dot, not to scale) **(b)** Satellite images (Google Earth) of PCFS (blue line), Field 10 (green line), the unplanted area surrounding the study site (yellow box), the study site inside the unplanted area (red box), and the rain gauge (turquoise star).

For this experiment, a strip of land at the southern border of Field 10 was left unplanted, inside which the microplot study site was implemented (Figure 3.1b). The field is sloped; however, the study was conducted on a section of the field that was flat. Throughout the experiment, no overland runoff was observed at the site. From 2015 to present, Field 10 had the

following crop sequence: winter wheat (2015), garbanzo beans (2016), winter wheat (2017), and spring canola (2018). Aside from the unplanted area surrounding the study area, the remainder of Field 10 was planted in winter wheat in 2019 and garbanzo beans in 2020 during the experiment. The tillage regime for Field 10 has been continuous no-tillage since 2001.

3.2.2. Experimental design

The 4.6 by 2.7 m study plot was divided into sixteen 1.14 by 0.61 m experimental microplots (Figure 3.2 and 3.3). Two consecutive studies were carried out on the microplots: a cover crop (CC) study between 15 May 2019 and 23 August 2019, and a winter wheat (WW) study between 16 October 2019 and 29 February 2020. The cutoff for the WW study was selected for the purposes of data analysis, however, data will continue to be collected until harvest in the fall. An automated flux chamber was installed on each microplot and each microplot/chamber was assigned a number (Figure 3.2).

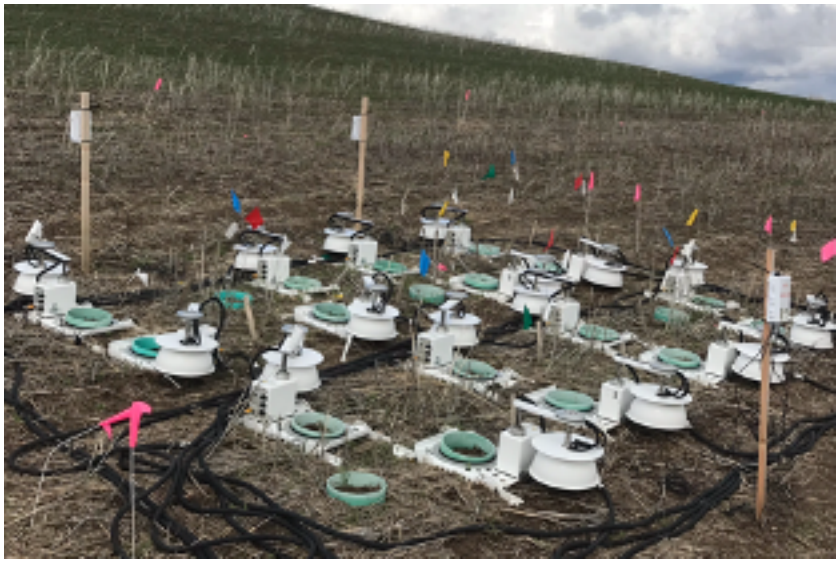

Figure 3.2. Picture of the study site and chamber setup.

3.2.2.1. Instrumentation

Continuous soil CO_2 and N_2O fluxes were measured at each of the 16 microplots using two nearly identical automated static chamber systems that were in operation during both the CC and WW studies. Each trailer system consists of eight (plus four more added during the WW study) automated flux chambers (LI8100-104 LI-COR Biosciences), a multiplexer connecting the chambers to the gas analyzers (LI-8150, LI-COR Biosciences), and a closed-path infrared gas analyzer measuring CO_2 and H_2O concentrations (LI-8100A, LI-COR Biosciences). A subsampling loop was inserted at the outlet of the LI-8100A and the inlet of the multiplexer (LI-8150) to pull the air sample through a laser spectroscopic Los Gatos Research (LGR) N_2O analyzer (Los Gatos Research Inc.) for N_2O concentration measurements. The instruments are housed inside two on-site trailers with connections to line-power. The LGR_1 used during the CC study failed on 23 August 2019 and was later exchanged for an enhanced precision LGR (LGR_{EP}) prior to commencing the WW study. Trailer 2 has an isotopic LGR (LGR_{ISO}) which measures N_2O as well as $\delta^{15}N$, $\delta^{17}O$, $\delta^{18}O$.

Each individual flux measurement lasted 22 minutes, which includes a 5 min pre-purge, a 12 min flux observation period, and a 5 min post-purge. During the purge periods, the multiplexer samples ambient air to restore the system to ambient concentrations. Chamber measurement and purge timing were slightly shorter for Trailer 2 (LGR_{ISO}) because it includes an automated reference bag sampling sequence that repeats every eight-chamber cycle for isotopic analysis purposes. This sampling schedule results in each chamber from each of the two trailer systems being sampled once every 3 hours, resulting in a total of approximately 128 chamber measurements per day from the 16 microplots.

Soil temperature and volumetric water content (VWC) sensors were installed vertically into the soil surface at each microplot to measure the top 0 – 10 cm (5-TM, METER Group, Inc.). The sensors take a measurement each minute of the soil VWC and temperature integrated over the 10 cm length of the sensor prongs. On-site dataloggers (EM50, METER Group, Inc.) were set to record 5-TM data at five-minute intervals, which averages the minute-average data every five minutes. The 5-TM's at microplots 9 and 15 were not functioning throughout the entirety of the experiment. Half-hourly precipitation measurements were recorded using a tipping bucket rain gauge located at PCFS approximately 1 km east of the study site (TRP-525I, Texas Electronics Inc; Figure 3.1b).

Prior to commencing the CC chamber measurements, several soil samples from the top 10 cm were collected at random locations around the perimeter of the study plot. The samples were oven-dried to remove moisture. An average bulk density value of 1.23 g cm^{-3} was calculated from the samples and was used to convert the VWC data from the 5-TM sensors to water-filled pore space (WFPS) using Equation 3.1 (Robertson and Groffman 2007). Soil bulk density changes over time and with depth, however, the same value was used throughout the experiment.

$$\%\, WFPS = \frac{soil\ water\ content \times bulk\ density \times 100}{1-(bulk\ density\ /\ 2.65)} \tag{3.1}$$

3.2.2.2 Cover crop study

For the CC study, four treatments with four replications were established on the microplots as a randomized block design, all of which are color-coded in Figure 3.3. The treatments were: lynx winter pea (WP), verdant winter barley (WB), a 50-50 mix of lynx winter pea and verdant winter barley (WP + WB), and fertilized verdant winter barley (WB_{fert}). For

WB_{fert} treatments, one half of the microplot (0.57 x 0.61 m) was used (grey color-coded boxes in Figure 3.3). The WB_{fert} half-microplot treatments were fertilized at a rate of 112 kg N ha^{-1} with 10 atom-percent ^{15}N-labeled KNO_3 fertilizer solution and the other half of the microplots remained unfertilized. The data from these four unfertilized half-microplots are not included in this work (color-coded white in Figure 3.3). In each microplot, seeding was done in two crop rows that were spaced approximately 0.30 m apart. A 1 m tall wooden frame was placed around the microplots during fertilizer and water application to contain the fertilizer and water to each microplot (Figure 3.4). Details on how the microplots were established, including timing, as well as seeding, fertilizer, and water application rates can be found in Table 3.1.

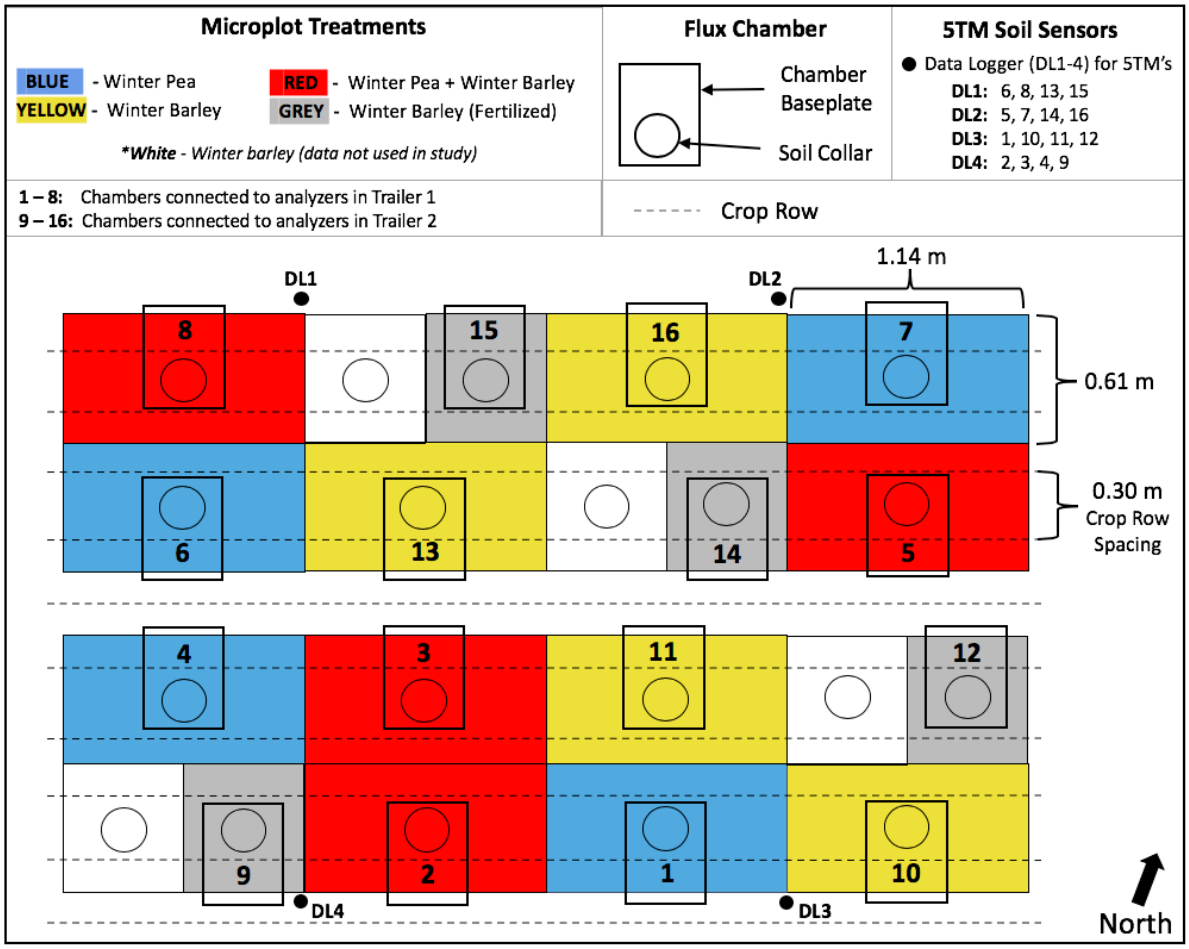

Figure 3.3. Schematic of the study plot during the CC study (15 May 2019 to 23 August 2019) containing four replicated CC treatments as indicated by the color-coded rectangles. Chambers labelled 1 – 8 are connected to analyzers in Trailer 1 and chambers labelled 9 – 20 are connected to analyzers in Trailer 2. The horizontal dotted lines traversing the microplots indicate crop rows. The circles in the middle of the microplots indicate soil collars and the solid rectangles around the circles indicate flux chamber baseplates. The black dots labelled DL1 - 4 indicate the locations of the dataloggers which are each connected to four 5-TM soil sensors installed beside the four chambers listed in parentheses.

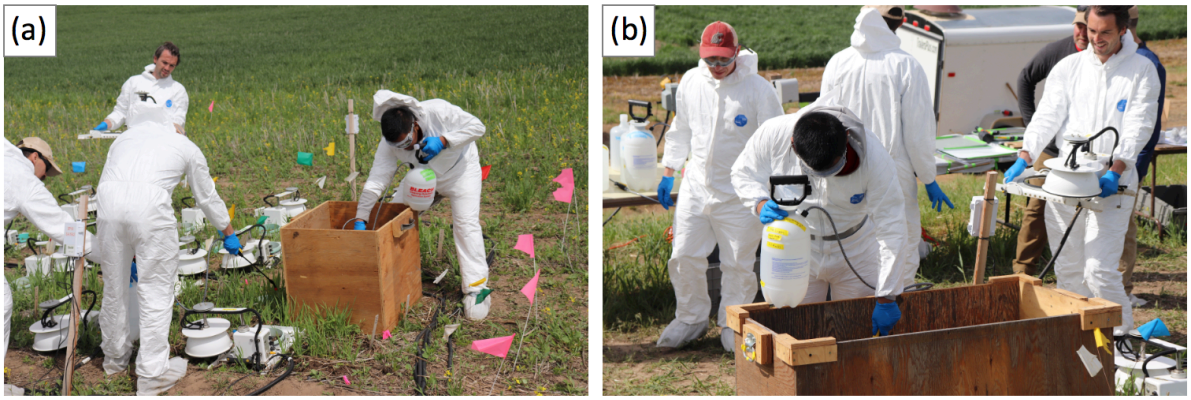

Figure 3.4. Picture showing ^{15}N-labelled fertilizer being applied on 22 May 2019 with a low-pressure sprayer to a WB_{fert} half-microplot. **(b)** Picture showing water being applied on 22 May 2019 with a low-pressure sprayer to a WB microplot.

3.2.2.3. Winter wheat study

The same plot setup was used for the WW study (Figure 3.5). The chamber frames were removed from the soil collars on 14 October 2019. On 15 October 2019, each microplot received three fertilized and seeded rows spaced approximately 20.3 cm apart (Figure 3.6). Row spacing was based off the middle row that transects the center of each collar for a given microplot. Collars were left in place and the fertilizing and seeding trenches were created inside the collars.

A fertilizer solution of ammonium hydroxide (NH_4OH) and ammonium sulfate ($(NH_4)_2SO_4$) was applied to each microplot along the bottom the three hand-dug 7.6 cm deep trenches using a syringe and then backfilled. This was repeated for all microplots one replicate at a time. Microplots that contained the WB treatment during the CC study were fertilized with a 20 atom-percent ^{15}N-labeled fertilizer solution; all other microplots were fertilized with an unlabeled fertilizer solution (Figure 3.4). This equated to a fertilization rate of 168 kg N ha^{-1} for all microplots. Upon completing fertilization, Northwest Tandem soft white winter wheat was seeded in each microplot in the three hand-dug 2.5 cm deep trenches approximately 1.3 cm

downslope of the fertilized rows, then the trenches were backfilled and lightly tamped down with soil (Figure 3.6). Details on fertilization and seeding rates can be found in Table 3.1.

On 16 October 2019, the chamber frames were returned to their soil collars and chamber measurements were restarted. Four additional chambers were added to the study plot during the WW study (chambers 17 – 20), however the chamber data from these microplots were not included in this work.

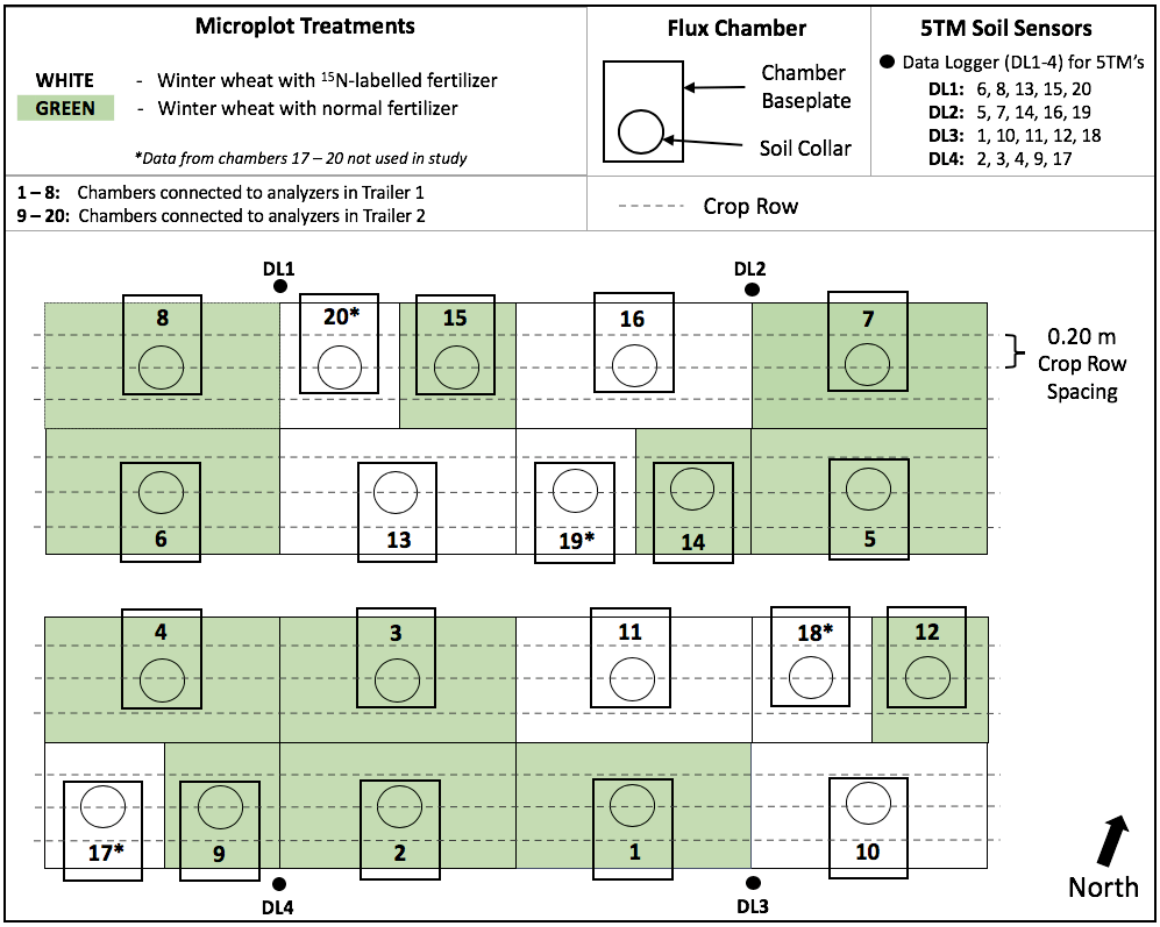

Figure 3.5. Schematic of the study plot during the WW study (16 October 2019 to 29 February 2020) containing winter wheat fertilized with either normal fertilizer or ^{15}N-labelled fertilizer, as indicated by the color-coded rectangles. The chambers labelled 1 – 8 are connected to analyzers in Trailer 1 and chambers labelled 9 – 20 are connected to analyzers in Trailer 2. Data from the chambers 17 – 20 were not included in this study. The horizontal dotted lines traversing the microplots indicate crop rows. The open circles in the middle of the microplots indicate soil collars and the solid rectangles around the circles indicate flux chamber baseplates. The black dots labelled DL1 - 4 indicate the locations of the dataloggers which are each connected to four 5-TM soil sensors installed beside the four chambers listed in parentheses.

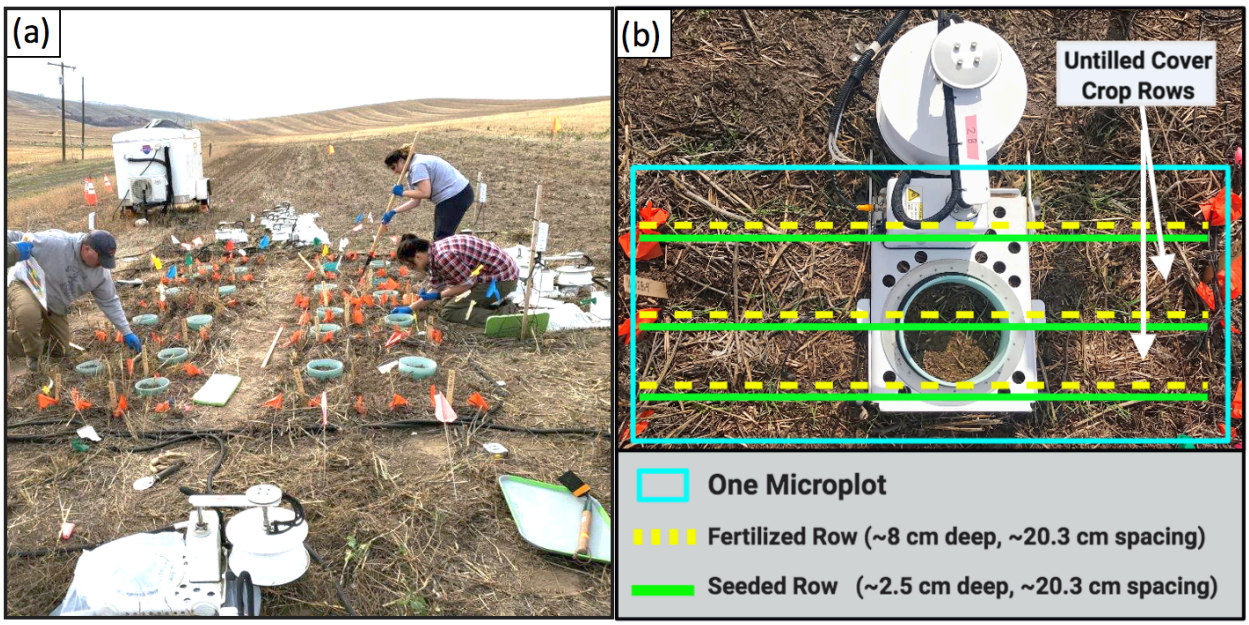

Figure 3.6. (a) Picture showing winter wheat being hand-seeded following fertilization at the study site on 15 October 2019. **(b)** Top-down schematic of the seeding and fertilization layout at each full microplot during the WW study.

Table 3.1. Timeline of crop management activities and fieldwork at the study site

Date	Crop management activities & fieldwork
Cover crop study	
3 October 2018	Seeded a 50/50 mix of lynx winter pea (WP) + verdant winter barley (WB) on all microplots *Seeding rate: 6 WP seed ft^{-1} + 12 WB seed ft^{-1}*
2 November 2018	Weeded WB from WP treatments and weeded WP from WB & WB_{fert} treatments Additional WP seed added to WP treatments for a total seeding rate of 11 WP seed ft^{-1} Additional WB seed added to WB & WB_{fert} treatments for a total seeding rate of 24 WB seed ft^{-}
5 November 2018	Soil collars installed
15 May 2019	Commenced chamber measurements
23 May 2019	Water applied (5.3 L) using low-pressure sprayer to WB treatments Fertilizer applied using low-pressure sprayer to WB_{fert} treatments *Fertilization rate: 112 kg N ha^{-1} of 10 atom% ^{15}N fertilizer (KNO_3)*
10 July 2019	Harvest (cover crops cut down and left on microplots)
23 August 2019	LGR_1 in Trailer 1 broken, chamber data acquisition halted from Trailer 1 and 2
Winter wheat study	
14 October 2019	Chambers removed from soil collars, collars left in place
15 October 2019	Seeded tandem soft white winter wheat (WW) on all microplots *Seeding rate: 15 WW seed ft^{-1}* ^{15}N-labelled fertilizer applied using banding method to previous WB and WB_{fert} microplots *Fertilization rate: 168 kg N ha^{-1} of 20 atom% ^{15}N fertilizer (NH_4OH + $(NH_4)_2SO_4$)* Unlabeled fertilizer applied using banding method to microplots previously seeded with WP an *Fertilization rate: 168 kg N ha^{-1} (NH_4OH + $(NH_4)_2SO_4$)*
16 October 2019	LGR_{EP} installed in Trailer 1 Chambers replaced onto soil collars and commenced chamber measurements

3.2.2.4. Site and instrumentation maintenance

During the growing seasons, the area in an around the chambers was weeded, and the canopy growing inside the soil collars was trimmed to the top of the collar so that there was no interference with chamber closure. The crop located within the trajectory of the swivel arm of the chamber was lightly pushed to the side to allow the arm to swing freely. The unplanted area surrounding the study site was regularly mowed throughout the duration of the experiment.

During the WW study, the instruments were shut down before snowstorms to avoid damage to the chambers from incomplete chamber closures. The system remained in operation

during lighter snow events and snow removal was done the following day. Typically, most of the snow was removed from the study plot, but if there was a significant amount of snow, berms were formed along the borders of the microplots in order to create enough clearance area for the chamber head swivel-path. Snow was removed up to the top of the soil collars, leaving about 3 – 4 cm of snow inside, depending on collar offset height.

3.2.4. Flux Calculations

Soil CO_2 and N_2O fluxes were calculated from the chamber measurement data using Soil Flux Pro software (v4.0.1; LI-COR Biosciences). Fluxes were calculated using both a linear and non-linear (exponential) regression fitted to the change in chamber headspace gas concentrations over time and were adjusted for the soil collar area (317.8 cm^3), system volume (chamber, tubing, and instruments), and ambient pressure and temperature. The first 60 s of each concentration curve were omitted from the flux calculation to account for the time needed to establish well-mixed conditions within the chamber headspace. The software selected the best-fitting model based on the sum of the SSN of the linear and exponential fit for each observation. Poor quality fluxes were discarded from the dataset by applying the quality control criteria described in Chapter 2. In order to effectively analyze nitrogen loss from the soil relative to nitrogen inputs from fertilizer, the flux units were converted to g N_2O-N ha^{-1} d^{-1}.

3.3 Results and discussion

3.3.1. Precipitation and Temperature

Daily total precipitation data collected during both studies at PCFS are reported in Figure 3.7. During the CC study (15 May 2019 to 23 August 2019), the mean daily temperatures ranged from 8.5 to 27.1 °C, the maximum recorded temperature was 35.5 °C on 7 August 2019, and the minimum was 2.6 °C on 19 July 2019, which occurred at night (Figure 3.7). The total rainfall during this period was 50 mm, where May and June were relatively wet (22 and 24 mm, respectively), and July and August were dry (2 and 4 mm, respectively; Figure 3.7).

During the WW study (16 October 2019 to 29 February 2020), the mean daily temperatures ranged from -8.5 to 13.2 °C, the maximum recorded temperature was 20.8 °C on 16 October, and the minimum was -12.0 °C on 14 January (Fig 2). October was wet (50 mm), November was comparatively dry (10 mm), and December (41 mm), January (92 mm), and February (75 mm) were wet, predominantly due to snowfall (Figure 3.7 and 3.12). The total precipitation accumulated during the WW study period was 265 mm, where about 186 mm was measured during snowfall/snowmelt events.

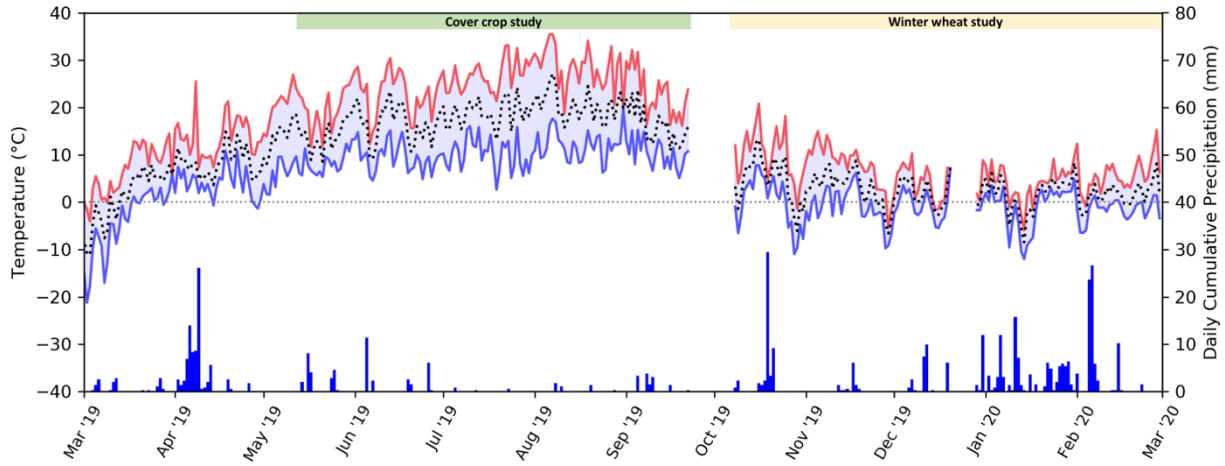

Figure 3.7. Daily mean, maximum, and minimum temperature data and daily cumulative precipitation data between March 2019 to March 2020 observed at the Palouse Conservation Field Station (PCFS) National Weather Service (NWS) Cooperative Observer Program (Co-op) weather station. The data gaps are due to the meteorological station being down.

3.3.2. Spatial and temporal patterns of N_2O flux in response to environmental parameters

3.3.2.1. Cover crop study

N_2O fluxes and environmental parameters measured during the CC study are presented as a time-series in Figure 3.8. Means and ranges of N_2O fluxes are shown in Table 3.2. Three rain events, plus a manual wetting and fertilization event on 22 May (WB and WB_{fert} microplots, respectively) caused sharp increases in WFPS from the baseline, which were correlated to hot spots and hot moments of N_2O fluxes. Arrows in Figure 3.8 show these as numbered events that are referenced throughout this section. Details about these events can be found in Table 3.3. Events 1, 2, and 4 caused the mean combined WFPS from all microplots to reach optimal ranges for denitrification (WFPS > 60%) while event 3 remained in the optimal WFPS range for nitrification (WFPS < 60%). WFPS decreased rapidly following each WFPS spike, suggesting rapidly draining soils and/or rapid surface soil moisture evaporation due to warm temperatures (Figure 3.8). Denitrification is more likely to occur in soils that are saturated for extended

periods of time, although the spikes in WFPS may have caused saturated pockets as soil is not homogenous. Figure 3.9 shows a slight positive linear correlation between soil WFPS and N_2O flux with respect to time. During the study, WFPS mostly remains below 60% WFPS; the favorable range for nitrification (Davidson et al., 1991).

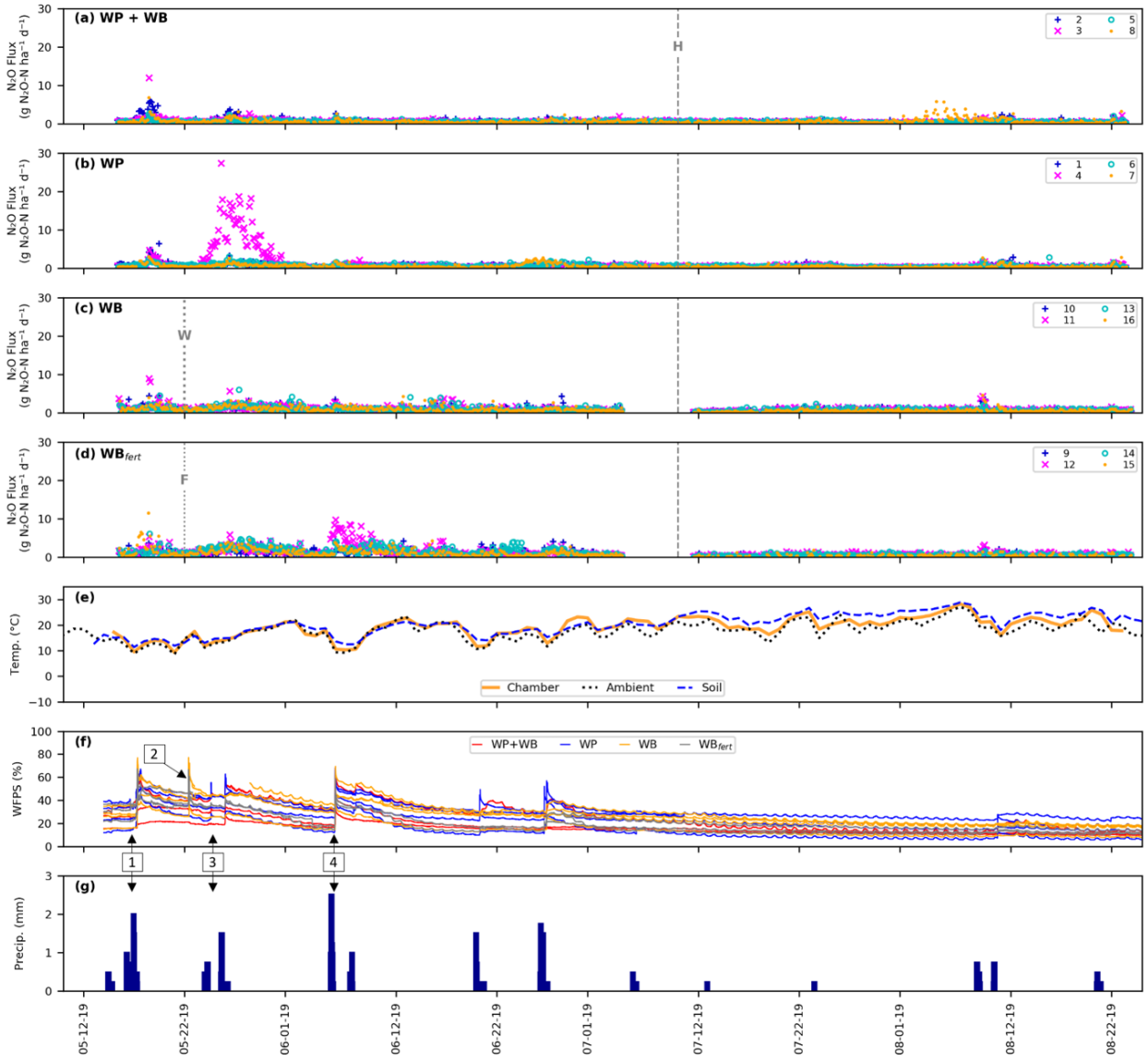

Figure 3.8. (a – d) Individual N_2O-N fluxes from each chamber during the CC study split up by treatment type, **(e)** daily mean chamber and soil temperature (0 – 10 cm) during, **(f)** soil water filled pore space (0 – 10 cm) from 14 of the 16 5-TM soil sensors, color-coded by treatment type, **(g)** half-hourly cumulative precipitation. Management activities are indicated by "W" = water application, "F" = fertilizer application, and "H" = harvest. There was a gap in GHG measurements from 5 – 10 July 2019 because Trailer 2 was under maintenance. The arrows number 1 – 4 depict specific rain events and flux responses that are referenced throughout Section 3.3.2.1.

Table 3.2. The mean, minimum (Min), and maximum (Max) N_2O-N fluxes, and the standard deviation (Std), measured for each chamber during the CC study (15 May to 23 August 2019) and WW study (16 October 2019 to 29 February 2020), split up by treatment group. The number of flux measurements (N) that were used for each chamber is also indicated. The last line of the table shows the mean, min, max, and mean of the std of all the measured fluxes from each study.

N_2O - N Fluxes (g ha^{-1} day^{-1})

		Cover Crops					Winter Wheat				
		Mean	Min	Max	Std	*N*	Mean	Min	Max	Std	*N*
WP + WB	Chamber 2	0.66	0.02	5.78	0.66	688	9.76	0.20	109.15	11.99	988
	Chamber 3	0.53	0.01	11.95	0.55	716	10.99	0.26	71.49	12.47	952
	Chamber 5	0.48	0.02	2.85	0.31	742	3.94	0.13	50.07	4.88	988
	Chamber 8	0.70	0.02	6.80	0.66	736	4.08	0.13	18.09	3.89	982
		0.59	**0.01**	**11.95**	**0.55**	**2882**	**7.19**	**0.13**	**109.15**	**8.31**	**3910**
WP	Chamber 1	0.62	0.02	6.49	0.54	737	18.56	0.20	174.42	22.97	993
	Chamber 4	1.14	0.03	27.36	2.70	739	7.42	0.41	36.86	6.63	990
	Chamber 6	0.60	0.03	3.13	0.42	732	14.49	0.49	81.33	12.91	962
	Chamber 7	0.60	0.02	3.09	0.47	743	15.42	0.27	106.29	22.25	954
		0.74	**0.02**	**27.36**	**1.03**	**2951**	**13.97**	**0.20**	**174.42**	**16.19**	**3899**
WB	Chamber 10	0.87	0.02	4.54	0.58	730	6.86	0.08	60.05	8.02	923
	Chamber 11	0.89	0.07	8.88	0.72	739	5.34	0.22	42.51	5.21	897
	Chamber 13	0.84	0.04	6.01	0.61	736	13.39	0.03	59.77	13.71	921
	Chamber 16	0.87	0.02	4.62	0.62	735	22.17	0.14	140.62	27.94	915
		0.87	**0.02**	**8.88**	**0.63**	**2940**	**11.94**	**0.03**	**140.62**	**13.72**	**3656**
WB_{fert}	Chamber 9	1.02	0.02	4.44	0.81	526*	6.40	0.04	71.24	6.96	826
	Chamber 12	1.21	0.04	9.77	1.28	726	4.85	0.05	22.52	4.31	928
	Chamber 14	1.12	0.02	6.13	0.96	711	6.86	0.17	67.89	9.05	793
	Chamber 15	1.10	0.03	11.61	1.04	585	3.70	0.21	16.35	2.72	923
		1.11	**0.02**	**11.61**	**1.02**	**2022**	**5.45**	**0.04**	**71.24**	**5.76**	**3470**
		0.83	0.02	27.36	0.81	10795	9.64	0.03	174.42	11.00	14935

Table 3.3. Soil wetting events during the CC study resulting in WFPS spikes correlated to N_2O hot spots and hot moments.

Event No.	Dates	Total Measured Precipitation	Maximum Peak WFPS (Combined Mean)
1	15 - 17 May 2019	14 mm	53 ± 17 %
2*	22 May 2019	**WB_{fert}:** 2.6 L fertilizer / half-microplot **WB**: 5.0 L water / microplot	**WB_{fert}**: 59 ± 10 % **WB**: 66 ± 11 %
3	24 - 25 May 2019	8 mm	40 ± 11 %
4	5 June 2019	12 mm	54 ± 10 %

* Combined mean maximum peak WFPS shown for WB_{fert} and WB treatments only

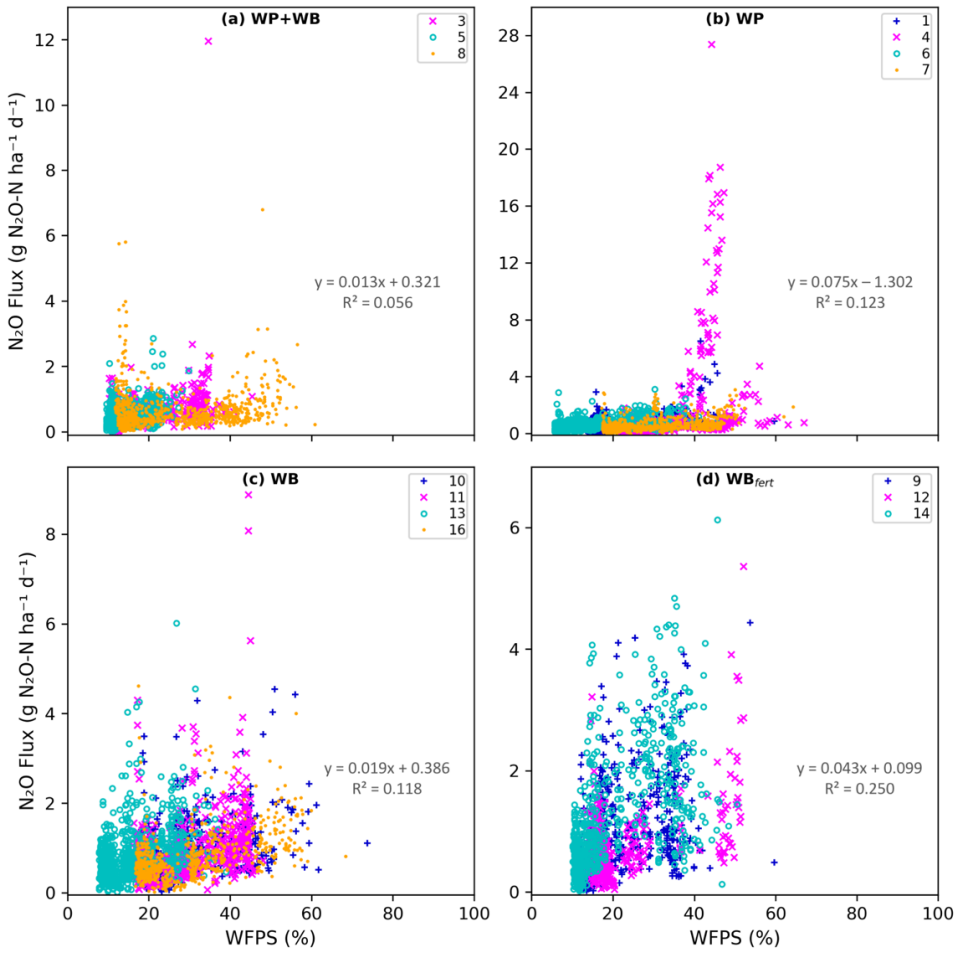

Figure 3.9. Relationship between N_2O fluxes and soil WFPS during the CC system for each chamber split up by treatment. Each panel has different y-axis limits.

During the entire study period, microplots had a combined average flux of 0.83 ± 0.81 g N_2O-N ha^{-1} d^{-1} (Figure 3.8, Table 3.2). Overall, the WB_{fert} microplots were consistently the highest N_2O emitting treatment group, followed by WB, WP, and finally WP+WB (Figure 3.8, Table 3.2). Most of the observed N_2O activity occurred during May and June as hot moments and pulses (Figure 3.8), which were likely caused by re-wetting of dry soils following precipitation events (McIntyre et al., 2009; Kuzyakov and Blagodatskaya, 2015; Leitner et al., 2017; Petitjean et al., 2019). Fluxes were reduced to near-zero following harvest as it became warmer and drier. Microbial activity has been consistently observed to be reduced in soils with low water content, resulting in N_2O emissions that generally remain low (Paul and Clark, 1996; Petitjean et al., 2019).

N_2O hot moments of varying magnitude were observed at nearly every microplot following rain events (Figure 3.8), indicating the presence of N_r and microbial activity in all treatments and not only the WB_{fert} microplots. Event 1 was the first rain event following a prolonged dry period of more than two weeks, with a mean combined baseline WFPS of 27 ± 8% prior to event. This was also the largest observed rain event during the CC study (Figure 3.7 and 8). Rewetting of the soil likely increased N_r availability from mineralization of SOM, and subsequently nitrification and denitrification potential, triggering N_2O hotspots and hot moments observed shortly after at the majority of the microplots (Figure 3.8). A closeup of the N_2O hotspots and hot moments are shown in Figure 3.10. The largest N_2O pulse observed during the study occurred at chamber 4 from the WP treatment group from 23 May to 1 June with a peak flux of 27.4 g N_2O-N ha^{-1} d^{-1}, approximately 75 times higher than pre- and post-background mean levels of 0.39 and 0.34 g N_2O-N ha^{-1} d^{-1}, respectively (Figure 3.10). This pulse commenced six days after event 1 ended, during which SOM mineralization was likely taking place. During

the N_2O pulse, soil conditions were still moist from event 1 and the daily mean temperature was also steadily increasing, creating favorable conditions for the microbial community to utilize the newly released N_r, producing a hot spot and prolonged pulse of N_2O emissions. Event 3 commenced about 10 h after the N_2O pulse began, adding about 8 mm of rain to the system, potentially prolonging the pulse.

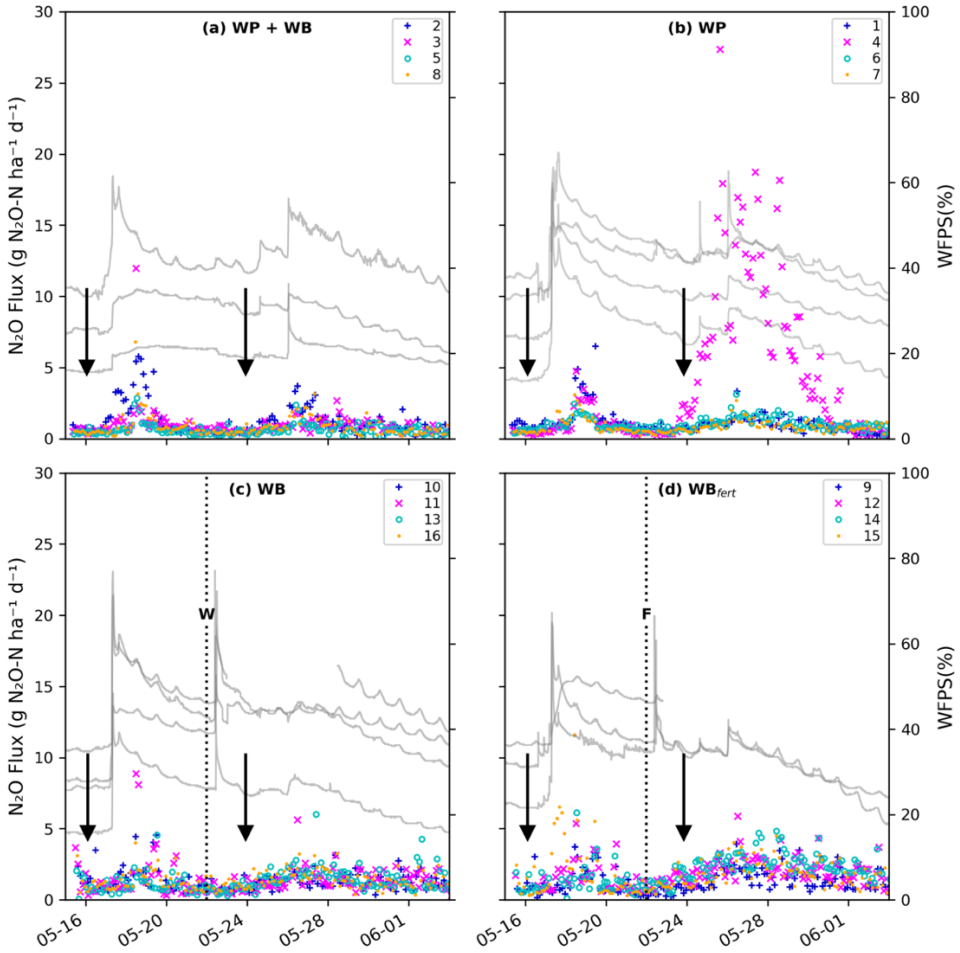

Figure 3.10. Closeup of N_2O fluxes and the WFPS corresponding to each chamber in response to events 1 and 3 from each treatment during the CC system. The first arrow in each panel depicts event 1 (15 – 17 May 2019; ~14 mm rain) and the second arrow depicts event 3 (24 – 25 May 2019; ~8 mm rain), and "W" and "F" indicates when the wetting and fertilizing events took place, respectively (event 2). An N_2O pulse is observed at chamber 4 in the second "WP" panel.

The second largest pulse was observed at chamber 12 from the WB_{fert} treatment group that is coincident to event 4 (Figure 3.8, Table 3.2). A closeup of the N_2O pulse is shown in Figure 3.11. The pulse lasted four and a half days and a peak flux of 9.76 g N_2O-N ha^{-1} d^{-1} was observed, approximately 7 times higher than pre- and post- background mean levels of 1.1 and 1.7 g N_2O-N ha^{-1} d^{-1}, respectively. The previous rain event was 10 days prior and high temperatures had caused the soil to dry out since then, where the mean combined baseline WFPS was 25 ± 8 %, (Figure 3.8). This was the second soil rewetting event observed during the CC study.

Following harvest on 10 July, combined mean WFPS remained at 16 ± 2 % until the conclusion of the CC study (Figure 3.8). Despite the fact that cover crop residue was left on the microplots, the dry soil conditions were unfavorable for mineralization, as well as for both nitrification and denitrification. This explains the low N_2O emissions that were observed during this dry period.

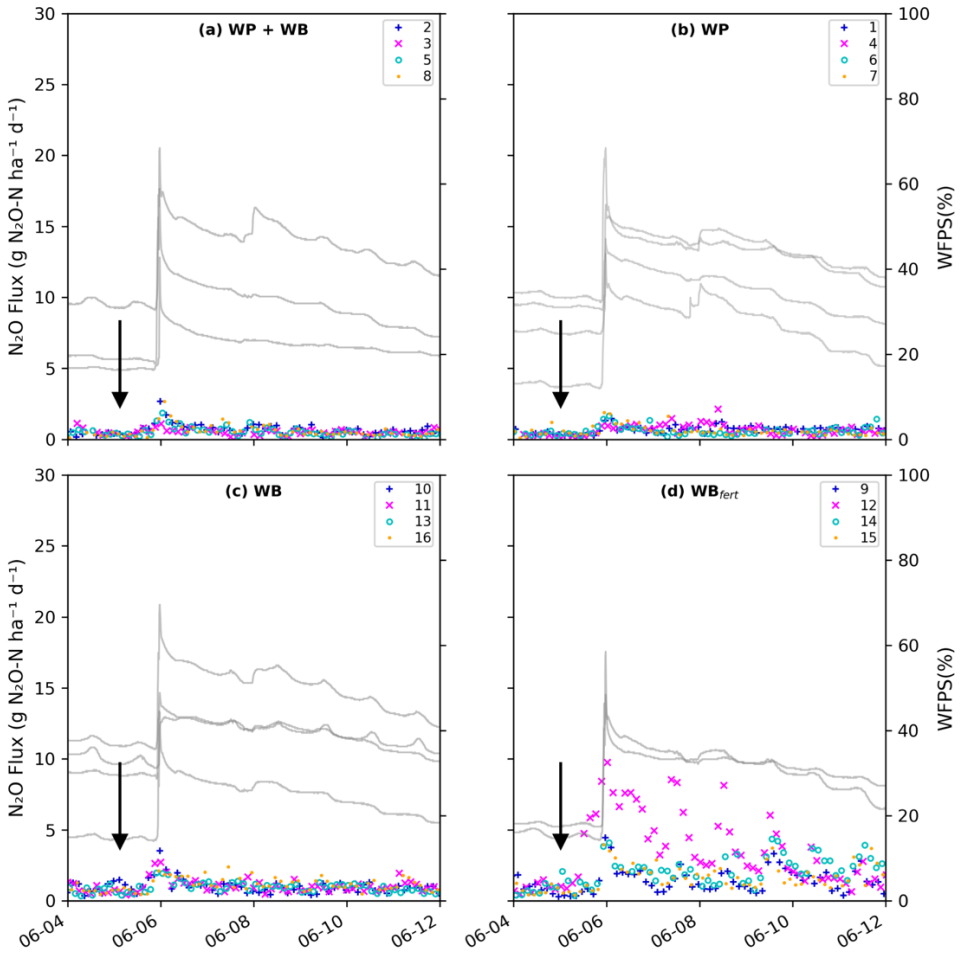

Figure 3.11. Closeup of N_2O fluxes and the WFPS corresponding to each chamber in response to event 4 from each treatment during the CC system. The arrow in each panel depicts event 4 (5 June; ~ 12 mm rain). An N_2O pulse is observed at chamber 12 in the fourth "WB_{fert}" panel.

3.3.2.2. Winter wheat study

N_2O fluxes and environmental parameters measured during the WW study are presented as a time-series in Figure 3.8. Means and ranges of N_2O fluxes are shown in Table 3.2. Snowmelt and freeze-thaw events were likely the main triggers of increased N_2O emissions via pulses during the WW system. Enhanced microbial activity and the release of N_2O trapped at depth during freezing have been observed during periods of increased fluxes (Wagner-Riddle et al.; 2008), although the latter was unlikely during the study as surface soil temperatures rarely

reached freezing temperatures. Due to the frequency and overlap of freeze-thaw cycles and snowmelt events, it was difficult to distinguish the effect of specific events on N_2O fluxes. Arrows in Figure 3.12 show several numbered precipitation events that are referenced in this section. Details about these events can be found in Table 3.4. Figure 3.13 shows that the WFPS and N_2O flux relationship during the WW study was found to have a bell-shaped optimum function, with N_2O peaking at around 60% WFPS. A similar relationship was observed by several authors during field experiments in agricultural soils, with maximum emissions being observed at 65% WFPS (Clayton et al., 1992); 72% WFPS (Scmidt et al., 2000), 70% WFPS (Bateman and Braggs, 2005); 60 – 80% WFPS (Rafique et al., 2011), 68% WFPS (Laville et al., 2011), and 60% WFPS (Petitjean et al., 2019), for example. WFPS levels of 60% and above is the range where soil moisture conditions have been observed to become more favorable for denitrification, as nitrification is minimal at these water content levels (Grundmann and Rolston, 1987; Davidson et al., 1991; Schmidt et al., 2000).

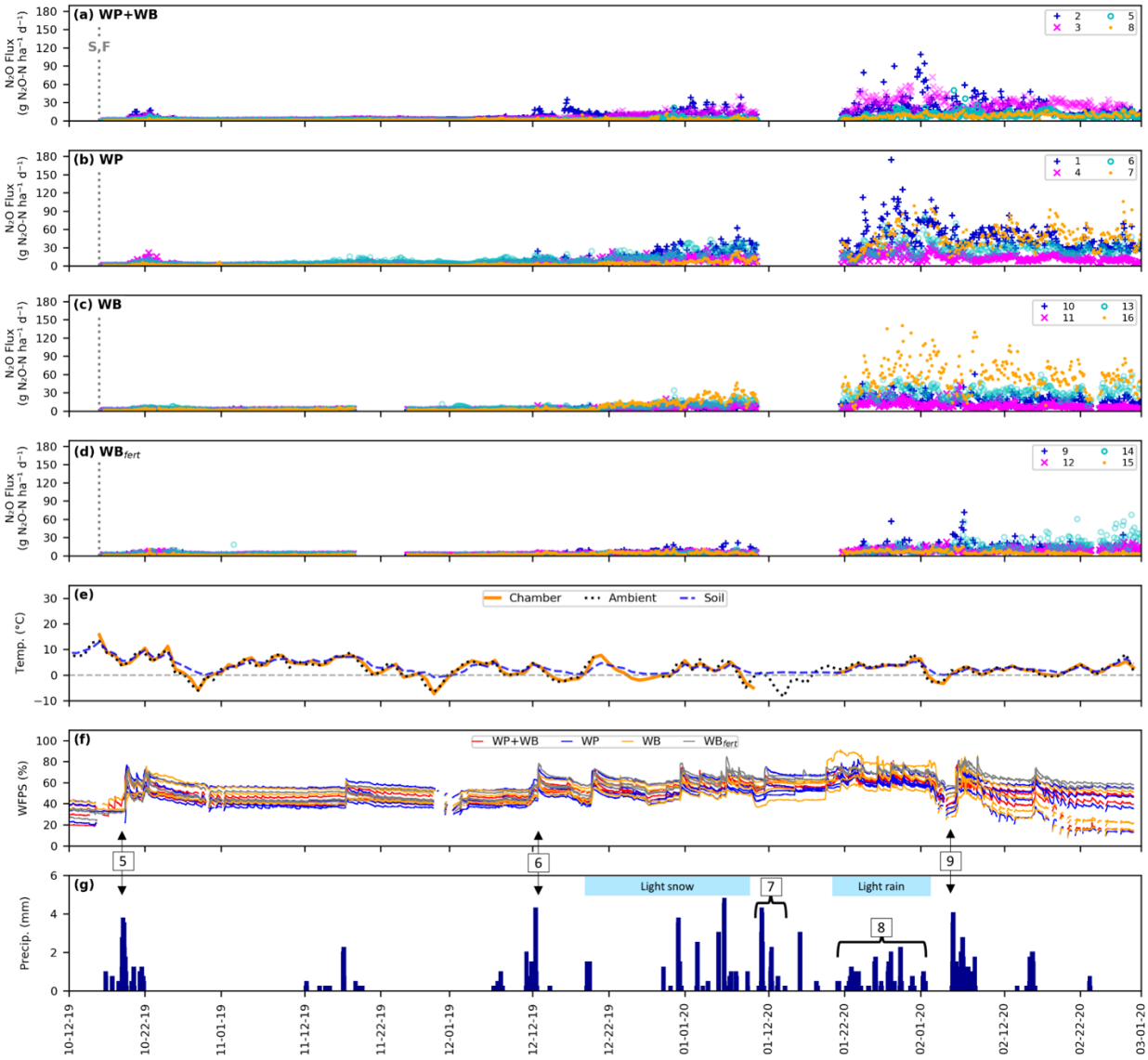

Figure 3.12. (a – d) Individual N_2O-N fluxes from each chamber during the WW study, split up by treatment type, **(e)** daily mean chamber and soil temperature (0 – 10 cm), **(f)** soil water filled pore space (0 – 10 cm) from 14 of the 16 5-TM soil sensors, color-coded by treatment type, **(g)** half-hourly cumulative precipitation. Management activities are indicated by "S" = seeding and "F" = fertilizer application. There was a gap in GHG measurements from 14 – 25 November 2019 because Trailer 2 was under maintenance, and between 11 – 20 January 2020 due to a snowstorm. Gaps in WFPS readings are due to sub-zero temperatures, which are outside of the 5-TM's operating range. The arrows depict rain events (black), snow events (blue), and snow following by rain (black and blue) that are referenced throughout Section 3.3.2.2.

Table 3.4. Soil wetting events during the WW study resulting in WFPS spikes correlated to N_2O hot spots and hot moments.

Event No.	Dates	Precipitation Type	Total Measured Precipitation	Maximum Peak WFPS (Combined Mean)
5	16 - 21 October 2019	Rain	47 mm rain (19 Oct: 30 mm)	63 ± 10 %
6	11 - 12 December 2019	Snow followed by rain	17 mm	66 ± 7 %
7	11 - 14, 16 January 2020	Heavy snow	30 cm + 10 cm (snow cover)*	61 ± 8 %
8	22 - 29 January 2020	Daily light rain events	92 mm†	76 ± 8 %
9	4 - 7 February 2020	Snow followed by rain	58 mm (10 cm snow cover)‡	72 ± 10 %

* On 15 Jan, ~ 30 cm of snow that had accumulated on the study site between 11 - 14 Jan was cleared/bermed. On 16 Jan, ~ 10 cm more snow fell.
† Total amount of precipitation measured in the tipping bucket is from melting snow and event 8 rain events.
‡ Total amount of precipitation measured in the tipping bucket is from melting snow and rain.

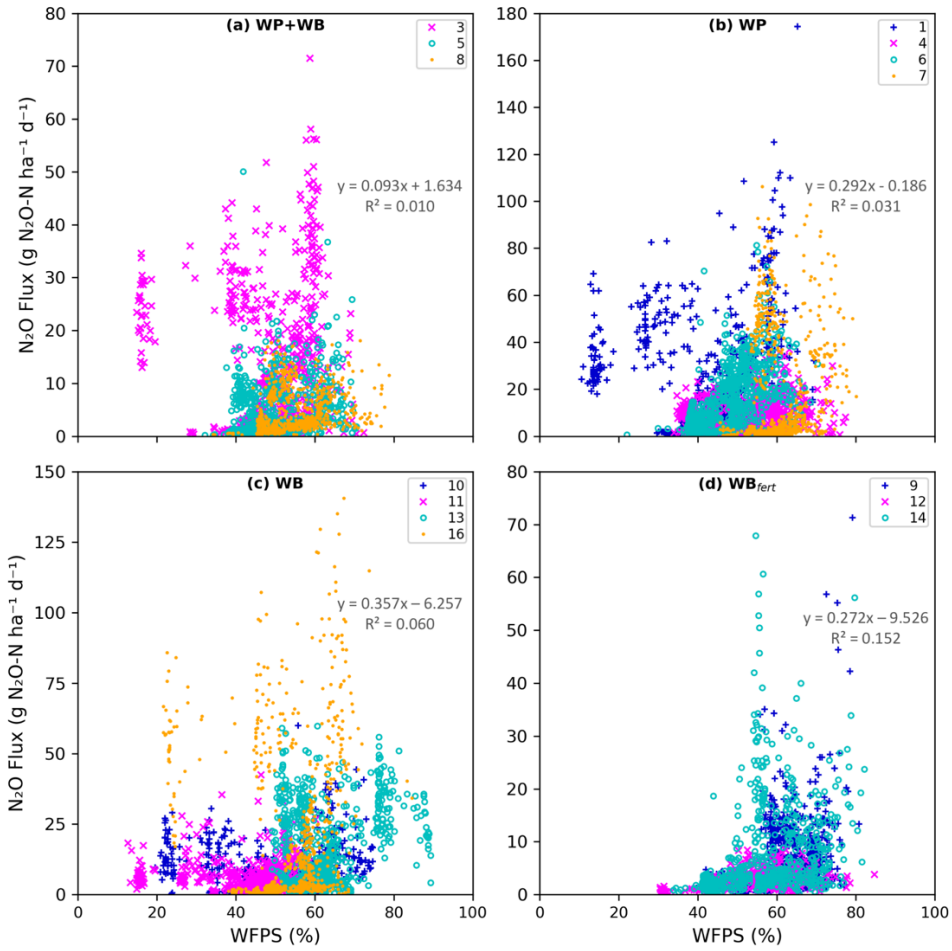

Figure 3.13. Relationship between N_2O fluxes and soil WFPS during the WW system for each chamber split up by treatment. Each panel has different y-axis limits.

During the WW study, the mean N_2O-N flux for all the microplots for the study was 9.64 ± 11.00 g ha^{-1} d^{-1} (Table 3.2). Based on the previous CC study treatment naming convention, during the WW study, the WP microplots had the highest mean flux, followed by WB, WP+WB, and finally WB_{fert} (Figure 3.12, Table 3.2). The WB microplots emissions were not particularly high overall, except for one chamber (16), one of two highest emitters throughout the WW study (Figure 3.12, Table 3.2).

Soil was dry on the day of seeding and fertilization (October 15), with a mean combined WFPS of 32 ± 7% across all microplots (Figure 3.12). Over the next six days following seeding and fertilization (event 5), 47 mm of rain fell, with 30 mm falling in a single day on 19 October, increasing WFPS to optimal denitrification levels (Figure 3.7 and 3.12, Table 3.4). N_2O pulses were triggered at every microplot about five days after fertilization (20 October), each lasting about 8 days. A closeup of the N_2O pulses are shown in Figure 3.14. Maximum N_2O emission values measured across all microplots were 9.06 ± 5.07 g N_2O-N ha^{-1} d^{-1}, a 375% increase from baseline levels of 0.70 ± 0.28 g N_2O-N ha^{-1} d^{-1}. This was the only rewetting event observed during the CC study as WFPS levels.

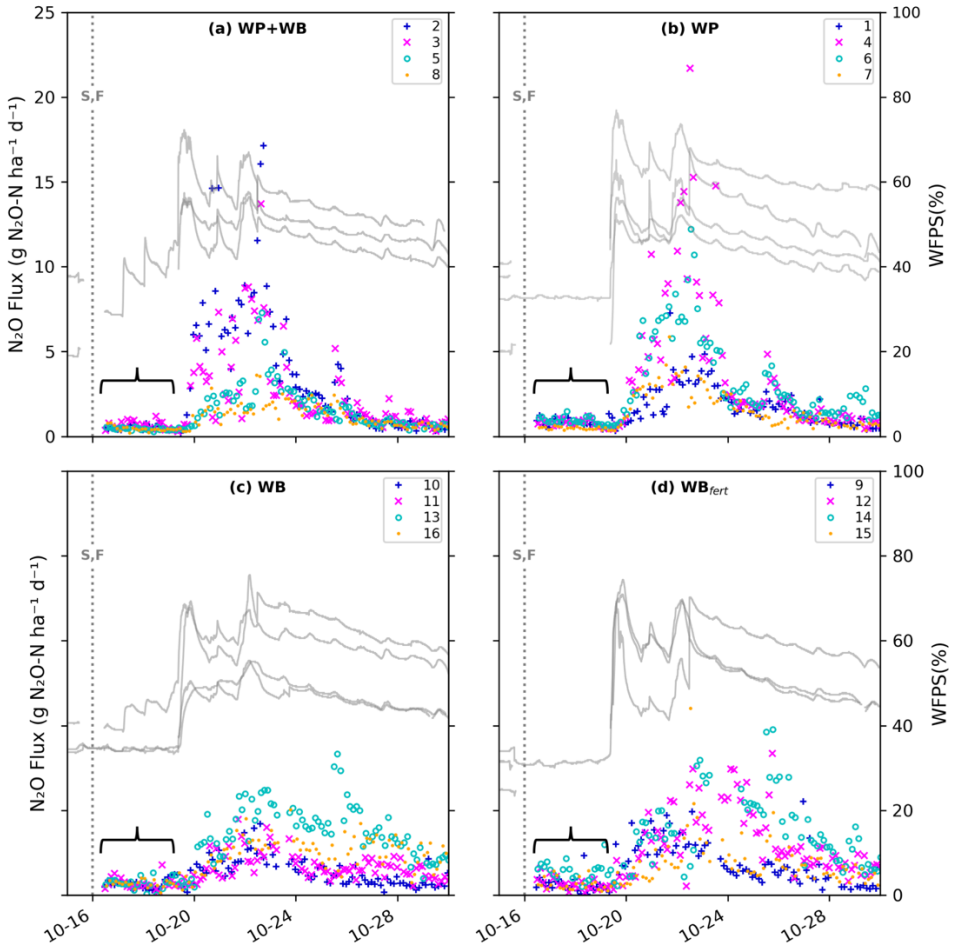

Figure 3.14. Closeup of N_2O fluxes and the WFPS corresponding to each chamber in response to event 5 from each treatment during the WW system. The parentheses depict event 5 (16 – 21 October 2019; ~ 47 mm rain), and "S,F" indicates seeding and fertilization.

The next series of rain events occurred over the course of 8 consecutive days (11 – 19 November; ~ 10 mm cumulative rain) and did not trigger any pulses (Figure 3.12). Following the event 5 pulses, fluxes remained low with a mean baseline of 1.7 ± 1 g ha^{-1} d^{-1} until event 6. Following event 6, fluxes began to steadily increase with the onset of several light snow events.

The largest prolonged N_2O pulses during the WW study were a combined effect of event 7 and 8 (Figure 3.12, Table 3.4). Maximum flux readings during these events were recorded from two hot spots; chamber 1 on 28 January (174.4 g N_2O-N ha^{-1} d^{-1}) and chamber 16 on 29

January (140.6 g N_2O-N ha^{-1} d^{-1}; Figure 3.12 and 3.15, Table 3.2). A closeup of the N_2O pulses following these events are shown in Figure 3.15. Event 7 was the largest snowstorm during the WW study which completely covered the chambers. On 15 January, as much snow was removed from the study plot as possible and the remaining snow was formed into berms around the microplots, then it snowed again the following day. Despite the freezing air temperatures and snowpack, soil temperature readings on all 5-TM sensors remained above 0°C and exhibited little diurnal variation due to the insulation provided by the snow (Figure 3.16). During this period, WFPS increased 17% above pre-snowstorm levels during the event, putting the soil within optimal denitrification range (Table 3.4). Between 22 – 29 January (event 8), several consecutive days of light rain events occurred, and temperatures began to steadily increase. By 24 January, the snowpack had completely melted. The highest recorded WFPS spikes measured during the WW study occurred between 20 and 30 January, with the highest maximum recorded reading reaching 91% from one of the sensors (Figure 3.12). WFPS decreased rapidly once event 8 rains ended and air temperatures dropped back down to freezing (Figure 3.12). Event 9 occurred shortly thereafter, sharply increasing WFPS by about 70% from pre-event 7 levels, prompting a second wave of more subdued N_2O pulses (Figure 3.15, Table 3.4). Denitrification was likely the main driver for N_2O fluxes following events 7, 8, and 9, as frequent snowfall and snowmelt maintained WFPS levels that were favorable for denitrifier bacteria.

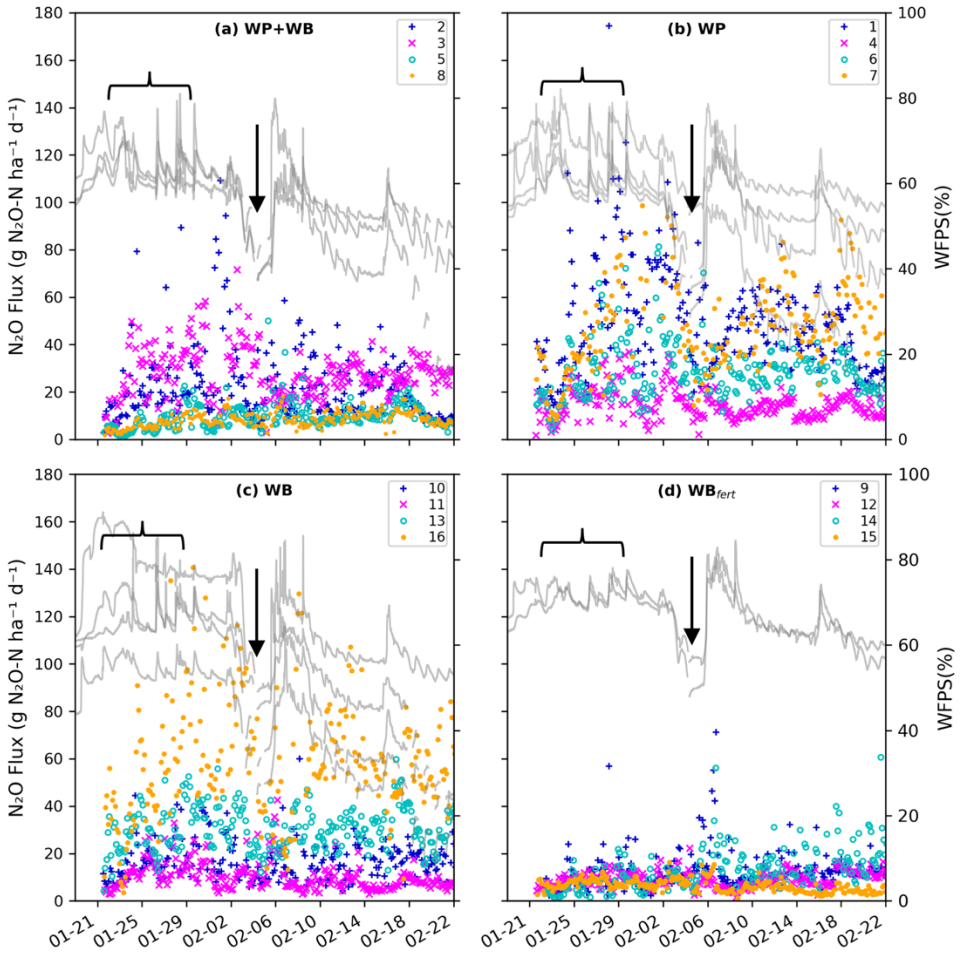

Figure 3.15. Closeup of N_2O fluxes and the WFPS corresponding to each chamber in response to event 7, 8, and 9 from each treatment during the WW system. The parentheses depict event 8 (22 – 29 January 2020; 92 mm precipitation from melting snowpack from event 7 followed by daily rain events), and the arrow indicates event 9 (4 – 7 February 2020; 58 mm).

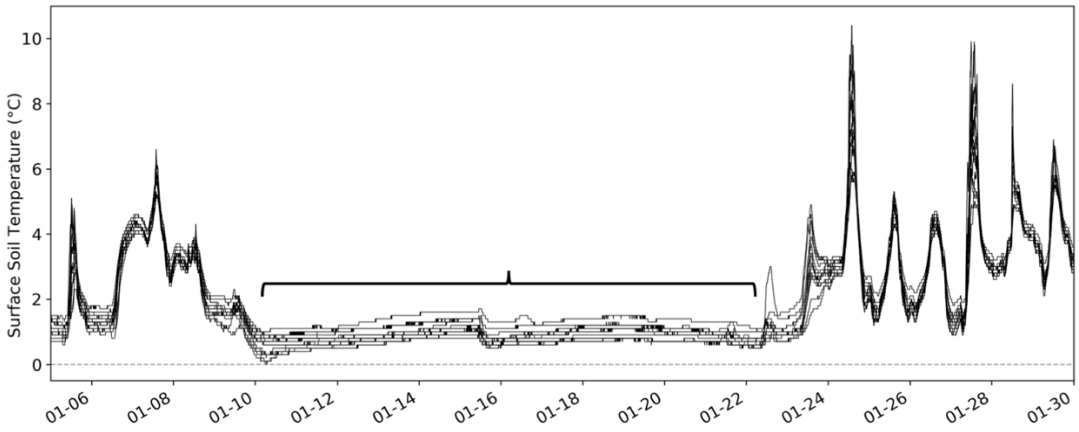

Figure 3.16. Surface soil temperature readings (0 – 10 cm) measured by all functioning 5-TM sensors at 5-minute intervals. The parentheses depict the period where the study plot was covered with frozen snow (11 – 22 January 2020).

3.3.3. Cumulative N_2O emissions

3.3.3.1. Cover crop study

The scaled cumulative emissions were determined using daily mean, minimum, and maximum flux values from each chamber, which averaged 78 ± 21, 39, and 137 g N_2O-N ha^{-1} d^{-1}, respectively, across all chambers for the duration of the CC study (Figure 3.17, Table 3.5). The cumulative emission magnitude from the WB_{fert} treatments was the highest, followed by WB, then WP, and finally WP+WB. The pulse from chamber 4 contributed to 138 % of the chamber's cumulative emissions. Without the pulse, the emissions from the WP treatment would have been similar to those of the WP+WB treatment. The pulse from chamber 12 in the WB_{fert} treatment was smaller, contributing to 32 % of the chamber's cumulative emissions.

The mean cumulative emissions from all three unfertilized treatments were 34 % lower than from the WB_{fert} treatments. This was likely the result of extra N_r additions to the WB_{fert} microplots through fertilization. Since cumulative emissions from unfertilized treatments were

comparable WB_{fert} treatments, this suggests that SOM and mineralization rates in unfertilized microplots were likely high enough before and throughout the study to produce similar quantities of N_r, and subsequently, N_2O through denitrification. Since N_2O from unfertilized WB treatments is mainly the product of soil N_r created through biological fixation and mineralization, it could be presumed that the mean net N_2O-N emissions from these treatments are "background" level for WB crops during this study. Subtracting this value from WB_{fert} net N_2O-N emissions, the difference in N loss is likely due to fertilizer N_r. The 17 % difference equates to 0.014 kg N ha^{-1}, which is only 0.01 % of the original 112 kg N ha^{-1} fertilizer input.

Figure 3.17. Daily cumulative N_2O-N emissions for each chamber (1 to 16) split up by treatment type during the CC study (15 May 15 to 23 August 2019; **a – d**) and WW study (16 October 2019 to 29 February 2020; **e – h**). The dotted lines are the cumulative emissions using daily mean fluxes, and the upper and lower solid lines are the cumulative emissions using daily maximum and minimum fluxes, respectively. Management activities are indicated by : H: = harvest, : W: = water application, and : F: = fertilizer application. There was a gap in flux measurements from 5 – 10 July and 14 – 25 November because Trailer 2 was under maintenance, and between 11 – 20 January due to a snowstorm. Other data gaps indicate days where the fluxes were below the minimum detectable flux limit of the LGR.

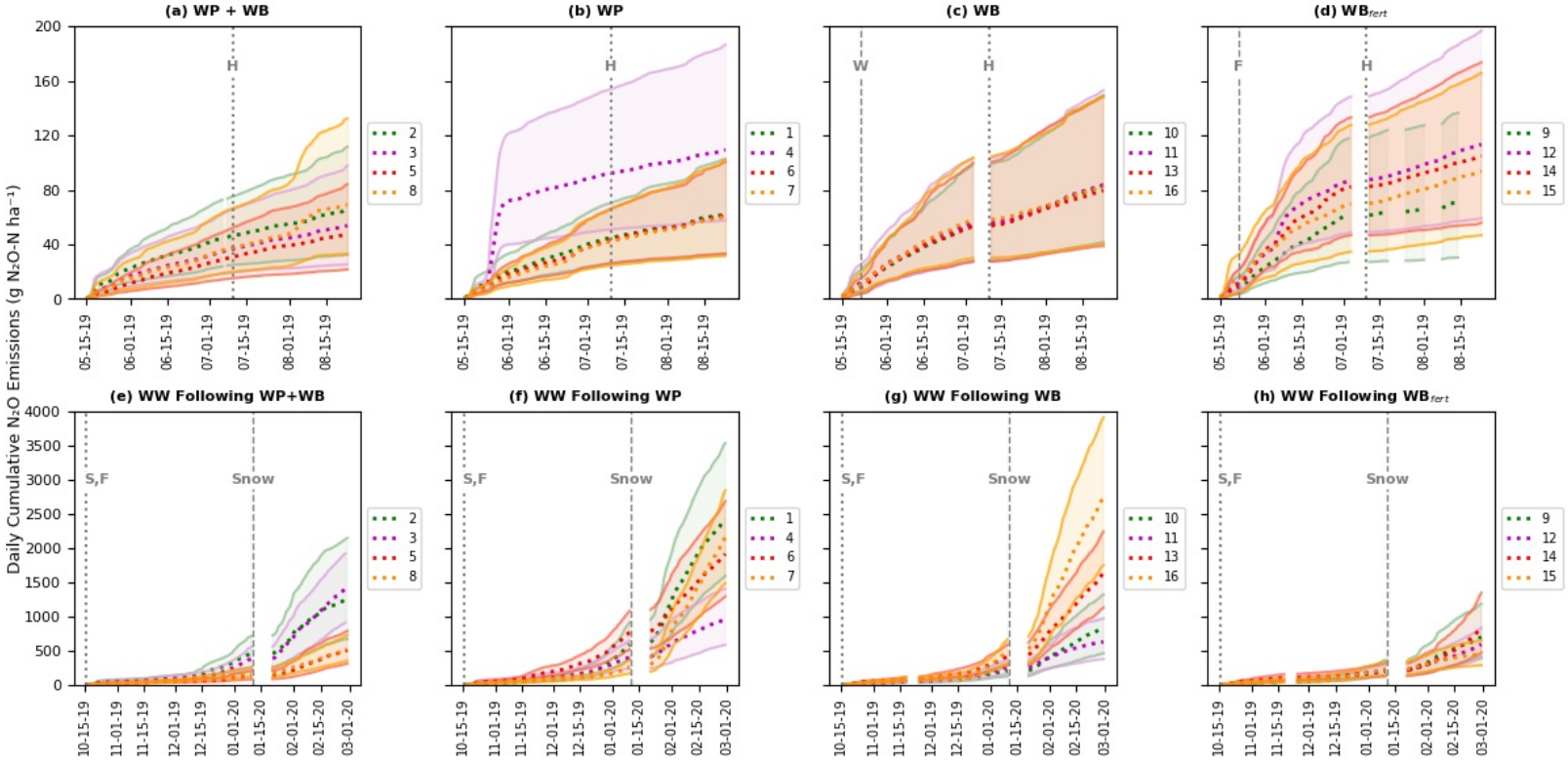

Table 3.5. The total cumulative N_2O-N emissions computed using the mean daily flux (Mean), the minimum daily flux (Min), and the maximum daily flux (Max) measured for each chamber during the cover crop study (15 May to 23 August 2019) and winter wheat study (16 October 2019 to 29 February 2020), split up by treatment group. The standard deviation of the mean daily flux (Std), and the number of days that flux measurements were collected (N) for each chamber are also indicated. The last line in the table shows the mean of the mean, min, max, and std values from all chambers, as well as the maximum amount of days that flux measurements were collected.

Cumulative N_2O-N Emissions (g ha^{-1})											
		Cover crop study					Winter wheat study				
		Mean	Min	Max	Std	*N*	Mean	Min	Max	Std	*N*
WP + WB	Chamber 2	66	32	112	16	100	1251	665	2145	154	127
	Chamber 3	54	25	98	15	101	1402	909	1920	103	126
	Chamber 5	48	22	84	12	101	501	304	782	45	127
	Chamber 8	69	33	132	16	101	519	348	725	40	127
		59	**22**	**132**	**15**	**101**	**918**	**304**	**2145**	**86**	**127**
WP	Chamber 1	62	33	103	14	101	2420	1591	3540	182	127
	Chamber 4	109	58	186	34	101	948	579	1404	103	127
	Chamber 6	61	33	101	12	101	1912	1290	2684	154	127
	Chamber 7	61	32	102	13	101	2150	1481	2845	101	127
		73	**32**	**186**	**18**	**101**	**1857**	**579**	**3540**	**135**	**127**
WB	Chamber 10	83	42	149	22	95	831	455	1316	78	121
	Chamber 11	84	40	153	25	95	624	371	967	66	119
	Chamber 13	80	39	148	22	95	1631	1126	2240	109	121
	Chamber 16	83	40	149	22	95	2729	1743	3916	187	121
		82	**39**	**153**	**23**	**95**	**1454**	**371**	**3916**	**110**	**121**
WB_{fert}	Chamber 9	71	30	136	22	73	693	405	1180	83	113
	Chamber 12	113	59	197	30	95	587	380	831	53	121
	Chamber 14	105	56	174	26	95	831	467	1344	80	120
	Chamber 15	94	47	166	29	95	445	281	648	51	121
		96	**30**	**197**	**27**	**95**	**639**	**380**	**1344**	**67**	**121**
		78	39	137	21	101	1217	775	1780	99	127

3.3.3.2. Winter wheat study

The daily mean, minimum, and maximum cumulative emissions from the microplots during the WW study (127 days) were 1217 ± 99, 775, and 1780 g N_2O-N ha^{-1}, respectively (Table 3.5). Cumulative fluxes increased exponentially with the commencement of the wet season around mid-December (Figure 3.17). Consecutive freeze-thaw and snow events followed by rain sustained consistent saturated soil conditions favorable for denitrification. Contributions from chamber 1 and 16 hot spot pulses increased overall cumulative emissions from their respective treatments. (Figure 3.17).

Although unlikely, if it is assumed that the all N_2O emissions from the study site were the result of N transformation of solely fertilizer N_r, then 1.2 of the original 168 kg N ha^{-1} fertilizer input were lost to the atmosphere via N_2O, or 0.7 %. This value will continue to increase as the study continues through to harvest in fall 2020.

The cumulative emissions from the microplots that were previously WB_{fert} treatments during the CC study were consistently lower that all other microplots and also exhibited less variability (Figure 3.17).

3.4 Conclusions

Soil moisture, measured as WFPS, and available soil N were the main variables controlling N_2O fluxes in both the CC and WW studies. The mean soil moisture and N_2O fluxes were higher during the WW study, attributed to frequent precipitation events (rain and snow) and N fertilization of all the microplots, compared to the CC study, which was generally dry and unfertilized except for the four WB_{fert} microplots.

WFPS generally did not surpass 60% during the CC season, indicating that nitrification was likely the main microbial activity contributing to N_2O emissions. N_2O fluxes were near-zero during the CC study, however, distinct N_2O pulses were still observed in May and June following drying/rewetting cycles ("Birch" effect). The total mean cumulative N_2O emissions from the CC treatments were 78 ± 21 g N_2O-N ha^{-1}, with WB_{fert} treatments consistently exhibiting the highest overall fluxes. This was likely due to the addition of supplemental N_r via N fertilization, increasing substrate availability and thus soil microbial activity. Pulses were also observed at unfertilized treatments, indicating that SOM mineralization likely occurred following rain events, supplying biologically available soil N_r for soil bacteria across all microplots. The largest CC study N_2O pulse was observed from a WP microplot. Rhizobia that live in the nodules of legumous plants are able to provide the roots with their own supply of NH_4^+ through N fixation of atmospheric N_2, potentially resulting in N build-up in the soil from mineralization of already present SOM that remains unused by the plant (Gage, 2006). This provides an excess of N_r for soil microbes, likely causing the N_2O pulse.

The WFPS and N_2O flux relationship during the WW study was found to have a bell-shaped optimum function, with N_2O peaking at around 60% WFPS. Periods of prolonged water saturation also caused the highest N_2O pulses during the WW study. The largest N_2O pulse

occurred following the largest observed snowstorm that took place during the study (~ 40cm cumulative snowfall), which slowly melted within a week of forming as temperatures progressively increased each day, followed by several days of light rain. The frozen snowpack had remained intact for almost two weeks, and despite a period of extended freezing temperatures, the near-surface soil temperature did not drop below freezing and WFPS slowly increased during this time into the denitrification range, suggesting that snow was melting at the soil-snow interface. Chambers were not operational during this time, but denitrifier bacteria still may have been active and N_2O was likely still being emitted. The total mean cumulative N_2O emissions from the WW treatments were 1217 ± 99 g N_2O-N ha^{-1}. The microplots that were previously WB_{fert} treatments during the CC study exhibited the lowest overall fluxes, the opposite of what was observed during the CC study.

Both the CC and WW study demonstrated that hot spots and hot moments increased the mean cumulative N_2O emissions. Overall, the mean total net N_2O-N lost from the WB_{fert} microplots during the CC study was about 17% higher than the "background" unfertilized WB treatments, accounting for only 0.01% of the original 112 kg N ha^{-1} fertilizer input. This value likely would have be higher had fertilization been done at the time of seeding, as the fertilizer N_r would have had more time to undergo transformations and moist soil conditions over the winter would have increased denitrification of fertilizer N_r.

All microplots were fertilized during the WW study at the time of seeding mid-October, which is common of a WW rotation. Fertilizing in excess is necessary as the wet fall, winter, and spring seasons result in N_r losses through multiple pathways. The only loss pathway that was measured during this study was denitrification, however, volatilization, leaching, and surface runoff are also common loss pathways from agricultural systems. Assuming all N_2O emissions

were the result of N transformations of fertilizer N_r only, then 0.7 % of the original 168 kg N ha^{-1} fertilizer input were lost to the atmosphere over the four and a half months following seeding and fertilization.

Measurement of other soil variables throughout the CC and WW studies, such as soil pH, SOM content, and soil N content (from both natural sources and fertilizer) could have provided insight into how they may have potentially impacted microbial abundance and diversity, ultimately affecting N_2O emissions. This information, combined with the data obtained from this study regarding N fertilizer placement, timing, rate, and application method, and how soil moisture affects N_2O emissions, can help to improve nutrient use efficiency in agroecosystems.

3.5 References

Bateman, E. J., & Baggs, E. M. (2005). Contributions of nitrification and denitrification to N2O emissions from soils at different water-filled pore space. *Biology and Fertility of Soils*, *41*(6), 379–388. https://doi.org/10.1007/s00374-005-0858-3

Behnke, G. D., Zuber, S. M., Pittelkow, C. M., Nafziger, E. D., & Villamil, M. B. (2018). Long-term crop rotation and tillage effects on soil greenhouse gas emissions and crop production in Illinois, USA. *Agriculture, Ecosystems and Environment*, *261*, 62–70. https://doi.org/10.1016/j.agee.2018.03.007

Bernhardt, E. S., Blaszczak, J. R., Ficken, C. D., Fork, M. L., Kaiser, K. E., & Seybold, E. C. (2017). Control Points in Ecosystems: Moving Beyond the Hot Spot Hot Moment Concept. *Ecosystems*, *20*(4), 665–682. https://doi.org/10.1007/s10021-016-0103-y

Boczulak, S. A., Hawkins, B. J., & Roy, R. (2014). Temperature effects on nitrogen form uptake by seedling roots of three contrasting conifers. *Tree Physiology*, *34*(5), 513–523. https://doi.org/10.1093/treephys/tpu028

Borken, W., & Matzner, E. (2009). Reappraisal of drying and wetting effects on C and N mineralization and fluxes in soils. *Global Change Biology*, *15*(4), 808–824. https://doi.org/10.1111/j.1365-2486.2008.01681.x

Camargo, G. G. T., Ryan, M. R., & Richard, T. L. (2013). Energy Use and Greenhouse Gas Emissions from Crop Production Using the Farm Energy Analysis Tool. *BioScience*, *63*(4), 263–273. https://doi.org/10.1525/bio.2013.63.4.6

Chen, Z., Yang, S. qi, Zhang, A. ping, Jing, X., Song, W. min, Mi, Z. rong, … Yang, Z. li. (2018). Nitrous oxide emissions following seasonal freeze-thaw events from arable soils in Northeast China. *Journal of Integrative Agriculture*, *17*(1), 231–246. https://doi.org/10.1016/S2095-3119(17)61738-6

Clayton, H., Arah, J. R. M., & Smith, K. A. (1994). Measurement of nitrous oxide emissions from fertilized grassland using closed chambers. *Journal of Geophysical Research*, *99*(D8), 16599. https://doi.org/10.1029/94JD00218

Davidson, E.A., Vitousek, P.M., & Matson, P.A. (1991). Soil emissions of nitric-oxide in a seasonally dry tropical forest of mexico. *Journal of Geophysical Research Atmospheres, 96*: 15439–15445. https://doi.org/10.1029/91JD01476

de Graaff, M. A., Hornslein, N., Throop, H. L., Kardol, P., & van Diepen, L. T. A. (2019). *Effects of agricultural intensification on soil biodiversity and implications for ecosystem functioning: A meta-analysis*. *Advances in Agronomy* (1st ed., Vol. 155). Elsevier Inc. https://doi.org/10.1016/bs.agron.2019.01.001

Fierer, N., & Schimel, J. P. (2002). Effects of drying-rewetting frequency on soil carbon and nitrogen transformations. *Soil Biology and Biochemistry*, *34*(6), 777–787. https://doi.org/10.1016/S0038-0717(02)00007-X

Firestone, M.K. & Davidson, E.A. (1989). *Microbiological basis of NO and N2O production and consumption in soil*. In: Andreae, M.O., Schimel, D.S. (Eds.), Exchange of Trace Gases between Terrestrial Ecosystems and the Atmosphere. John Wiley, New York, pp. 7–21.

Fowler, D., Pyle, J. A., Raven, J. A., Sutton, M. A., Fowler, D., Pyle, J. A., & John, A. R. (2013). The global nitrogen cycle in the twenty-first century: introduction, *368*(1621), 1–2.

Galloway, J. N., Aber, J. D., Erisman, J. W., Seitzinger, S. P., Howrath, R., Cowling, E. B., & Cosby, B. J. (2003). The Nitrogen Cascade. *BioScience*, *53*(4), 341. https://doi.org/10.1641/0006-3568(2003)053[0341:tnc]2.0.co;2

Grierson, P.F., Comerford, N.B., Jokela, E.J., 1998. Phosphorus mineralisation kinetics and response of microbial phosphorus to drying and rewetting in a Florida Spodosol. *Soil Biology and Biochemistry, 30:* 1323–1331. https://doi.org/10.1016/S0038-0717(98)00002-9

Groffman, P. M., Butterbach-Bahl, K., Fulweiler, R. W., Gold, A. J., Morse, J. L., Stander, E. K., … Vidon, P. (2009). Challenges to incorporating spatially and temporally explicit phenomena (hotspots and hot moments) in denitrification models. *Biogeochemistry*, *93*(1–2), 49–77. https://doi.org/10.1007/s10533-008-9277-5

Grundmann, G.L. & Rolston, D.E. (1987). A water function approximation to degree of anaerobiosis associated with denitrification. *Soil Science, 144*: 437–441.

Hénault, C., Grossel, A., Mary, B., Roussel, M., & Léonard, J. (2012). Nitrous Oxide Emission by Agricultural Soils: A Review of Spatial and Temporal Variability for Mitigation. *Pedosphere*, *22*(4), 426–433. https://doi.org/10.1016/S1002-0160(12)60029-0

IPCC (2013). *Climate Change 2013: The Physical Science Basis. Contribution of Working Group I to the Fifth Assessment Report of the Intergovernmental Panel on Climate Change* [Stocker, T.F., D. Qin, G.-K. Plattner, M. Tignor, S.K. Allen, J. Boschung, A. Nauels, Y.

Xia, V. Bex and P.M. Midgley (eds.)]. Cambridge, United Kingdom and New York, NY, USA: Cambridge University Press.

Jarvis, P., Rey, A., Petsikos, C., Wingate, L., Rayment, M., Pereira, J., … Valentini, R. (2007). Drying and wetting of Mediterranean soils stimulates decomposition and carbon dioxide emission: The "Birch effect." *Tree Physiology*, *27*(7), 929–940. https://doi.org/10.1093/treephys/27.7.929

Jeuffroy, M. H., Baranger, E., Carrouée, B., De Chezelles, E., Gosme, M., Hénault, C., … Cellier, P. (2013). Nitrous oxide emissions from crop rotations including wheat, oilseed rape and dry peas. *Biogeosciences*, *10*(3), 1787–1797. https://doi.org/10.5194/bg-10-1787-2013

Kuzyakov, Y., & Blagodatskaya, E. (2015). Microbial hotspots and hot moments in soil: Concept & review. *Soil Biology and Biochemistry*, *83*, 184–199. https://doi.org/10.1016/j.soilbio.2015.01.025

Laville, P., Lehuger, S., Loubet, B., Chaumartin, F., & Cellier, P. (2011). Effect of management, climate and soil conditions on N2O and NO emissions from an arable crop rotation using high temporal resolution measurements. *Agricultural and Forest Meteorology*, *151*(2), 228–240. https://doi.org/10.1016/j.agrformet.2010.10.008

Leitner, S., Homyak, P. M., Blankinship, J. C., Eberwein, J., Jenerette, G. D., Zechmeister-Boltenstern, S., & Schimel, J. P. (2017). Linking NO and N2O emission pulses with the mobilization of mineral and organic N upon rewetting dry soils. *Soil Biology and Biochemistry*, *115*, 461–466. https://doi.org/10.1016/j.soilbio.2017.09.005

Linn, D. M., & Doran, J. W. (1984). Effect of Water-Filled Pore Space on Carbon Dioxide and Nitrous Oxide Production in Tilled and Nontilled Soils. *Soil Science Society of America Journal*, *48*(6), 1267–1272. https://doi.org/10.2136/sssaj1984.03615995004800060013x

Liu, C., Cutforth, H., Chai, Q., & Gan, Y. (2016). Farming tactics to reduce the carbon footprint of crop cultivation in semiarid areas. A review. *Agronomy for Sustainable Development*, *36*(4). https://doi.org/10.1007/s13593-016-0404-8

Ludwig, B., Wolf, I., & Teepe, R. (2004). Contribution of nitrification and denitrification to the emission of N2O in a freeze-thaw event in an agricultural soil. *Journal of Plant Nutrition and Soil Science*, *167*(6), 678–684. https://doi.org/10.1002/jpln.200421462

McClain, M. E., Boyer, E. W., Dent, C. L., Gergel, S. E., Grimm, N. B., Groffman, P. M., … Pinay, G. (2003). Biogeochemical Hot Spots and Hot Moments at the Interface of

Terrestrial and Aquatic Ecosystems. *Ecosystems*, *6*(4), 301–312. https://doi.org/10.1007/s10021-003-0161-9

McIntyre, R. E. S., Adams, M. A., Ford, D. J., & Grierson, P. F. (2009). Rewetting and litter addition influence mineralisation and microbial communities in soils from a semi-arid intermittent stream. *Soil Biology and Biochemistry*, *41*(1), 92–101. https://doi.org/10.1016/j.soilbio.2008.09.021

Miller, A. E., Schimel, J. P., Meixner, T., Sickman, J. O., & Melack, J. M. (2005). Episodic rewetting enhances carbon and nitrogen release from chaparral soils. *Soil Biology and Biochemistry*, *37*(12), 2195–2204. https://doi.org/10.1016/j.soilbio.2005.03.021

Mosier, A. R. (2002). Environmental challenges associated with needed increases in global nitrogen fixation. *Nutrient Cycling in Agroecosystems*, *63*(2–3), 101–116. https://doi.org/10.1023/A:1021101423341

Mulvaney, R. L., Khan, S. A., & Mulvaney, C. S. (1997). Nitrogen fertilizers promote denitrification. *Biology and Fertility of Soils*, *24*(2), 211–220. https://doi.org/10.1007/s003740050233

Papen, H., & Butterbach-Bahl, K. (1999). A 3-year continuous record of nitrogen trace gas fluxes from untreated and limed soil of a N-saturated spruce and beech forest ecosystem in Germany. 2. NO and NO2 fluxes. *Journal of Geophysical Research Atmospheres*, *104*(15), 487–503.

Perlman, J., Hijmans, R. J., & Horwath, W. R. (2013). Modelling agricultural nitrous oxide emissions for large regions. *Environmental Modelling and Software*, *48*, 183–192. https://doi.org/10.1016/j.envsoft.2013.07.002

Petitjean, C., Le Gall, C., Pontet, C., Fujisaki, K., Garric, B., Horth, J.-C., … Perrin, A.-S. (2009). Soil N2O, CH4, and CO2 Fluxes in Forest, Grassland, and Tillage/No-Tillage Croplands in French Guiana (Amazonia). *Soil Systems*, *33*(3), 617–623. https://doi.org/10.3773/j.issn.1005-264x.2009.03.021

Pilegaard, K. (2013). Processes regulating nitric oxide emissions from soils. *Philosophical Transactions of the Royal Society B: Biological Sciences*, *368*(1621). https://doi.org/10.1098/rstb.2013.0126

Poth, M., & Focht, D. D. (1985). 15N Kinetic Analysis of N2O Production by Nitrosomonas europaea: an Examination of Nitrifier Denitrification. *Applied and Environmental Microbiology*, *49*: 1134-1141. https://doi.org/10.1128/AEM.49.5.1134-1141

Qin, C., Yi, K. K., & Wu, P. (2011). Ammonium affects cell viability to inhibit root growth in Arabidopsis. *Journal of Zhejiang University: Science B*, *12*(6), 477–484. https://doi.org/10.1631/jzus.B1000335

Rafique, R., Hennessy, D., & Kiely, G. (2011). Nitrous Oxide Emission from Grazed Grassland Under Different Management Systems. *Ecosystems*, *14*(4), 563–582. https://doi.org/10.1007/s10021-011-9434-x

Risk, N., Snider, D., & Wagner-Riddle, C. (2013). Mechanisms leading to enhanced soil nitrous oxide fluxes induced by freeze-thaw cycles. *Canadian Journal of Soil Science*, *93*(4), 401–414. https://doi.org/10.4141/CJSS2012-071

Schmidt, U., Thöni, H., & Kaupenjohann, M. (2000). Using a boundary line approach to analyze N2O flux data from agricultural soils. *Nutrient Cycling in Agroecosystems*, *57*, 119–129. https://doi.org/10.1023/A:1009854220769

Smith, P., House, J. I., Bustamante, M., Sobocká, J., Harper, R., Pan, G., … Pugh, T. A. M. (2016). Global change pressures on soils from land use and management. *Global Change Biology*, *22*(3), 1008–1028. https://doi.org/10.1111/gcb.13068

United States Environmental Protection Agency (2020). *Inventory of U.S. Greenhouse Gas Emissions and Sinks: 1990–2018*. Available at https://www.epa.gov/ghgemissions/inventory-us-greenhouse-gas-emissions-and-sinks-1990-2016

Van Cleemput, O. and Samater, A. H. (1996). Nitrite in soils: accumulation and role in the formation of gaseous N compounds. *Fertilizer Research*, *45*: 81–89. https://doi.org/10.1007/BF00749884

Vitousek, P. M., Mooney, H. A., Lubchenco, J., & Melillo, J. M. (1997). Human domination of Earth's ecosystems. *Urban Ecology: An International Perspective on the Interaction Between Humans and Nature*, *277*(July), 3–13. https://doi.org/10.1007/978-0-387-73412-5_1

Wagner-Riddle, C., Hu, Q. C., van Bochove, E., & Jayasundara, S. (2008). Linking Nitrous Oxide Flux During Spring Thaw to Nitrate Denitrification in the Soil Profile. *Soil Science Society of America Journal*, *72*(4), 908–916. https://doi.org/10.2136/sssaj2007.0353

Wagner-Riddle, C., Thurtell, G. W., Kidd, G. K., Beauchamp, E. G., & Sweetman, R. (1997). Estimates of nitrous oxide emissions from agricultural fields over 28 months. *Canadian Journal of Soil Science*, *77*(2), 135–144. https://doi.org/10.4141/S96-103

Zhu, X., Burger, M., Doane, T. A., & Horwath, W. R. (2013). Ammonia oxidation pathways and nitrifier denitrification are significant sources of N2O and NO under low oxygen availability. *Proceedings of the National Academy of Sciences of the United States of America*, *110*(16), 6328–6333. https://doi.org/10.1073/pnas.1219993110

CHAPTER FOUR:

CONCLUSIONS AND FUTURE WORK

This thesis analyzed and reported measurements of greenhouse gas (GHG) emissions from a small-scale study plot on an agricultural field from a cover crop (CC) system followed by a winter wheat (WW) system. Measurements were conducted over a three-month study period during spring and summer for the CC system, and over a four-and-a-half-month study period during the fall and winter for the WW system. Carbon dioxide (CO_2) and nitrous oxide (N_2O) fluxes were quantified using automated closed static chambers (CSCs) that were closely placed together to achieve high spatial coverage over a small and seemingly heterogeneous area of soil.

Few field studies based in agricultural sites have documented long-term soil flux datasets at the same high temporal resolution as this study due to the lack of on-site electrical power. The flux data obtained from this study showed that hotspots and hot moments had large contributions to the overall cumulative emissions from the soil during both systems, which likely would not have been captured had manual CSCs been used, particularly nighttime emissions, as this method is labor intensive and realistically cannot be operated continuously. Long-term soil GHG flux data offer a valuable contribution to the currently limited but expanding information on soil N cycling processes and the diurnal, seasonal, and annual variability of soil respiration between agroecosystems and the atmosphere.

Peak and prolonged pulses of N_2O fluxes measured during WW system confirmed that fertilization before the wet fall and winter months increases denitrification activity and thereby N_2O production. Due to time constraints, not all of the flux data from the WW study were presented herein, but monitoring is on-going and the flux data from the entire growing season will eventually be analyzed and reported, from which an emission factor can be calculated.

Additional data will also be released from a concurrent isotope analysis that was on-going throughout this study from the half-microplots that were fertilized with ^{15}N-labelled fertilizer. This data will provide further evidence into which microbial mechanisms (nitrification or denitrification) were responsible for N_2O emissions at specific times, as this study was only able to speculate what mechanism was dominant based on soil moisture and the likely N substrate that was available.

Suggested future work includes:

- Measurement of other soil variables throughout both the CC and WW study, such as pH, soil organic matter content (SOM), and soil N content (from both natural sources and fertilizer), to study their impact on soil microbial abundance and diversity, and ultimately how this may be affecting N_2O emissions. This information may have helped us understand why the N_2O fluxes from the WB_{fert} microplots during the WW study were lower.
- Analyze the impact of naturally derived reactive nitrogen (N_r) supplied via SOM mineralization of a preceding "alternative" CC legume rotation on a subsequent crop rotation without the addition of chemical N fertilizers. This could be achieved by leaving some microplots unfertilized during a "business-as-usual" crop rotation, such as winter wheat, which is typically fertilized, and monitoring the effect on N_2O emissions and crop yield from both the fertilized and unfertilized microplots. Legumes are able to fix substantial quantities of atmospheric N_2, which is returned to the soil as SOM following crop termination. Mineralization of SOM during the summer has been found in previous studies to be a significant source of reactive nitrogen (N_r) to the soil, which could mean a

reduction in synthetic N fertilizer inputs, and thereby a reduction in N_2O emissions from agricultural soils. Additionally, SOM mineralization occurs over extended periods of time, supplying crops with a constant source of N_r under the right conditions and with high enough amounts of available SOM. Unlike SOM, N fertilizer is more vulnerable to losses from soil via nitrification/denitrification, volatilization, leaching, and surface runoff.

- Decrease chamber flux measurement timing and incorporate more automated chambers to the flux system. This would decrease temporal frequency of individual chambers but would increase spatial coverage. It was observed during this study that while N_2O soil emissions are high and producing well-behaved flux data, a shorter measurement time is possible.
- Addition of eddy covariance flux measurements with a high-precision N_2O analyzer to quantify soil N_2O emissions. This would allow for a larger flux footprint, increasing the potential to capture more hot moments and hot spots that chamber-based measurements are prone to missing. Combining measurement techniques would provide insight into the viability of scaling up chamber-based measurements to landscape scale emissions.
- Monitoring the effects of a snowpack on soil N_2O emissions could contribute valuable information to the still limited data available on wintertime N_2O fluxes. Our soil sensor data showed that the insulating properties of snow increased soil moisture to within optimal denitrification range, likely driving N_2O emissions.

It has been well established within the literature that diminishing uncertainties in global emission estimates of N_2O may help in constraining the global N budget. The high spatial and

temporal variability of soil N_2O emissions make this difficult, however, improvements in measurement tools, techniques, and strategies are bringing researchers closer to this goal. The future work suggested in this chapter could provide added value to this research study and future similar studies, which unfortunately were not possible due to time and funding constraints.